Interplay between disorder and interactions: from non-Fermi liquid superconductivity to iterative quantum optimization

A DISSERTATION
SUBMITTED TO THE FACULTY OF THE GRADUATE SCHOOL
OF THE UNIVERSITY OF MINNESOTA
BY

Hanteng Wang

IN PARTIAL FULFILLMENT OF THE REQUIREMENTS
FOR THE DEGREE OF
DOCTOR OF PHILOSOPHY

Advisor: Professor Alex Kamenev

August, 2021

Acknowledgements

The graduate journey couldn't be smooth, if there is no support from many peoples, especially during the pandemic. I would like to express my deepest gratitude to them.

First and foremost, I am deeply indebted to my adviser Prof. Alex Kamenev, for his continuous and tireless support in academia. Alex inspires me with his critical thinking, scientific creativity, and especially the simplicity to demonstrate the hardest physics. All the work I demonstrate in the thesis, could not be accomplished without Alex's help and partnership.

I am also greatly thankful to the faculty members of the School of Physics at the University of Minnesota, especially Boris Shklovskii, Andrey Chubukov, Misha Shifman, and Jorge Vinals where I learn a lot from their advanced courses. I have also benefited from the collaboration with Sasha Chudnovskiy, Dmitry Bagrets, and Alexander Gorsky. I am grateful to Rafael Fernandes and Vlad Pribiag for serving as my graduate preliminary and final examining committee.

Special thanks to many friends of mine, who accompany and help me through many years, including Junyu Zhang, Yiming Wu, Hsiu-Chung Yeh, Zhen Jiang, and many others.

Last but not least, I want to say thank you to my parents, who raised me for 18 years in Shanghai, and endured my away from home for 4 years in Beijing and 6 years in Minnesota. Without your love and patience, I could not have come this far.

Dedication

This dissertation is dedicated to my parents, Tiehua Wang and Jihong Han.

Abstract

In this thesis, we use analytical and numerical methods to shed light on the interplay between disorder and interactions in discorded systems. We investigate existence of replica off-diagonal solutions in the field-theoretical description of Majorana version of Sachdev-Ye-Kitaev (SYK) model. We conclude that all our numerical results are in a quantitative agreement with the theory based on the replica-diagonal saddle point plus Schwarzian and massive Gaussian fluctuations, which indicate a non-Fermi liquid phase rather than glassy phase in SYK. Besides the Majorana version of SYK model, We also investigate a possibility of having a superconducting off-diagonal long-range order and a pseudogap phase in SYK model with spin-1/2 fermions attracted by Hubbard interaction. We figure out the SYK + Hubbard model is approaching a certain generalization of the integrable Richardson model at large Hubbard term and exists a quantum phase transition described by synchronization effect in a quantum version of the Kuramoto model at small Hubbard term. The thesis also include the investigation of localization-delocalization transition in SYK_4 + SYK_2 model, and a non-ergodic extend phase could be found in certain parameter space. This indicate two extensive states in Hilbert space of SYK_4 + SYK_2 model, are not necessarily have level repulsion with each, which is similar to the case of single-particle Anderson transition on a Cayley tree lattice. At last, we demonstrate our attempt to the diabatic iterative version of the quantum optimization, with an addition reference Hamiltonian during annealing process. By choosing certain optimal trajectory in phase space, in one iteration of a four-stage annealing protocol, one may search a better solution compare to previous inputted ansatz (i.e. reference state) within power-law rather than exponentially long time with a high probability. This algorithm may overcome the issue of the exponentially small gap at the end of the annealing procedure of the standard "forward" quantum annealing due to many-body localization effect, and find out an outcome of the optimization problem with desired accuracy within a power-law annealing time.

Contents

Chapter 1

Introduction

1.1 Overview

Disorder is everywhere. Disorder effects may show up in a condensed matter material in physics lab which ruin the result one expect compared to clean samples, or in an optimization problem struggle by a traveling salesman, or even a black hole which is far away from our daily life. The main point of this thesis is to offer idealized models and possible method/solutions to settle the issue when disorder appears.

The most profound and useful model in disordered kingdom is however constructed by the simplest way one can imagine, just grabbing plenty of random numbers and organize them into a 2-dimensional array (or say matrix). This seemingly naive structure surprisingly present almost all the information we need in a hidden manner. The first example to show the power of random matrices in physics world is presented by Wigner who settle the problem of the great complexity in nuclei (late 1950s, see collection in Ref. [1]) . Without solving any complicated Schrodinger equations one may expect which construted by orbitals or spins, Wigner simply diagonalize a 2 by 2 random matrix and argue that the spectrum in a complicated nuclei would share the similar properties as that 2 by 2 random matrix. After that, physicist start to construct more sophisticated versions of random matrices, and develop the formal theory of random matrix theory (RMT). Many interesting observation was made, and one of the interesting one is the universal symmetry class [2]. By putting different types of number (real or complex, or even quaternion) into the matrix, one may found the strength of the level repulsion

differs qualitatively, which lead to a visualized check to the underlining symmetry of the random systems.

Few years later, physicists start to divert their attention from nuclei physics (which are concentrated area due to the transparent usage of the nuclear at those days) to more daily life style physics, solid physics (or more general condensed matters). Around the early days of the invention of the quantum mechanics, Bloch understand that, the electrons in lattice would not be scattered, as long as the lattice structure is perfectly organized, until there are impurities/disorder in lattice to let the electron detour. Nevertheless, though existing the disorder effect to obstruct electron from moving forward, people believe the electron should maintain its exploration wherever it wants inside the material. In other words, the disordered electronic systems should still be in the metal phase and have no chance to become a insulator, which is the situation that the electrons are stuck at very limited region. P. W. Anderson (1958, in Ref. [3]), use a toy model which is nothing different from another 2 by 2 matrix, argued that if one has strong randomness for the on-site energy as diagonal part of the random matrix with the hopping energy between different sites as off-diagonal part relatively weak, the electron could be localized on one of the impurity and the system should be regard as an insulator. The metal-insulator transition may be translated into delocalization-localization transition, which open a era for new types of transition may beyond the Landau paradigm.

The concept of delocalization-localization transition, though originally proposed and worked out in single-particle electronic system, could be expand to the context with strongly interacting systems, i.e. many-body systems. People start to realize, that one of the common material in daily life, the glass, could be interpreted as a type of many-body localized material. In the sense, that the glassy systems are always stuck/localized in one of the meta-stables among exponentially many of them. Similar to the disordered electronic system that electrons can be localized at one of the site among full lattice rather than explore the whole lattice space, the glass is localized in the Hilbert space lattice and cannot explore the whole Hilbert space. This coincide with the notion of lack of thermalization/ergodicity. For the quantitative investigations of the glassy systems, physicists found the systems consists spins forms good playground to deal with analytic analysis. Sherrington-Kirkpatrick (SK) model (1975, in Ref. [4]), a

canonical example of spin-glass, has simplest random spin-spin coupling, while the outcoming results of the SK is fruitful. To analytically calculate the physical quantities of the Sherrington-Kirkpatrick model, people invent the replica trick to replicate the partition function, and argue the equivalent replicas (replica symmetric) indicate delocalized phase while inequality between replicas (replica symmetry breaking) indicate the exsistance of multiple meta-stables and the system would be localized at one of the meta-stables. Sherrington-Kirkpatrick is replica symmetric at high temperature, while the replica symmetry is broken at low temperature. So the common sense of melting glass to fluid could be now interpreted as localization-delocalization transition, and the replica structure would be serve as the order parameter to distinguish between glass and fluid. At the same time, this theoretical machinery, i.e. replica field theory, becomes a strong tool to investigate different types of disordered systems.

Additional to the Sherrington-Kirkpatrick model, many other spin models were proposed to explore the nature of spin-glass. Sachdev and Ye (1993, in Ref. [5]) also join in the trend of tourism and describe the so-called Sachdev-Ye (SY) model. Contrary to initial suspicious, the Sachdev-Ye model, though have very similar appearance compare to Sherrington-Kirkpatrick model in its Hamiltonian, people found that there may not have a glassy phase. This might become the reason why the SY model was not heavily mentioned in the literature at those days. Until very recent (2015, in Ref. [6]), Kitaev rediscovered the same model in terms of fermionic degrees of freedom, arguing this model itself is (dual to) a black hole and make the model popular again with a new name: Sachdev-Ye-kitaev (SYK) model. This SYK model, in some sense, can be regard as a structured random matrix, because the level statistics for the nearest neighbor ordered in energy shares the same type with the RMT which classified by the same symmetry classes. This resembled feature in RMT in the smallest energy scale (or the longest time scale), is the defining signature of quantum chaos. What's more interesting is that, at a short time scale, SYK shows its strongest ability to scramble the information, i.e. the system would forgot where it comes from with fastest speed with only tiny perturbation, just like the butterfly effect. So this toy model characterize the type of the most chaotic stuff in the universe, and would prefer delocalize itself in any time scale. This model also present us the playground to study the localization-delocalization transition and would become useful when one wants to "melt" something.

Apart from the quantum chaotic nature as we discussed, SYK is a strange metal. One should be careful strange metal here is a terminology rather than oral English. It is a metal/fluid rather than a glass or insulator, in the sense it is a gapless system without replica symmetry breaking. It is strange in the sense that it differs from a Fermi-liquid type of metal, where excitation are quasi-particles. This feature reminds people of the metal phase in the high-temperature superconductivity. At certain doping regime of the high-Tc superconductivity, metal state at intermediate energy scale has linear-temperature dependence rather than quadratic, which is caused by the lack of notion of quasi-particle excitations. Though with a unrealistic disordered Hamiltonian, mean-field theory of SYK started to be used as paradigm to treat strange metal (i.e. non-Fermi liquid) phase in superconductivity, and there are lots of fruitful results to shed light on high-Tc problem.

On the other side of the world, disordered systems can be mapped to an optimization problem one may care about in daily life. Combinatorial optimization can be regard as a topic that consists of finding an optimal object (i.e. spin-configuration in spin-type Hamiltonian language) among all objects which lead to the least cost. The cost is equivalent to the energy (Hamiltonian) of the problem, which one may want to minimize, i.e. finding the ground state (GS) of the Hamiltonian. Unfortunately, many important combinatorial optimization problems, are mapped to Hamiltonians which establish a spin-glass phase. This means finding the ground state is a tremendously hard job, since with high probability, one would search a solution which stuck around meta-stable (i.e. local minimum) states of the problem. In order to fix the problem of localization at wrong solutions, people provide the quantum fluctuation in order to hop the state from one local minimum to another. This is the idea of quantum annealing (1998, in Ref. [7]) in optimization problem. There are many different types of quantum annealing protocols which may do the job, and the understanding of the validity of these protocols may heavily rely on the knowledge of localization-delocalization transition.

1.2 Dissertation Structure

This dissertation will focus on these disordered system, and be ordered in following manner

- In Chapter 2, we introduce two important toy models in the disorder kingdom: random matrix theory and Sachdev-Ye-Kitaev model. The visualizable feature of them are the Wigner-Dyson level statistics in their eigen-energies, which indicate their quantum chaotic nature. We also briefly demonstrate how replica field theory could be established in these two contexts, and study the preliminary aspects of the replica structure. Only replica diagonal and symmetric solutions are studied in this chapter.

- In Chapter 3, we dig more into the replica structure of the SYK model. The mean-field solutions and fluctuation around the mean-field are studied, with more sophisticated replica structure. Both analytical and numerical results are present to verify different scenarios one may encountered, i.e. replica-diagonal vs replica-off-diagonal calculations. This chapter is mainly constructed according to the published work [8]: H. Wang, D. Bagrets, A. L. Chudnovskiy, and A. Kamenev, *On the replica structure of Sachdev-Ye-Kitaev model*, J. High Energy Phys. 09 (2019) 057.

- In Chapter 4, with the knowledge of the dominance of replica diagonal solution established in Chapter 3, we discuss how to construct superconductivity on top of the strange metal (i.e. non-Fermi liquid) phase of the SYK. A resemble picture compare to real world high-Tc superconductivity could be found in the SYK-superconductor models. This chapter is mainly constructed according to the published work [9]: H. Wang, A. L. Chudnovskiy, A. Gorsky, and A. Kamenev, *Sachdev-Ye-Kitaev superconductivity: Quantum Kuramoto and generalized Richardson models*, Phys. Rev. Research **2**, 033025 (2020).

- In Chapter 5, we focus on the possible glass phases in disorder systems and discuss the melting process of glass which could be interpreted as many-body localization-delocalization transition. We also discuss the application of the spin-glass systems in optimization problem. An iterative version of quantum annealing protocol with a reference Hamiltonian was proposed in this chapter, where each iteration of the protocol will lead a better solution compare to previous inputted solution/ansatz within only power-law long time. The chapter is partially based on unpublished work collaborated with Hsiu-Chung Yeh and A. Kamenev.

- Chapter 6 concludes the dissertation.

Chapter 2

Disordered systems: level statistics and replicas

In this chapter, Two important toy models which involve quenched randomness would be discussed and service as main characters throughout the thesis. In contrast to thermal or quantum fluctuations, quenched randomness are the "frozen" disorder, and does not change on the time scale we care about.

The most widely used toy model to characterize disordered system is the random matrix theory (RMT). One of its earliest usage is from nuclear physics. Due to the hardness in solving the wavefunction and analysis the property in nuclei, Wigner invent a coarse graining point of view, namely regarding strong interaction between the orbitals of the nuclei that the system could be representing by a random Hamiltonian [10]. Surprisingly, though the randomness and roughness in the presence of the Hamiltonian, there is a high precision in predicting the statistics of eigenvalues and eigenfunctions of those complex many–body quantum systems. On side of the physics world involves condensed matter, RMT treatment was introduced by Anderson in study the disordered metals, especially for the aspect of the localization transition [3]. Later, people open the new era for the study of the many-body physics of the disordered metal under this construction. To be concrete, let's consider a disordered metal, with electrons hopping

here and there with Hamiltonian

$$\hat{H}_{\text{hopping}} = \sum_{i,j} t_{ij} c_i^\dagger c_j \tag{2.1}$$

where i, j can be recognized as the sites on lattice, and the hopping from i to j should be nearest neighbor in a realistic set-up. More abstractly (i.e. do not limit yourself in the 3d real space), these i, j can be regarded as any orbital you want to describe and the interaction between i, j can be randomly chosen. If we allow all to all interaction with certain quenched random distribution of the hooping, this becomes the standard random matrix theory:

$$H_{\text{RMT}} = \begin{pmatrix} t_{11} & t_{12} & ... & t_{1N} \\ \vdots & \vdots & \ddots & \vdots \\ t_{N1} & t_{N2} & ... & t_{NN} \end{pmatrix} \tag{2.2}$$

This can be regard as the "first quantized" version of the quantum mechanics in orbital basis. If one have a powerful computer which let you find all eigenvalues and eigenfunctions of Eq. (2.2), one basically got all the information of the single particle electron spectrum. One can study many different aspects of the physics (say single particle Anderson transition and quantum chaos). Under the investigation of RMT, people start to realize that one may define the concept of quantum chaos with help of the RMT. If the systems have the similar statistics in eigenvalues and eigenfunctions to RMT, it could be defined as a chaotic system at quantum level, even the system may not have classical counterpart. We will discuss the details of RMT in Sec. 2.1.

Recently, a new type of "random matrices" called Sachdev-Ye-Kitaev (SYK) model becomes the focus of physicists' attention. It could be regard as a many-body version of the random matrices. SYK model consists 4-point (or higher-point) interactions between Fermions and its Hamiltonian can be constructed

$$\hat{H}_{\text{SYK-complex}} = \sum_{i,j;k,l} J_{ij;kl}\, c_i^\dagger c_j^\dagger c_k c_l \tag{2.3}$$

It is seeming a naive upgrade from single particle random matrix (2-point interaction)

to a many-body random matrix (4-point interaction), but actually SYK has many fancy properties compare to standard RMT. People find (a) SYK is a metal but a strange metal (i.e. non-Fermi liquid). (b) Though different from RMT at short time scale, SYK will be thermalized at long time and mimic the behavior of RMT. This indicate SYK as a many-body version of quantum chaos. (c) SYK has the fastest scrambling rate at short time regime. (d) SYK is dual to certain gravity theory, i.e. looks like a black hole at finite temperature. We will have more detailed introduction for the SYK in Sec. 2.2.

In order to investigate these types of quantum chaotic systems, I will present some basic knowledge treating the RMT and SYK, both analytically and numerically.

2.1 Random matrix theory (RMT)

We are interested in the spectral properties of the random $N \times N$ Hermitian Hamiltonians $H_{\text{RMT}} = \{H_{ij}\}$, with entry H_{ij} are random variables. The probability for one specific realization of H to show up is following the Gaussian distribution

$$P(H_{\text{RMT}}) \propto \exp\left[-\frac{N}{2}\text{Tr}\, H_{\text{RMT}}^2\right] \tag{2.4}$$

Once one generate a random instance of H, the eigenvalue and eigenfunctions can be found by a brute force exact diagonalization procedure. Nowadays, people can deal with the matrix size around $2^{20} \times 2^{20}$ to find all the eigenvalue and eigenfunctions. For different symmetry of the Hamiltonian, one may find different level statistics. And very strong level repulsion at smallest energy difference scale is observed. We will discuss these information in Sec. 2.1.1.

Besides viewing the Hamiltonian as a random matrix and diagonalizing it directly, physicists also invent the field theory treatment to solve it and find similar result compare to experiments. We will discuss this treatment in Sec. 2.1.2.

2.1.1 Level repulsion and level statistics

Let's first focus on the statistics of the eigen-energies. If we randomly generate a matrix, which only have diagonal part as $\text{diag}\{\epsilon_1, \epsilon_2, ..., \epsilon_N\}$, i.e. all off-diagonal part is zero. We understand that these $\{\epsilon_i\}$'s are the eigen-energies without any correlations. We

can order these energies from smallest to largest and call them diag$\{E_1, E_2, ..., E_N\}$, and calculate the distribution of nearest neighbor level space, i.e. $P(s)$, where s picked from the list $\{E_2 - E_1, E_3 - E_2, ..., E_N - E_{N_1}\}$. One can find the Poisson distribution

$$P(s) = \exp(-s) \tag{2.5}$$

That means smaller s, more probable it will. There is no forbidden for two eigen-energies to sit on top of each other, as long as there is no off-diagonal term in Hamiltonian.

One the other hand, the RMT do have strong off-diagonal term in its Hamiltonian. As a consequence, the levels will repel with each other, so $P(s \to 0) \to 0$. In order to understand the physical origin of the level repulsion, let us consider a situation where occasionally two levels are very close to each other $\Delta E = |E_1 - E_2| \ll \Delta$, where Δ is the mean level separation. To sack the life from complexity, it is enough to consider only one block of the random matrix:

$$\begin{pmatrix} \epsilon_1 & V \\ V^* & \epsilon_2 \end{pmatrix} \tag{2.6}$$

where ϵ_1, ϵ_2 are two diagonal matrix element, which are two unperturbed orbital basis energy, while V is the interaction/hopping between them. Then the eigen-energies of the 2 matrix should be:

$$E_{1,2} = \frac{1}{2}\left(\epsilon_1 + \epsilon_2 \mp \sqrt{(\epsilon_1 - \epsilon_2)^2 + |V|^2}\right) \tag{2.7}$$

Then the nearest neighbor level space s, should follow the distribution

$$P(s) = \int d\epsilon_1 d\epsilon_2 \mathcal{D}V P(\epsilon_1) P(\epsilon_2) P(V)\, \delta\left(s - \sqrt{(\epsilon_1 - \epsilon_2)^2 + |V|^2}\right) \tag{2.8}$$

where the integration measure of V has two different scenario: (1) real value of V. the random matrix is orthogonal (GOE). label the case with $\beta = 1$ (2) complex value of V. the random matrix is unitary (GUE). label the case with $\beta = 2$. To be specific

$$\mathcal{D}V = \begin{cases} dV & H \text{ is real, GOE, } \beta = 1 \\ d\,\mathrm{Re}V\, d\,\mathrm{Im}V & H \text{ is complex, GUE, } \beta = 2 \end{cases} \tag{2.9}$$

Calculate Eq. (2.8) with this two choice of measure, one can immediately find the distribution of he nearest neighbor level space for GOE and GUE type:

$$P(s) \propto s^{\beta} \exp\left(-\#s^2\right) \tag{2.10}$$

where # is a positive number that is irrelevant in our discussion. We can see that $P(s \to 0) \to 0$ which is the indication of the level repulsion, and different scaling $P(s \to 0) \to s^{\beta}$ can identify different symmetry of the Hamiltonian. Though here we only use a 2×2 matrix to demonstrate these concept, truth be told that for larger system size, the result of Eq. (2.10) didn't change qualitatively (Wigner surmise), and the distribution is called Wigner-Dyson statistics [2].

Fig. 2.1.1 (a) shows the real life experiment of nuclear eigen-energy level statistics. It shows that the nuclear system can be well approximate by a random matrix Hamiltonian of GOE type. Fig. 2.1.1 (b) shows the $P(s)$ for different symmetry class, i.e. GOE, GUE and GSE. The GSE is the case where the interaction V's are Quaternions, or equally well as a 2×2 matrix as if it has internal spin degrees of freedom.

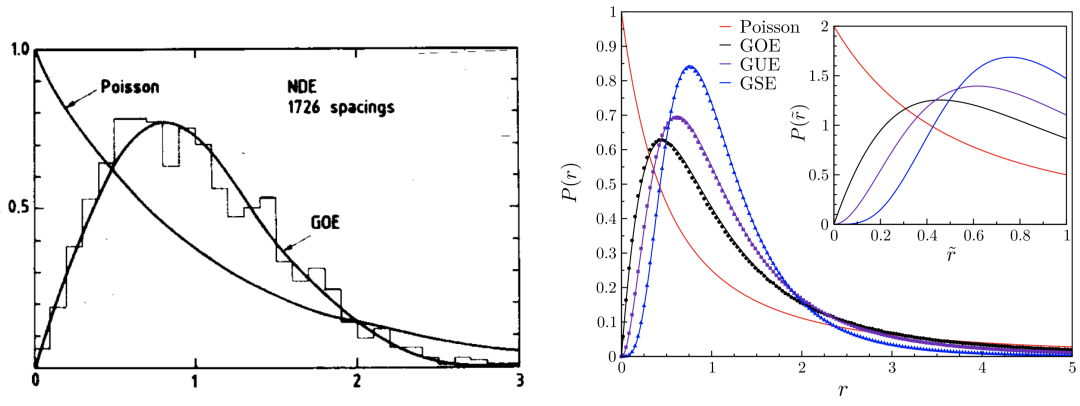

Figure 2.1: (a) Nearest neighbor spacing distribution for the "Nuclear Data Ensemble". Taken from Ref. [11]. (b) Distribution of the ratio of consecutive level spacings for Poisson and RMT ensembles. Taken from Ref. [12].

2.1.2 Field theory treatment and replica structure.

In this section, we will introduce one of the standard field theory treatments in the random matrix set-up, that is the replica field theory in RMT.

As we will see in this section, many important direct observable quantities (density of state, level statistics, etc.) would have close relationship to the correlation functions, which may be calculated by the machinery of the field theory. Now we would like to view the Hamiltonian H of the random matrix as "first quantized" version of quantum mechanics, one can define the 1-point correlation function (sometime refer as Green's function) as

$$G_1(E) = \frac{1}{N}\left\langle \mathrm{Tr}\frac{1}{E - H_{\mathrm{RMT}}}\right\rangle_{\mathrm{dis}} \tag{2.11}$$

where E refers to the single particle energy, and $\langle\cdots\rangle_{\mathrm{dis}} = \int \mathcal{D}H_{\mathrm{RMT}}\, P(H_{\mathrm{RMT}})(\cdots)$ means average over different realizations. One can rewrite the 1-point correlation function as

$$G_1(E) = \frac{1}{N}\frac{\partial}{\partial E}\langle \mathrm{Tr}\log(E - H_{\mathrm{RMT}})\rangle_{\mathrm{dis}} = \frac{1}{N}\frac{\partial}{\partial E}\langle \log Z\rangle_{\mathrm{dis}} \tag{2.12}$$

where one define the partition function $Z(E) = \det(E - H_{\mathrm{RMT}})$ for one realization of H. One need to average $\log Z$ or its derivative $\frac{\partial Z/\partial E}{Z}$ over disorder realizations to get meaningful quantities such as free-energy or density of states. But general speaking, it is very hard to average $\log Z$ or $\frac{\partial Z/\partial E}{Z}$. Physicists so far have invent three intelligent way to solve the problem: the supersymmetry approach, the Keldysh technique, and the replica trick. Here we will focus on the replica trick and this method is unreasonably useful in many disordered system especially in RMT and glass system.

Replica trick starts from the observation of the following identities:

$$\log Z = \lim_{n\to 0}\begin{cases}\frac{Z^n-1}{n}\\ \frac{d}{dn}Z^n\end{cases} \tag{2.13}$$

Here n should be a infinitesimal value. While in practice (i.e. for physicists) one choose n to be a integer value and do almost every calculation in integer n with an analytical expression. Until the special step of the calculation, set $n \to 0$. This is the reason why n is called replicas, because one evaluate the n replicas of Z times together as $Z \cdot Z \cdots Z$.

This procedure is far from rigorous but can produce accurate prediction compare to experiments. Now we use the second line of Eq. (2.13) to decompose the log and the Green's function becomes

$$G_1(E) = -\frac{2}{N}\frac{\partial}{\partial E}\lim_{n\to 0}\frac{\partial}{\partial n}\langle Z^{(n)}(E)\rangle_{\text{dis}} \tag{2.14}$$

where we defined the replicated partition function $Z^{(n)}(E) = \left(\frac{1}{E-H_{\text{RMT}}}\right)^{n/2}$. Now we decomposed the replicated partition function $Z^{(n)}$ by n bosonic fields ϕ_i^a using Gaussian integral, where $a = 1, 2, ..., n$. And since it is replicated version, the formula can be easily averaged over disordered distribution as shown following:

$$\langle Z^{(n)}(E)\rangle_{\text{dis}} = \left\langle \left(\frac{1}{E-H_{\text{RMT}}}\right)^{n/2} \right\rangle_{\text{dis}} \tag{2.15}$$

$$= \int \mathcal{D}\phi_i^a \left\langle \exp\left[-\frac{1}{2}\sum_{i,j}^{N}\sum_{a}^{n}\phi_i^a(E\delta_{ij} - H_{ij})\phi_j^a\right] \right\rangle_{\text{dis}} \tag{2.16}$$

$$= \int \mathcal{D}\phi_i^a \exp\left[-\frac{1}{2}\sum_{ij;a}\phi_i^a(E\delta_{ij})\phi_j^a - \frac{1}{4N}\sum_{ij;ab}\phi_i^a\phi_j^a\phi_i^b\phi_j^b\right] \tag{2.17}$$

Now we got a field theory with static bosonic field. One can define the static order parameter Q which is a $n \times n$ matrix as

$$Q_{ab} = \frac{1}{N}\sum_i \phi_i^a\phi_i^b \tag{2.18}$$

The physical meaning of the order parameter Q will be illustrated later. It will be the main character in the replica field theory, and its structure could be very fuzzy and indicating the existence of glass phase for certain scenario. Go back to the calculation and inserting the following fat identity into Eq. (2.17)

$$1 = \int \mathcal{D}Q\,\delta(NQ_{ab} - \sum_i \phi_i^a\phi_i^b) \tag{2.19}$$

$$= \int \mathcal{D}Q\,\mathcal{D}\mathcal{P}\exp\left[\frac{1}{2}\sum_{a,b}\mathcal{P}_{ab}(NQ_{ab} - \sum_i \phi_i^a\phi_i^b)\right], \tag{2.20}$$

We get the so-called σ-model of the RMT case:

$$\langle Z^{(n)}(E)\rangle = \int \mathcal{D}Q\,\mathcal{D}\mathcal{P}\exp\left[-\frac{N}{2}\mathrm{Tr}(E\,Q - \frac{1}{2}Q^2 - Q\mathcal{P} + \log\mathcal{P})\right], \tag{2.21}$$

where the matrix Q and its conjugate matrix $\mathcal{P}$ are the effective degrees of freedom of the theory. Notice that both Q and $\mathcal{P}$ are both bosonic matrix field, with a large N sitting at the action, one can calculate the quantities with saddle point approximation. So at the mean-field level, one notice that $\mathcal{P}$ is the inverse matrix of Q by solving the saddle point equation of the action, i.e. $Q_{ab} = (\mathcal{P}^{-1})_{ab}$. And one can define a replicated free energy density at mean-field level

$$f^{(n)}(Q) = \mathrm{Tr}(EQ - \frac{1}{2}Q^2 - \log Q), \tag{2.22}$$

where the relation between the partition function and free energy density is

$$\langle Z^{(n)}(E)\rangle = \int \mathcal{D}Q\exp\left[-\frac{N}{2}f^{(n)}(Q)\right] \tag{2.23}$$

Now we should take care the (replica) structure of the Q_{ab} and make some ansatz to proceed. In general, Q_{ab} could be a very complicated matrix even at mean-field level. We will see cases in the Sachdev-Ye-Kitaev model and Sherrington-Kirkpatrick model in the following sections. For now, we just take the knowledge, if we only want to calculate the shape of the density of states in RMT at large N, a *replica symmetric* ansatz of matrix Q should be enough. The term "replica symmetric", means every off-diagonal matrix element of the matrix Q are equivalent, no matter what replica a you comes from. With this assumption, we set the replica symmetric ansatz on the form of the saddle point solution:

$$Q_{ab} = q\delta_{ab} + p(1 - \delta_{ab}), \tag{2.24}$$

where q and p are the parametrization of the matrix Q on diagonal and off-diagonal

part. Now the saddle point equation is only the function of q and p:

$$0 = \frac{\partial f^{(n)}}{\partial q} = n\left[E - q - \frac{1}{q-p} + \frac{p}{(q-p)^2}\right] \tag{2.25}$$

$$0 = \frac{\partial f^{(n)}}{\partial p} = n\left[p - \frac{p}{(q-p)^2}\right] \tag{2.26}$$

with the saddle point solution denoted as q^* and p^*:

$$q^* = \frac{E - \sqrt{E^2-4}}{2}, \quad p^* = 0 \tag{2.27}$$

We evaluate the free energy density and the partition function in terms of q^*, and it is not surprising that the free energy is proportional to the number of replicas (at small n limit):

$$Z^{(n)}(E) = \exp\left[-\frac{N}{2} f^{(n)}(q^*)\right] \tag{2.28}$$

$$f^{(n)}(q^*) = n(Eq^* - q^{*2}/2 - \log q^*) + \mathcal{O}(n^2) \tag{2.29}$$

So we can find that the Green's function for the energy E state as following

$$G_1(E) = -\frac{2}{N}\frac{\partial}{\partial E}\lim_{n\to 0}\frac{\partial}{\partial n}\exp\left[-\frac{N}{2} f^{(n)}(q^*)\right] \tag{2.30}$$

$$= \frac{\partial}{\partial E}(Eq^* - q^{*2}/2 - \log q^*) \tag{2.31}$$

$$= \frac{E - \sqrt{E^2-4}}{2} \tag{2.32}$$

In a sudden, we find the density of states for the RMT at the mean-field level:

$$\rho(E) = \frac{1}{\pi}\mathrm{Im}\, G_1(E + i0^+) = \begin{cases} \frac{1}{2\pi}\sqrt{4-E^2} & \text{with } |E| < 2 \\ 0 & \text{with } |E| > 2 \end{cases} \tag{2.33}$$

This the Wigner semicircle law. In general, one can include the $1/N$ fluctuation around the saddle point, and this will generate oscillatory $1/N$ correction. A good reference for the derivation in fermionic replica formalism could be found in Ref. [13]

Actually the information of the level repulsion can be also formulated in this machinery, which is closely related to the 2-point correlation function:

$$G_2(E,E') = \frac{1}{N^2}\left\langle \mathrm{Tr}\frac{1}{E-H_{\mathrm{RMT}}}\mathrm{Tr}\frac{1}{E'-H_{\mathrm{RMT}}}\right\rangle_{\mathrm{dis}} \tag{2.34}$$

With help of the replica trick, one can calculate the 2-point correlation function in its replicated form

$$G_2(E,E') = \frac{1}{N^2}\frac{\partial^2}{\partial E\partial E'}\lim_{n,n'\to 0}\frac{\partial^2}{\partial n\partial n'}\langle Z^{(n)}(E)Z^{(n')}(E')\rangle_{\mathrm{dis}} \tag{2.35}$$

The procedure to calculate the $\langle Z^{(n)}(E)Z^{(n')}(E')\rangle_{\mathrm{dis}}$ is similar compare to previous one, since one can just double the n replicas to $n+n'$ with a vector energy $\hat{E}=(E,E')$. The detailed procedure is quite complicated, and one need to properly treat *replica symmetry breaking* solution to get the correct answer for the $G_2(E,E')$. Let me just discuss its final result and what's the consequence and skip the derivation.

Study the level statistics of nearest neighbor is equivalent to investigate the density-density correlation $R_2(\omega)=\Delta^2\langle\rho(E+\omega/2)\rho(E-\omega/2)\rangle_c$, where c refers to the connected part of the correlation function and $\Delta=\langle\rho(E)\rangle^{-1}$ is the level spacing at E. The information of $R_2(\omega)$ is actually fully encoded inside the 2-point correlation function $G_2(E+i0^+,E'-i0^+)$. Once one calculate the G_2 in its replica form, one can immediately get (for GUE case):

$$R_2(\omega) = \Delta\,\delta(\omega) - \left[\frac{\sin(\pi\omega/\Delta)}{\pi\omega/\Delta}\right]^2 \tag{2.36}$$

Now one calculate the number variance $\Sigma_2(\epsilon)$, namely the number of levels fluctuating inside a strip of width ϵ, i.e. $\Sigma_2(\epsilon)=\langle\mathcal{N}(\epsilon)^2\rangle_c$, where $\mathcal{N}(\epsilon)=\int_{E-\epsilon/2}^{E+\epsilon/2}d\epsilon'\rho(\epsilon')$ is the number of levels inside the ϵ strip for certain instance of realization. It relation to density-density correlation is

$$\Sigma_2(\epsilon) = \frac{1}{\Delta^2}\int_{E-\epsilon/2}^{E+\epsilon/2} d\epsilon_1 d\epsilon_2\, R_2(\epsilon_1-\epsilon_2) \tag{2.37}$$

$$\simeq \frac{1}{\pi^2}\log\left(\frac{2\pi\epsilon}{\Delta}\right) \tag{2.38}$$

This is a non-trivial statement, saying that the fluctuation inside strip of width ϵ, is

logarithmic growing. One can compare it with Poissonian level statistics, i.e. the case without level repulsion. Then $R_2^{\text{Poisson}}(\omega) = \Delta\,\delta(\omega)$, and $\Sigma_2^{\text{Poisson}}(\epsilon) \propto \epsilon$ is linearly growing. The fluctuation for Poisson type energy levels are much stronger than the random matrices. This lack of long range strong fluctuation in energy spectrum is called "spectral rigidity", and people can diagnose which universality class the systems stay in by evaluate the number variance.

2.2 Sachdev-Ye-Kitaev (SYK) model

In the introduction part of the chapter, we introduced a 4-point interacting fermionic system as a many-body version of RMT. The earliest version of the model was introduced by Sachdev and Ye in 1993 [5] in order to investigate the spin-glass. So the original version has the degrees of freedom spin rather than fermion. And Sachdev and Ye found that, though mimic the Hamiltonian of spin-glass (say Sherrington-Kirkpatrick with higher spin), the system itself may not have the glassy phase. In 2015, Kitaev [6] re-invent the model in language of Majorana fermions and discuss it mainly in the duality to the gravity theory.

To be concrete, let's use the Majorana (real-valued) fermions to be the underline degrees of freedom of the SYK model. There should not be too much quantitative difference from its spin-less complex version except complex fermions may have charge. The Sachdev-Ye-Kitaev (SYK) model consist of N Majorana fermions with quenched random interaction of four fermions at a time. The Hamiltonian of this quantum mechanical system is

$$H_{\text{SYK}} = \sum_{i<j<k<l}^{N} J_{ijkl}\chi_i\chi_j\chi_k\chi_l, \tag{2.39}$$

where χ_i is the Majorana fermion, J is the quenched random coupling with its mean $J_{ijkl} = 0$ and variation $J_{ijkl}^2 = 3!J^2/N^3$. Random couplings are usually to be chosen as Gaussian distribution for simplicity in analytical calculation.

Luckily enough, the SYK model is solvable in the large N limit at even strong coupling limit [14, 15, 16]. We will discuss the replica theory of it and solve it at mean-field level in Sec. 2.2.3. More detailed analysis of replica structure will leave at Chap. 3.

Another important feature of this model is that the model has the maximum chaos. A numerical examination demonstrate that the many-body spectrum of the model obeys the Wigner-Dyson statistics in a special way which depend on N [17, 18]. This is the most conventional way to identify a quantum chaotic system as illustrated in previous section. Translate the level statistics to its time domain (Fourier transform), one can found that, after a so called Thouless time, which scales as $\log N$, the system would be have same as a certain RMT type [19, 20]. Besides the mimic RMT behavior at extremely long time regime, people also find its chaotic nature at short time. The speed to scramble the system, characterized by the Lyapunov exponent in the out-of-time-correlator (OTOC)[21, 22], is maximized among all other materials at a fixing temperature. This universal speed bound at short time regime is quite amazing, and people are trying to understand the chaotic nature of quantum materials by connecting the knowledge of both (short/long) time regime.

In addition to the quantum chaos, SYK model also provide the playground for condensed matter physicists to investigate the so called strange metal[23, 24]. As will discuss in Sec. 2.2.3, the Green's function of the SYK do not have a simple pole, which may indicate that this system may not have a quasi-particle description. This also could be understand by using its many-body low energy spectrum, where the density of states is exponentially dense rather than power law dense as Fermi liquid system. The normal metal state build by SYK is very resemble to the normal state for the high-Tc superconductivity. In Chapter 4, we will demonstrate a possible non-BCS type superconductivity formulated by SYK paradigm.

2.2.1 Level statistics and symmetry

In this section, we will study the level statistics for the SYK model as we did for standard RMT. In order to do so, we would treat the Hamiltonian of SYK back to its "first quantized" version, by assigning the Majorana χ_i by its matrix representation following the Ref. [18].

Here we only consider the number of the Majoranas N to be even number. The reason for that is two Majoranas can combine to a real-life complex fermion and it is a easy set-up. Odd number version can be find in Ref. [17]. Let $\gamma_i^{(N)}$ to be the matrix representation of χ_i, where subscript (N) refers to how many Majoranas we have (i.e.

capture the dimension of the matrix). One can construct the γ matrices with higher dimension iteratively. When $N = 2$, one have

$$\gamma_1^{(2)} = \sigma_1, \quad \gamma_2^{(2)} = \sigma_2, \quad \gamma_3^{(2)} = \sigma_3, \tag{2.40}$$

where $\sigma_1, \sigma_2, \sigma_3$ are the Pauli matrices. Assume we have got $\gamma_i^{(d)}$, then we define

$$\begin{aligned} \gamma_i^{(d+2)} &= \sigma_1 \otimes \gamma_i^{(d)},\ i = 1, ..., d+1 \\ \gamma_{d+2}^{(d+2)} &= \sigma_2 \otimes \mathbb{1}_{2^{d/2}} \\ \gamma_{d+3}^{(d+2)} &= \sigma_3 \otimes \mathbb{1}_{2^{d/2}} \end{aligned} \tag{2.41}$$

In this representation, we will see that four gamma times together which is $\gamma_i\gamma_j\gamma_k\gamma_l$ will be block diagonalized.

Now define two anti-unitary operator

$$\begin{aligned} C_1 &= \gamma_1 \prod_{i=2}^{N} \gamma_{2i} K \\ C_2 &= \gamma_2 \prod_{i=2}^{N-1} \gamma_{2i+1} K \end{aligned} \tag{2.42}$$

There are symmetry relation for them

$$\begin{aligned} C_1 K \gamma_\mu + (-1)^{N/2} \gamma_\mu C_1 K = 0 \\ C_2 K \gamma_\mu - (-1)^{N/2} \gamma_\mu C_2 K = 0 \end{aligned} \tag{2.43}$$

This implies the fact that

$$[C_1 K, H_{\text{SYK}}] = [C_2 K, H_{\text{SYK}}] = 0 \tag{2.44}$$

Now we can define $\Gamma_5 = i^{-N/2} \prod_{i=1}^{N} \gamma_i$, so we know that the Hamiltonian is block diagonal. We can divide into following three different symmetry class [**?**].

- Orthogonal: if we have the situation $C_1 K C_2 K = \pm\Gamma_5$, then one can define project operator $P = \frac{1}{2}(1 + C_1 K C_2 K)$. Now $[C_1 K, P] = 0$. if $(C_1 K)^2 = 1$, it is possible to find an H-independent basis in which H becomes real, which means the matrix

is orthogonal.

- Symplectic: if we have the situation $C_1KC_2K = \pm\Gamma_5$ which is same as orthogonal case. But now $(C_1K)^2 = -1$, the Hamiltonian is self-dual quaternion up to an H independent unitary transformation, which means the matrix is symplectic.

- Unitary: if we have the situation $C_1KC_2K = \pm i\Gamma_5$, then one can define project operator $P = \frac{1}{2}(1 \pm iC_1KC_2K)$. Differ from orthogonal and symplectic case, now $[C_1K, P] \neq 0$, due to the existence of imaginary unit i. So there is no anti-unitary symmetry in the matrix.

All these difference coming from the term like $i^{N/2}$. Now we figure out when N has different values, the symmetry of the block part of the Hamiltonian are different. We understand that in "first quantized" version, the Hamiltonian of the SYK is a large sparse matrix, with different symmetry, either to be orthogonal, unitary or symplectic. What is interesting is that when one really diagonalize the sparse matrix, one found the eigen-energies have the same level repulsive feature as the standard RMT (a dense matrix). Depending on N, the system goes to the universality class of Gaussian orthogonal, unitary or symplectic ensemble. Here is the Table 2.1 of the universality class the SYK belongs to with different N and the Fig. 2.2 shows the Wigner-Dyson statistics for SYK.

N (mod 8)	0	1	2	3	4	5	6	7
level stat.	GOE	GOE	GUE	GSE	GSE	GSE	GUE	GOE

Table 2.1: The symmetries of the matrix depends on N. The level statistics can be described by GOE, GUE or GSE.

For completeness, let's talk about the many-body density of state of the SYK. For the traditional non-interacting particle system with random hopping amplitude, the density of state is given by semi-circle law. In SYK, the interaction is strong, which indicate the spectrum will deviate from the semi-circle law. The numeric result from exact diagonalization is shown in Fig. 2.3. Around the center of the many-body spectrum band, the distribution is similar to Gaussian, and the band-with is scale as $\sqrt{N}$. The low lying eneries (including the ground state) are scaling as N, as designed by the scaling of the random coupling $J_{ijkl} \sim 1/N^{3/2}$. The low energy density is exponentially dense as

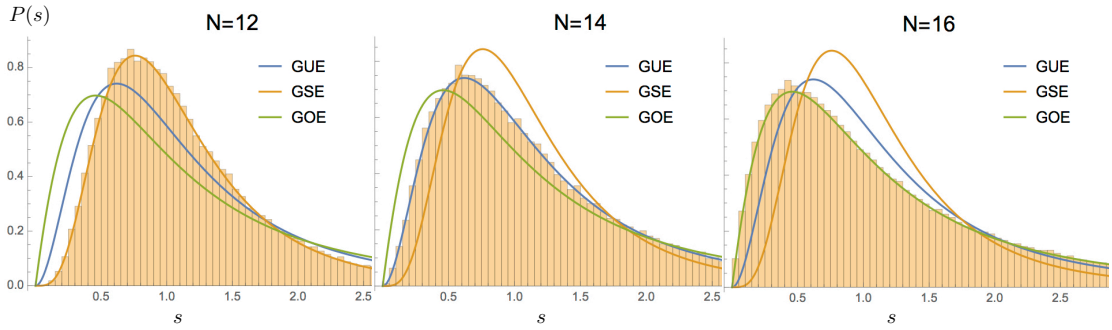

Figure 2.2: (a)(b)(c) refer to the level statistics under many realizations. $N = 12$: GSE; $N = 14$: GUE; $N = 16$: GOE.

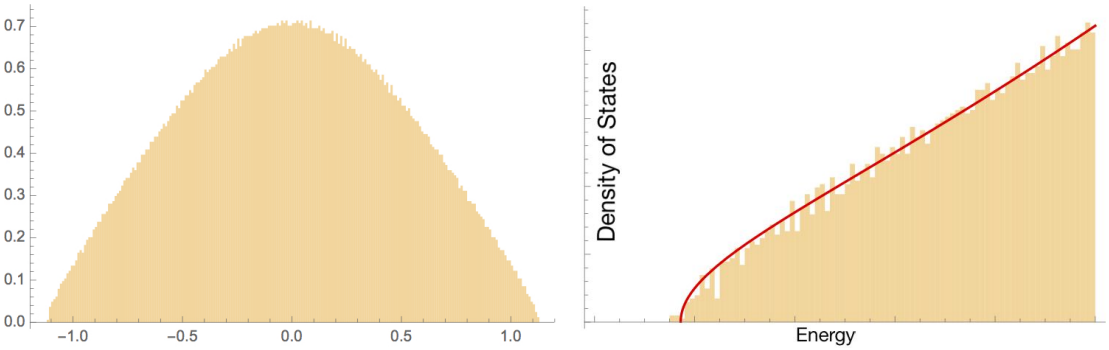

Figure 2.3: (a) The many-body density of states for $N = 30$ for one realization. (b) Zoom in density of states around the GS. The red curve is the fit by using the sinh curve as theory predicted.

$\rho(\epsilon) \propto \sinh[\#\sqrt{\epsilon}]$ which will disscused in detail in Sec. 2.2.3. This exponentially small level spacing gives us a first glance of the non-Fermi liquid states in SYK.

2.2.2 Field theory at mean-field level and the strange metal phase

In this section, we will discuss how the machinery of field theory works in SYK model. As standard approach in path-integral construction of a fermionic field theory, one introduce the dynamical Grassmann degrees of freedom $\chi_i(\tau)$ in the imaginary time domain and writing down free-energy $\log Z$ with these degrees of freedom. As a quenched disordered system similar to RMT, the replica trick is again a good method to replacing averaging

$\log Z$ by averaging Z^n in SYK models. So we introduce replica fields $\chi_i^a(\tau)$, where replica indices are $a = 1, 2, ..., n$, then the replica averaged partition function is

$$\langle Z^{(n)}(\beta)\rangle_J = \left\langle \int \mathcal{D}\chi \exp\left[-\sum_a^n \int_0^\beta d\tau \left(\frac{1}{2}\chi_i^a(\tau)\partial_\tau \chi_i^a(\tau) + H_{\rm SYK}^a(\tau)\right)\right]\right\rangle_J, \quad (2.45)$$

where $\langle\cdots\rangle_J$ refers to average over different disorder coupling configuration and $H_{\rm SYK}^a(\tau)$ is replicated Hamiltonian

$$H_{\rm SYK}^a(\tau) = \frac{1}{4!}\sum_{ijkl}^N J_{ijkl}\,\chi_i^a(\tau)\chi_j^a(\tau)\chi_k^a(\tau)\chi_l^a(\tau). \quad (2.46)$$

Now the disorder averaging can be easily finished by performing the Gaussian integral, since we choose the distribution of the disorder to be Gaussian distribution:

$$\left\langle \exp\left[-\sum_a^n \int_0^\beta d\tau H_{\rm SYK}^a(\tau)\right]\right\rangle_J \quad (2.47)$$

$$= \exp\left[\frac{J^2}{8N^3}\sum_{a,b}^n \int d\tau d\tau' \sum_{ijkl}^N \chi_i^a(\tau)\chi_j^a(\tau)\chi_k^a(\tau)\chi_l^a(\tau)\cdot \chi_i^b(\tau')\chi_j^b(\tau')\chi_k^b(\tau')\chi_l^b(\tau')\right] \quad (2.48)$$

$$= \exp\left[\frac{NJ^2}{8}\sum_{a,b}^n \int d\tau d\tau' \left[G_{\tau,\tau'}^{ab}\right]^4\right], \quad (2.49)$$

where we use the notation of $G_{\tau,\tau'}^{ab}$, which will later be recognized as 2-point correlation function, defined as

$$G_{\tau,\tau'}^{ab} = -\frac{1}{N}\sum_i^N \chi_i^a(\tau)\chi_i^b(\tau'), \quad (2.50)$$

In this stage, we will trying to write a theory for G, which hopefully be the good degrees of freedom to characterize the many-body phase (as Q did in RMT case). That means we better to integrate out the original microscopic d.o.f χ, by introducing the Lagrangian multipler Σ (which will be recognized as the self-energy later). Very similar

to introduce $\mathcal{P}$ which is the conjugate of Q in RMT case, we write down the fat identity

$$1 = \int \mathcal{D}G\,\delta\left(NG^{ab}_{\tau,\tau'} + \sum_i^N \chi_i^a(\tau)\chi_i^b(\tau')\right) \tag{2.51}$$

$$= \int \mathcal{D}G\mathcal{D}\Sigma \exp\left[\frac{1}{2}\sum_{a,b}^n \int d\tau d\tau' \Sigma^{ab}_{\tau,\tau'}\left(NG^{ab}_{\tau,\tau'} + \sum_i^N \chi_i^a(\tau)\chi_i^b(\tau')\right)\right] \tag{2.52}$$

and insert the unity identity back to Eq. (2.45). We will get

$$\langle Z^{(n)}(\beta)\rangle_J = \int \mathcal{D}\chi \exp\left[-\sum_{a,b}^n \int_0^\beta d\tau d\tau' \frac{1}{2}\chi_i^a(\tau)(\partial_\tau \delta^{ab} + \Sigma^{ab}_{\tau,\tau'})\chi_i^b(\tau)\right] \tag{2.53}$$

$$\times\, \mathcal{D}G\mathcal{D}\Sigma \exp\left[\sum_{a,b}^n \int_0^\beta d\tau d\tau' \frac{N}{2}\left(\frac{J^2}{4}\left[G^{ab}_{\tau,\tau'}\right]^4 + \Sigma^{ba}_{\tau',\tau} G^{ab}_{\tau,\tau'}\right)\right] \tag{2.54}$$

Now we can integrate out χ and this lead to the Pfaffian $|\partial_\tau \delta^{ab} + \Sigma^{ab}_{\tau,\tau'}|^{N/2}$ (i.e. half of the determinate since Majorana is half of the complex fermion), we now get the partition function $\langle Z^{(n)}\rangle = \int \mathcal{D}G\mathcal{D}\Sigma \exp\left[-S[G,\Sigma]\right]$, where the action

$$-S[G,\Sigma] = \frac{N}{2}\left[\mathrm{Tr}\log(\partial_\tau \delta^{ab} + \Sigma^{ab}_{\tau,\tau'}) + \left[G^{ab}_{\tau,\tau'}\right]^4 + \Sigma^{ba}_{\tau',\tau} G^{ab}_{\tau,\tau'}\right] \tag{2.55}$$

In the large N limit, the properties of the model are determined by the saddle point of the path integral over the effective fields $G^{ab}_{\tau\tau'}$ and $\Sigma^{ab}_{\tau\tau'}$. The corresponding saddle point equations read

$$\Sigma^{ba}_{\tau'\tau} = -J^2 (G^{ab}_{\tau\tau'})^3, \qquad \left(\hat{\mathbf{1}}\partial_\tau + \hat{\mathbf{\Sigma}}\right) \circ \hat{\mathbf{G}} = -\hat{\mathbf{1}}, \tag{2.56}$$

where $\hat{\mathbf{1}} = \delta_{ab}\delta(\tau - \tau')$ and $\hat{\mathbf{G}}$, $\hat{\mathbf{\Sigma}}$ is the shorthand for the matrix $G^{ab}_{\tau\tau'}$ and $\Sigma^{ab}_{\tau\tau'}$. Generically, the saddle point solution will both depend on replica structure as well as the imaginary time evolution in a mixing way. So Eq. (2.56) is impossible to solve analytically without certain approximation. People later figure out that, in the long time limit, one can neglect the time-derivative term in the second equation in (2.56), which makes the equations scale invariant and possible to solve analytically. In such a limit, one may look for a solution in a separable form, i.e. where matrix form in replica

and time spaces separates as:

$$\hat{\mathbf{G}} = g^{ab} G_{\tau,\tau'}, \qquad \hat{\mathbf{\Sigma}} = \sigma^{ab} \Sigma_{\tau,\tau'}. \tag{2.57}$$

Here $G_{\tau'\tau}$ and $\Sigma_{\tau'\tau}$ would be the time-dependent part which will be discussed in detail in this section, while time-independent *symmetric* $n \times n$ matrices $\mathbf{g}$ and $\boldsymbol{\sigma}$ would be our main topic in Chapter 3 and they satisfy the relation:

$$\sigma_{ab} = \big(g_{ab}\big)^3, \qquad \boldsymbol{\sigma} \cdot \mathbf{g} = \mathbf{1}. \tag{2.58}$$

Apparently, there is a simple replica-diagonal solution for time-independent part, i.e. $g_{ab} = \delta_{ab}$ and $\sigma_{ab} = \delta_{ab}$. This is the standard conjecture appears in Ref. [15, 16, 25, 26, 27], which looking for a replica-diagonal saddle point solution of the form $\hat{\mathbf{G}} = \delta_{ab} G_{\tau\tau'}$ and correspondingly $\hat{\mathbf{\Sigma}} = \delta_{ab} \Sigma_{\tau\tau'}$. Let us emphasize that, although we call such a choice *replica-diagonal*, fluctuations around the replica-diagonal saddle may and should include replica-off-diagonal components $\delta G^{ab}_{\tau\tau'}$. We discuss them in detail in Appendix ??.

Now let's focus on the time-dependent structure, and the solution in time-domain is power law decay at zero temperature as

$$G_{\tau,\tau'} = -\frac{J^{-1/2}}{(4\pi)^{1/4}} \frac{\mathrm{sgn}(\tau - \tau')}{|\tau - \tau'|^{1/2}}; \quad \Sigma_{\tau,\tau'} = -\frac{J^{1/2}}{(4\pi)^{3/4}} \frac{\mathrm{sgn}(\tau - \tau')}{|\tau - \tau'|^{3/2}} \tag{2.59}$$

Or in its energy representation

$$G_\epsilon = -i \frac{\sqrt{2\pi}}{(4\pi)^{1/4}} \frac{\mathrm{sgn}(\epsilon)}{|J\epsilon|^{1/2}}; \quad \Sigma_\epsilon = -i \frac{\sqrt{8\pi}}{(4\pi)^{3/4}} \mathrm{sgn}(\epsilon) |J\epsilon|^{1/2} \tag{2.60}$$

The proportionality $\Sigma \sim |J\epsilon|^{1/2}$ indeed justifies omission of $\partial_\tau \to -i\epsilon$ in the trace of the logarithm, as long as $\epsilon \ll J$. And proportionality $G \sim |J\epsilon|^{-1/2}$ tells use, the 1-point Green's function do not have a simple pole. This means even the system can be considered as metal (replica-diagonal solution means metal/fluid phase), it cannot become a Fermi-liquid. This is because, even one define the quasi-particle life time as the inverse proportional to the self-energy Σ, the decay from a quasi-particle to the continuum happens much before that the system can oscillate itself one cycle as a wave-package, i.e. $\tau_{\text{quasi-particle}} \propto 1/\Sigma_\omega \sim |J\omega|^{-1/2} \ll 1/\omega$. This contradict to the definition

of quasi-particle excitation which should preserve for long time. This is why people called SYK metal as strange metal (or non-Fermi liquid).

2.2.3 Fluctuation around mean-field and reparameterization soft mode

We now turn to the discussion of fluctuations around the above mean-field configuration. Driving away from the replica-diagonal configurations is one of the possible fluctuations that may modify the dynamical behavior of SYK. We will leave the details of considering this type of fluctuation in Chapter 3, and it turns out in the strange metal phase, the fluctuation due to replica structure is less important compare to the one which we present in this section.

This dominate fluctuation comes from the hidden symmetry of the saddle point equation, and was first recognized in Refs [6, 28]. They noticed that Eq. (2.59) is only one of the solutions of saddle point equations (2.56) in conformal limit, where conformal limit means $\partial_\tau \to 0$ and the system at this stage is conformally invariant. More precisely, any time-reparameterization transformation $\tau \to f(\tau)$ in diffeomorphism group $\mathrm{Diff}(\mathbb{R})$, will preserve the solution $G(\tau) \to G(f(\tau))$ be one of the saddle point solutions, i.e. the value of the action didn't change $S[G(\tau), \Sigma(\tau)] = S[G(f(\tau)), \Sigma(f(\tau))]$.

This reparameterization of time from τ to any other arbitrary monotonic differentiable function $f(\tau)$, is the root of the soft mode around the mean-field saddle, and indicating a spontaneously broken scenario. When calculate fluctuation around the saddle, one should carefully collect all possible $f(\tau)$ as new degrees of freedom for the fluctuating field theory. Apart from the reparameterization symmetry makes action invariant, the saddle point solution 2.56 itself is invariant under the transformation

$$f(\tau) = \frac{A\tau + B}{C\tau + D}, \quad AD - BC = 1 \tag{2.61}$$

which is $\mathrm{SL}(2, \mathbb{R})$ group. This indicate that any transformation function $f(\tau)$ one choose to be located inside $\mathrm{SL}(2, \mathbb{R})$ group, becomes a zero mode and will not cost action changing even you put temporal fluctuation ∂_τ back into action. So now we state that, the soft fluctuation around the replica-diagonal saddle point is dominate by reparameterization symmetry of time $f(\tau)$, which lives in the coset space $\mathrm{Diff}(\mathbb{R})/\mathrm{SL}(2, \mathbb{R})$, see Fig.2.4. In

other words, the field theory of soft mode for replica-diagonal part is

$$Z^{(n=1)}(\beta) = \int \mathcal{D}f \exp\left(-S[f(\tau)]\right), \quad f(\tau) \in \mathrm{Diff}(\mathbb{R})/\mathrm{SL}(2,\mathbb{R}). \tag{2.62}$$

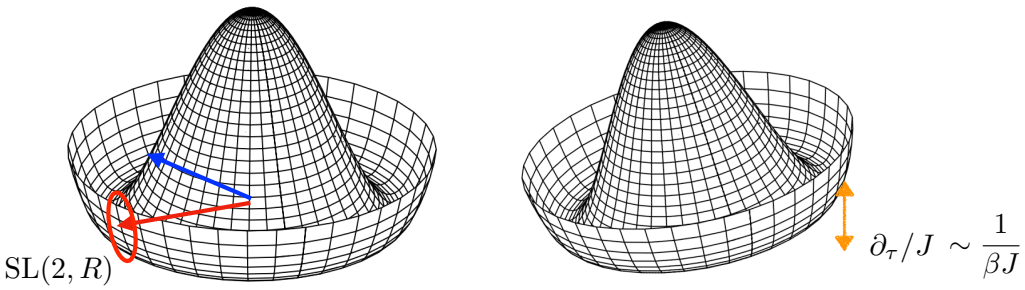

Figure 2.4: (a) Cartoon for the saddle point manifold in conformal limit. The red arrow pin point a saddle point solution Eq. with $f(\tau) = \tau$, any SL(2,R) transformation of this red arrow will not change it. Blue arrow refers to another choice of reparameterization function f. The have the degenerate saddle point action. Any movement from one solution (say red arrow) to another one (say blue arrow) will cost zero energy (Zero mode). (b) ∂_τ will lift the degenerate. So there is a true ground state and any deviation from it will cost ∂_τ, in long time limit, it is soft.

Now we need to construct the action for $f(\tau)$. We understand that the following G and Σ which reparameterized by $f(\tau)$

$$G_{\tau,\tau'} = -\frac{J^{-1/2}}{(4\pi)^{1/4}} \frac{f'(\tau)^{1/4} f'(\tau')^{1/4}}{|f(\tau) - f(\tau')|^{1/2}} \mathrm{sgn}(f(\tau) - f(\tau')) \tag{2.63}$$

$$\Sigma_{\tau,\tau'} = -\frac{J^{1/2}}{(4\pi)^{3/4}} \frac{f'(\tau)^{3/4} f'(\tau')^{3/4}}{|f(\tau) - f(\tau')|^{3/2}} \mathrm{sgn}(f(\tau) - f(\tau')) \tag{2.64}$$

should still be the saddle point solutions in the conformal limit. We need now deviate our theory from conformal limit $\partial_\tau = 0$ to the near conformal limit $\partial_\tau \ll J$ and to see

how $f(\tau)$ will lift the degeneracy. Measuring the lifting action around the saddle point

$$\begin{aligned} S[f] &= \mathrm{Tr}\left[\log(\partial_\tau + \Sigma) - \log \Sigma\right] \\ &= \frac{N}{4}\mathrm{Tr}(\partial_\tau G \partial_\tau G) + ... \\ &= -\frac{N}{32\sqrt{\pi}J}\iint d\tau d\tau' \frac{f'(\tau)^{3/2} f'(\tau')^{3/2}}{|f(\tau) - f(\tau')|^3} \end{aligned} \tag{2.65}$$

where we use the saddle relation $\Sigma^{-1} = -G$ (be careful it is a matrix identity in τ, τ' space) and only keep the second order of ∂_τ in the second line since only long time limit are concerned. The action $S[f]$ is non-local. In Ref. [16], the author argue that the integral kernel is $\omega^2 \log(J/|\omega|)$ in frequency domain with Fourier conjugation $f(\tau) = t \to \omega$. Since we can only care about the long time behavior where $\omega \ll J$, so this kernel in frequency domain will be mainly controlled by ω^2. One can define frequency scale that cut logarithm at $\omega = \Lambda$, that the kernel would be regularized as $\omega^2 \log(J/\Lambda)$. The cut-off Λ should be understood self-consistently, where $\Lambda < \omega < J$, the theory goes back to mean-field result i.e. $G_{\tau,\tau'} \sim 1/|\tau - \tau'|^{1/2}$, while $\omega < \Lambda$ we got a new $G_{\tau,\tau'}$ dependence that dominated by reparameterization fluctuations. Using the local kernel $\omega^2 \log(J/\Lambda)$ and transform back to time domain, one found the effective action for $f(\tau)$

$$S[f] = \frac{M}{2}\int d\tau \left(\frac{f''(\tau)}{f'(\tau)}\right)^2 \tag{2.66}$$

where the pre-factor $M \propto N/J \log(J/\Lambda)$. In Ref. [29], there is another way to get the effective action, by considering the symmetry of the action. We understand that under the $\mathrm{SL}(2,\mathbb{R})$ group transformation, the saddle solution of Eq. (2.56) is invariant, which means the effective action for the fluctuation coming from $f(\tau) \in \mathrm{SL}(2,\mathbb{R})$ should be vanished, i.e. $S[f(\tau) \in \mathrm{SL}(2,\mathbb{R})] = 0$. The lowest order in derivatives that vanishes for the global $\mathrm{SL}(2,\mathbb{R})$ transformation is nothing but the Schwarzian action

$$S[f] = -M\int d\tau\, \mathrm{Sch}(f,\tau) \tag{2.67}$$

where $\mathrm{Sch}(f,\tau)$ is called Schwarzian derivative and defined as

$$\mathrm{Sch}(f,\tau) = \frac{f'''}{f'} - \frac{3}{2}\left(\frac{f''}{f'}\right)^2 \tag{2.68}$$

One can check that Eq.(2.66) are equivalent to Eq.(2.67) up to a boundary term.

Now with the effective theory of fluctuation field $f(\tau)$, we are in the stage to calculate physical quantities that one may care about in experiment (e.g. density of states, 2-point correlation function). And the same time, don't forget we left the energy cut-off of the theory Λ to be determined. Without tolerant with cumbersome calculation, we refer the details of calculation to the Ref. [16, 30] and just state the idea and results behind it. By introduce an exponential representation of reparametrization

$$f(\tau) = \int^{\tau} \exp[\phi(\tau)] d\tau, \tag{2.69}$$

the author find that the Schwarzian theory can be mapped to Liouville Quantum Mechanics, and the Schwarzian action becomes

$$S[\phi] = \frac{M}{2} \int d\tau [\phi'(\tau)]^2. \tag{2.70}$$

In the Chapter 3, we will use the same technique to deal with the Schwarzian theory with non-trivial replica structure. One can calculate the "measurable" replica-diagonal 2-point correlation function

$$G(\tau, \tau') = -\frac{1}{N} \sum_{i}^{N} \langle \chi_i(\tau) \chi_i(\tau') \rangle \tag{2.71}$$

$$\tag{2.72}$$

One need be careful its difference from the replicated version Eq. (2.50), which is not a measurable quantities unless your are in the glass phase. In glassy system (e.g. Sherrington-Kirkpatrick model which discussed in the last chapter), one can have different local minimum energy states which are metastable compare to the true ground state of the system. One now can assign replica indices on different local minimum states and measure the replica off-diagonal correlation functions. We will discuss the replica off-diagonal correlation functions could probability be detected by non-local correlation functions which demonstrate in Chapter 3.

Now go back to the calculation of replica-diagonal in Eq. (2.71)

$$G(\tau,\tau') \tag{2.73}$$

$$=\frac{1}{J^{1/2}(4\pi)^{1/4}}\int \mathcal{D}\phi \frac{e^{\frac{\phi(\tau)}{4}}e^{\frac{\phi(\tau')}{4}}}{|e^{\phi(\tau)}-e^{\phi(\tau')}|^{1/2}}\exp\left[-\frac{M}{2}\int d\tau[\phi'(\tau)]^2\right] \tag{2.74}$$

$$=\frac{1}{(\pi J)^{1/2}(4\pi)^{1/4}}\int_0^\infty \frac{d\alpha}{\sqrt{\alpha}}\int \mathcal{D}\phi\, e^{\frac{\phi(\tau)}{4}}e^{\frac{\phi(\tau')}{4}}\exp\left[-\int_{\tau'}^{\tau}d\tau\left(\frac{M}{2}[\phi'(\tau)]^2+\alpha e^{\phi(\tau)}\right)\right] \tag{2.75}$$

$$=\int_0^\infty \frac{d\alpha}{\sqrt{\alpha}}\left\langle e^{\frac{\phi(\tau)}{4}}e^{\frac{\phi(\tau')}{4}}\right\rangle^{(\alpha)}_{\text{Q-Liouville}} \tag{2.76}$$

where the Liouville action

$$S^{(\alpha)}_{\text{Q-Liouville}}[\phi]=\int_{\tau'}^{\tau}d\tau\left(\frac{M}{2}[\phi'(\tau)]^2+\alpha e^{\phi(\tau)}\right) \tag{2.77}$$

This means in order to calculate $\langle\chi\chi\rangle_{\text{Schwarzian}}$, we need to calculate $\langle e^{\frac{\phi}{4}}e^{\frac{\phi}{4}}\rangle_{\text{Q-Liouville}}$, which is nothing but solving quantum mechanical system with a mass M particle driving by potential αe^{ϕ} at position ϕ. Skip the details of solving the Quantum Liouville model, one can arrive at the result for the replica-diagonal 2-point correlation function

$$G(\tau,0)\propto\begin{cases}\frac{1}{|\tau|^{1/2}} & \text{for } |\tau|\ll M\\ \frac{M}{|\tau|^{3/2}} & \text{for } |\tau|\gg M\end{cases} \tag{2.78}$$

Now we understand that the cut-off in frequency space $\omega\simeq\Lambda$ is nothing but the inverse of the separation of time scale $\tau\simeq M$, i.e. $\Lambda\simeq 1/M$. Recall that the $M\propto N/J\log(J/\Lambda)$ and solve it self-consistently, we can have

$$M\approx\frac{N\log N}{J},\quad \Lambda\approx\frac{J}{N\log N} \tag{2.79}$$

The numerical data to verify the statement of Eq. (2.78) is shown in Fig. 2.2.3 for $N=32$ case. Its time-decay exhibits two qualitatively different regimes. At short times ($1\lesssim\tau\lesssim 10$ in units of $1/J$) the correlation function decays as $\tau^{-1/2}$. This behavior corresponds to a saddle point solution, Eq. (3.1). At longer times, for $10\lesssim\tau\lesssim 100$,

the time decay changes to $\tau^{-3/2}$. Such a behavior signals the dominant effect of soft reparametrization fluctuations around the saddle point.

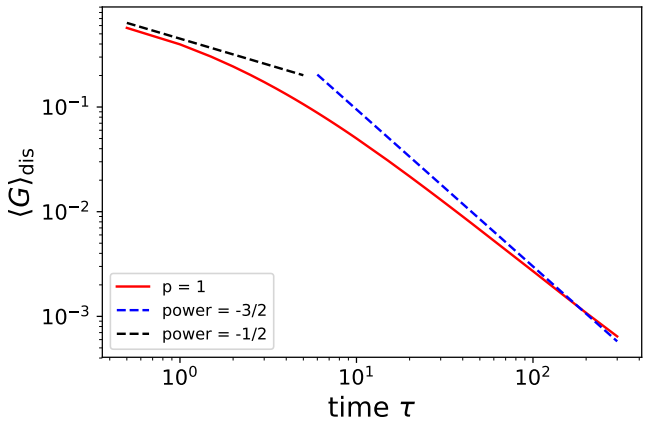

Figure 2.5: (a) Numerical results for $\langle G(\tau, 0)\rangle_{\text{dis}}$ at $N = 32$ averaged over 30 realizations (Log-Log plot). At short time, it decays with power $-1/2$, while at long time it decays with power $-3/2$.

In addition to the correlation function, the many-body density of states can be also evaluated under this construction. By calculate the partition function $Z(\beta)$ in finite temperature (unfortunately the finite temperature technique is not discussed in this thesis, one can check Ref. [30]), they can inverse Laplace transform the relation $Z(\beta) = \int d\epsilon\, \rho(\epsilon) \exp(-\beta\epsilon)$ and obtain $\rho(\epsilon)$. At low energy, the density of state $\rho(\epsilon) \propto \sinh[2\pi\sqrt{2M\epsilon}]$[30, 31]. The comparison between the theoretical prediction and the numeric result would be shown in Fig. 2.3(b).

Chapter 3

Replica structure in SYK

As we discussed in Chapter 2, SYK model are represented by interacting Majorana fermions with quenched random matrix elements and naturally admits a description in terms of a replica field theory [32]. The structure of this theory in the replica space has important bearings on all aspects and applications of the SYK-like models. In particular, an existence and properties of a glass phase is most naturally discussed in terms of the replica symmetry breaking (RSB). Indeed, RSB was first introduced by Parisi [33, 34] to describe glass transition in the Sherrington-Kirkpatrick model [4]. The existence of the glass phase in SYK and similar models is a subject of intense discussions since the very introduction of the model [5, 35, 36, 37, 38]. A recent discussion, Ref. [39], came on the side of the absence of the glass phase.

Non-trivial replica structures, associated with some form of RSB, were discussed in many other fields of the statistical physics. Most relevant to the present context are replica studies of the random matrix theory. The latter may be classified as SYK_2 model as opposed to SYK_4. The corresponding replica field theory of SYK_2 is known as non-linear sigma model. Its long time (i.e. small energy) correlation functions were understood in terms of the broken replica symmetry [13, 40, 41, 42, 43]. To some extent these studies mirror Altshuler-Andreev description [44] in terms of the broken supersymmetry. The important point is that RSB is only noticeable on the time scale associated with the inverse level spacing (Heisenberg time) and practically does not have consequences at shorter times.

It was recently suggested [45] that non-trivial replica structure (i.e. replica non-diagonal saddle point) may be responsible for the behavior of the structure factor of SYK_4 model at a time scale parametrically shorter than the Heisenberg time. Another recent study [46] discusses thermodynamic relevance of the replica off-diagonal saddle points in SYK model.

The goal of this chapter is to investigate possible signatures of RSB and replica off-diagonal saddles on the behavior of correlation functions at moderately long times. By those we understand time scales longer than $\tau > N/J$, yet shorter than the Heisenberg time (i.e. inverse many-body level spacing). The correlation functions considered in this chapter are motivated by mesoscopic physics [47], where one is interested in quench disorder averages of higher moments of certain quantum observables. (One may also look for an entire probability distribution function of a given observable over quench disorder realizations.) Here we show that the corresponding correlation functions exhibit qualitatively distinct behavior being calculated on replica diagonal vs. replica off-diagonal saddle points. The difference stems from the ways the corresponding saddle points break the reparameterization symmetry [6, 14] of the model. The distinct patterns of the symmetry breaking are reflected in the structure of the low-energy (Schwarzian) action. We found that in case of replica-diagonal saddle points the latter consists of n (number of replica) independent Schwarzians. However, for a generic replica off-diagonal saddle point there is only one Schwarzian degree of freedom, while the remaining $n-1$ acquire a stiffer action. These observations translate into a different behavior of correlation functions at moderately long times.

We then perform a detailed comparison of our analytical expectations with numerical simulations of $N \leq 32$ SYK_4 model. Our simulations use exact diagonalization and exact matrix elements to evaluate corresponding "mesoscopic" correlation functions. We consider p-th moments, $p = 1, \ldots, 5$, of both site-local and site-non-local two-point correlation functions. The comparison shows no evidence for contributions from replica off-diagonal saddles. On the contrary, all the data may be quantitatively accounted for by the theory based on replica diagonal saddle point along with reparameterization fluctuations and massive Gaussian fluctuations around it. The massive fluctuations, which include replica off-diagonal components, must be retained to account for small site non-local correlations.

In Sec. 3.1, we discuss soft reparameterization modes and how their action is different between replica diagonal and replica off-diagonal saddle point configurations. In Sec. 3.2.1, we discuss consequences of these differences for the long-time behavior of mesoscopic correlation functions. We put these differences to numerical test in Sec. 3.2.2. In Sec. 3.2.3, the similar program is implemented to a different family of mesoscopic correlation functions - those with site non-local correlations.

3.1 More on replica structure and reparameterization fluctuations

In Chapter 2, we demonstrate how the SYK model represented by interacting Majorana fermions can be fomulated in replica field theory. At the conformal limit, we have saddle point solution which can be separated in diagonal time-dependent part and off-diagonal time-independent as following (i.e. Eq. (2.57) in previous chapter):

$$\hat{\mathbf{G}} = -\mathbf{g}\,\frac{J^{-1/2}}{(4\pi)^{1/4}}\frac{\mathrm{sgn}(\tau-\tau')}{|\tau-\tau'|^{1/2}}, \qquad \hat{\mathbf{\Sigma}} = -\boldsymbol{\sigma}\,\frac{J^{1/2}}{(4\pi)^{3/4}}\frac{\mathrm{sgn}(\tau-\tau')}{|\tau-\tau'|^{3/2}}, \tag{3.1}$$

where replica matrices $\mathbf{g}$ and $\boldsymbol{\sigma}$ satisfy (i.e. Eq. (2.58) in previous chapter):

$$\sigma_{ab} = \left(g_{ab}\right)^3, \qquad \boldsymbol{\sigma}\cdot\mathbf{g} = \mathbf{1}. \tag{3.2}$$

The $n \times n$, where n is number of replica, matrix equations (3.2) admit a wealth of both diagonal and off-diagonal solutions. It is thus necessary to spell out selection criteria on which of these solutions should be taken into account and why. The most natural of such criteria seems to be a requirement of having a minimal action (i.e. free energy). In particular one may ask if the widely accepted choice $\mathbf{g} = \boldsymbol{\sigma} = \delta_{ab}$ indeed has the smallest action. In Appendix A.1 we show that one can find a discrete set of solutions of the form

$$g_{ab} = \tilde{g}\delta_{ab} + g(1-\delta_{ab}), \tag{3.3}$$

where $\tilde{g}$ and g are n-dependent complex numbers. Moreover, in the $n \to 0$ limit the (real part of) corresponding action is *smaller* than that on the diagonal (i.e. $\tilde{g} = 1$, $g = 0$) solution. Similar conclusions were recently reached in Ref. [46]. The question

thus arises whether these (or others) replica-off-diagonal solutions are indeed relevant for the physics of the model.

This question is farther complicated by the fact that besides the saddle point action one needs to evaluate fluctuation determinants and perform summation over the set replica-off-diagonal saddles for any desired observable. Since we do not know how to perform this program in general, we seek for generic signatures, which help to distinguish between diagonal and off-diagonal solutions. Below we argue that long time behavior of certain correlation functions serves as a sensitive test for the presence of the off-diagonal components. To argue why this is indeed the case one needs to consider a structure of soft-mode fluctuations around diagonal and off-diagonal solutions. For the conformal solutions of the form Eq. (3.1) such soft modes are given by reparameterization fluctuations [6, 15, 16, 25, 26, 27].

In the conformal limit (i.e. neglecting ∂_τ term) the action (2.55) and the saddle point equations Eqs. (2.56), are invariant under the time reparametrization transformations

$$G^{ab}(\tau_1,\tau_2) \to [f_a'(\tau_1)]^{1/4} G^{ab}(f_a(\tau_1), f_b(\tau_2))[f_b'(\tau_2)]^{1/4}, \tag{3.4}$$

$$\Sigma^{ab}(\tau_1,\tau_2) \to [f_a'(\tau_1)]^{3/4} \Sigma^{ab}(f_a(\tau_1), f_b(\tau_2))[f_b'(\tau_2)]^{3/4}, \tag{3.5}$$

where $G^{ab}(\tau_1,\tau_2)$ and $\Sigma^{ab}(\tau_1,\tau_2)$ are conformal solutions (3.1). Here $f_a(\tau)$ with $a = 1,\dots n$ is a *replica-specific* reparametrization transformation. This defines the symmetry group $\mathcal{G}$ of the action (2.55) in the infra-red limit, $\mathcal{G} = \otimes_{a=1}^{n} \mathrm{Diff}(\mathbb{R})$, where $\mathrm{Diff}(\mathbb{R})$ denotes the diffeomorphism group of time axis. The product over replicas reflects the fact that reparametrization transformations can be chosen independently in different replicas, i.e. $f_a(\tau) \neq f_b(\tau)$. The symmetry under time-reparametrizations is a crucial property, that relates the SYK model to the AdS_2 gravity theories [48, 28, 49, 25, 50, 51, 24, 52, 53, 54]. This time-reparametrization symmetry is however spontaneously broken by the saddle point solutions (3.1) down to the subgroup $H = \mathrm{SL}(2,\mathbb{R}) \subset \mathcal{G}$ resulting in the appearance of a soft modes, which span the coset $\mathcal{G}/H$. Specifically, the group H is formed by all Möbius maps of the form $h(\tau) = (A\tau + B)/(C\tau + D)$ with $AD - BC = 1$.

Here, the major difference shows up between the diagonal and off-diagonal saddle point solutions. For the diagonal case the subgroup is $\widetilde{H} = \otimes_{a=1}^{n} \mathrm{SL}(2,\mathbb{R})$. Indeed, for

a diagonal saddle point the independent Möbius maps $h_a(\tau) = (A_a\tau + B_a)/(C_a\tau + D_a)$ may be taken for each replica, leaving the diagonal solution (3.1) invariant. The diagonal soft mode coset is thus $\mathcal{G}/\widetilde{H} = \big[\otimes_{a=1}^{n} \mathrm{Diff}(\mathbb{R})\big]/\big[\otimes_{a=1}^{n} \mathrm{SL}(2,\mathbb{R})\big]$.

This should be contrasted with the off-diagonal case, where the subgroup is $H = \mathrm{SL}(2,\mathbb{R})$ - the *same* for all replicas. Indeed, performing different Möbius transformations in different replicas does *not* leave (3.1) invariant, if $\mathbf{g}$ and $\boldsymbol{\sigma}$ have off-diagonal components. Therefore the coset is different: $\mathcal{G}/H = \big[\otimes_{a=1}^{n} \mathrm{Diff}(\mathbb{R})\big]/\mathrm{SL}(2,\mathbb{R})$ (similar structure of the coset space was mentioned recently in Ref. [55] in context of two-boundary Jackiw-Teitelboim Gravity). The different structure of the coset is reflected in the soft mode action.

The latter action originates from the explicit breaking of the reparametrization symmetry by the time derivative term $\delta_{ab}\partial_\tau$. In the diagonal case, where the coset is the product of n independent $\mathrm{Diff}(\mathbb{R})/\mathrm{SL}(2,\mathbb{R})$ components, the corresponding action is the sum of n Schwarzian derivatives [14]

$$S_{\mathrm{diag}} = -M \sum_{a=1}^{n} \int d\tau\, \mathrm{Sch}(f_a, \tau) \tag{3.6}$$

where $M \sim N \log N$ is the mass of the soft fluctuations [16].

In the off-diagonal case the subgroup H consists of a single $\mathrm{SL}(2,\mathbb{R})$, suggesting that only a single degree of freedom is governed by the Schwarzian action. Indeed, the explicit calculation, outlined in details in Appendix A.4, shows that the off-diagonal matrix elements $g_{ab} \neq 0$ in the saddle point solution generate additional terms in the action for reparametrization fluctuations. These terms overpower $n-1$ Schwarzian derivatives in the long-time limit.

Let us use the exponential representation of reparametrizations [16]

$$f_a(\tau) = \int^{\tau} \exp[\phi_a(\tau)] d\tau, \tag{3.7}$$

which has an advantage that the corresponding invariant integration measure is flat in ϕ_a variables. In this representation, the additional action can be cast in the form of an

effective potential:

$$S_2[\phi] = -\frac{NJ}{2^7\sqrt{2\pi}} \sum_{a\neq b} g_{ab}^2 \int\limits_{\mathcal{C}} \frac{d\tau}{\cosh^{3/2}\left[\phi_a(\tau_1(\tau)) - \phi_b(\tau_2(\tau))\right]}. \tag{3.8}$$

Here the integration goes along the line $\mathcal{C} = (\tau_1(\tau), \tau_2(\tau))$ drawn in $\mathbb{R}^2$ space of two times, at which two reparametrizations take equal values, $f_a(\tau_1(\tau)) = f_b(\tau_2(\tau))$. When expanded in small deviations $\phi_a - \phi_b$, each term in the action Eq. (3.8) acquires the form of a "mass" term

$$S_2[\phi] \simeq \frac{5NJ}{2^{10}\sqrt{2\pi}} \sum_{a\neq b} g_{ab}^2 \int (\phi_a - \phi_b)^2 d\tau, \tag{3.9}$$

where in the last expression the integral already goes along the straight line. It is clear that this term is minimized when reparametrizations in all replicas are identical and penalizes deviations from such configuration. To formalize this observation we introduce new variables as $\phi_a = \Phi + \varphi_a$, where $\sum_{a=1}^n \varphi_a \equiv 0$ and therefore $\Phi = \frac{1}{n}\sum_{a=1}^n \phi_a$. Then the soft mode action for, e.g., off-diagonal ansatz (3.3) takes the form

$$S_{\text{off}-\text{diag}} = -\tilde{g}^2 M \int d\tau\, \text{Sch}(\Phi, \tau) + 2ng^2 \frac{5NJ}{2^{10}\sqrt{2\pi}} \sum_{a=1}^n \int d\tau\, \varphi_a^2, \tag{3.10}$$

where we have used that $\sum_{a\neq b}(\phi_a - \phi_b)^2 = \sum_{ab}(\varphi_a - \varphi_b)^2 = 2n\sum_a \varphi_a^2$, since $\sum_a \varphi_a = 0$. In the long time limit the last term here suppresses fluctuations of $n-1$ degrees of freedom φ_a, leaving the single degree of freedom Φ, to be governed by the Schwarzian action. This effectively locks reparameterization degrees of freedom in different replicas to

$$f_a(\tau) = f(\tau) = \int^\tau \exp[\Phi(\tau)] d\tau. \tag{3.11}$$

Finally, let us mention that the structure of action Eq. (3.10) is consistent with the coset space $\mathcal{G}/H$ of the replica off-diagonal SYK action. For the infinitesimal reparametrizations $f_a(\tau) = \tau + \epsilon_a(\tau)$ the phases $\phi_a(\tau) \simeq \epsilon_a'(\tau)$. We see that the action Eq. (3.8), if written in terms of $\epsilon_a(\tau)$, remains *massless* vis-a-vis n degrees of freedom. However only single degree of freedom is "super soft": $\text{Sch}(\Phi, \tau) \propto (\mathcal{E}'')^2$ (where $\mathcal{E} = \sum_{a=1}^n \epsilon_a$), while remaining $n-1$ acquire stiffer action $\propto (\epsilon_a')^2$. This is *not* the case in

the diagonal case where all n modes are super soft $\propto (\epsilon_a'')^2$.

The locking of reparameterization modes in different replicas, Eq. (3.11), for off-diagonal saddle points has important consequences for long time behavior of the correlation functions, which we explore in the next section.

3.2 Correlation functions

3.2.1 Site-local correlation functions

It is well known, that the reparameterization fluctuations modify the long-time decay of correlation functions. The simplest example is the two-point site-local function:

$$G(\tau,0)=\frac{1}{N}\sum_{i}^{N}\langle\chi_i(\tau)\chi_i(0)\rangle. \tag{3.12}$$

While at short times, $1/J<|\tau|<N/J$, the decay is governed by the conformal mean field behavior $G\sim|\tau|^{-1/2}$, Eq. (3.1), its long-time behavior, $|\tau|>N/J$, is very different: $G\sim|\tau|^{-3/2}$ due to the effect of the reparametrization fluctuations [16]. Moreover, the $2p$-point correlation functions ($p<N$) of the form

$$G_{2p}(\tau,0)=\frac{1}{N^p}\sum_{i_1\ldots i_p}^{N}\langle\chi_{i_1}(\tau)\ldots\chi_{i_p}(\tau)\chi_{i_1}(0)\ldots\chi_{i_p}(0)\rangle. \tag{3.13}$$

at long time decay with the *same* universal exponent $-3/2$, i.e. $G_{2p}\sim|\tau|^{-3/2}$ [16]. The short time behavior is, of course, p-dependent: $G_{2p}\sim|\tau|^{-p/2}$. It is important to notice that the angular brackets in Eqs. (3.12) and (3.13) imply both quantum mechanical ground-state expectation value (hereafter we restrict ourselves to zero temperature) along with the averaging over disorder realizations.

We now introduce different objects, inspired by mesoscopic fluctuations physics [47]

$$\langle[G(\tau,0)]^p\rangle_{\rm dis}=\left\langle\left[N^{-1}\sum_{i=1}^{N}\langle GS|\chi_i(\tau)\chi_i(0)|GS\rangle\right]^p\right\rangle_{\rm dis}, \tag{3.14}$$

where $|GS\rangle$ stays for a disorder specific ground-state of the SYK_4 model (the same for all p expectation values), while $\langle\ldots\rangle_{\rm dis}$ denotes averaging over realizations of random

matrix elements J_{ijkl}. In the replica formalism, the correlation function Eq. (3.14) can be written as

$$\langle [G(\tau,0)]^p \rangle_{\rm dis} = \left(\frac{1}{N}\right)^p \sum_{i_1 \dots i_p=1}^{N} \left\langle \chi_{i_1}^{a_1}(\tau) \dots \chi_{i_p}^{a_p}(\tau) \chi_{i_1}^{a_1}(0) \dots \chi_{i_p}^{a_p}(0) \right\rangle , \tag{3.15}$$

where angular brackets denote averaging with respect to the replicated action and all the replicas $a_1, ..., a_p$ are different. The leading contribution to the correlation function Eq. (3.15) is given by the product of replica-diagonal contractions. Indeed, each contraction of fermions with different replicas enforces the equality of the sites of the contracted fermions, for example $\langle \chi_{i_1}^{a_1} \chi_{i_2}^{a_2} \rangle \propto g_{a_1 a_2} \delta_{i_1 i_2}$ thus eliminating one summation over sites. Such contribution is therefore suppressed by the factor $1/N$ (in case of the replica diagonal saddle point, $g_{a_1 a_2} = 0$ and such contractions originates from Gaussian fluctuations of $\delta G_{a_1 a_2}$ and $\delta \Sigma_{a_1 a_2}$, bringing additional factors of $1/N$). The leading contribution from the product of replica diagonal contractions has furthermore to be averaged over the reparametrization fluctuations

$$\langle [G(\tau,0)]^p \rangle_{\rm dis} \approx \int \prod_{a=1} [D\phi_a(\tau)] \prod_{a=1}^{p} G^{aa}(f_a(\tau), f_a(0))\, e^{-S[\phi]}, \tag{3.16}$$

where $G^{aa}(f_a(\tau), f_a(0))$ is given by Eqs. (3.4), (3.7).

In the case of the off-diagonal saddle point, the reparametrizations are locked, Eq. (3.11), and therefore the integration in Eq. (3.16) runs over the single field Φ. This makes Eqs. (3.13) and (3.15) essentially equivalent in the long time regime. One thus expects to find $\langle [G(\tau,0)]^p \rangle_{\rm dis}$
$\sim \tau^{-3/2}$ independent on p. On the other hand, in the replica diagonal case the reparametrizations are not locked, the integration in Eq. (3.16) runs over p independent field and one expects $\langle [G(\tau,0)]^p \rangle_{\rm dis} \sim \tau^{-3p/2}$ again in the long time regime. For short times reparameterizations are not relevant and one expects mean-field $\langle [G(\tau,0)]^p \rangle_{\rm dis} \sim$

$\tau^{-p/2}$ irrespective of the replica structure. To summarize:

$$(\langle [G(\tau,0)]^p \rangle_{\rm dis})^{1/p} \sim \begin{cases} \tau^{-1/2}, & \tau < N/J \\ \tau^{-3/2}, & \tau > N/J \qquad \text{replica diagonal} \\ \tau^{-3/2p}, & \tau > N/J \qquad \text{replica off-diagonal.} \end{cases} \tag{3.17}$$

This can be checked numerically to distinguish between diagonal and off-diagonal scenario.

3.2.2 Numerical results for site-local correlation functions

The basic quantity for numerical calculations is the two-time ground-state expectation value:

$$G_{ii}(\tau) = \langle GS|\chi_i(\tau)\chi_i(0)|GS\rangle = \sum_n \langle GS|\chi_i|n\rangle\langle n|\chi_i|GS\rangle\, e^{-(E_n - E_{GS})\tau}. \tag{3.18}$$

In the second equation $|n\rangle$ denote many-body excited states (with the parity opposite to that of the ground-state). Numerically, the correlation function Eq. (3.18) is calculated from the spectrum of energies and matrix elements obtained by exact diagonalization. The correlation function Eq. (3.18) is then used to construct the higher order correlation functions as defined by Eq. (3.14). Numerical results for the correlation function Eq. (3.14) are shown in Fig. 3.1.

The correlation function $\langle G(\tau,0)\rangle_{\rm dis}$ ($p = 1$) is shown in the left panel in Fig. 3.1. Its time-decay exhibits three qualitatively different regimes. At short times ($1 \lesssim \tau \lesssim 10$ in units of $1/J$) the correlation function decays as $\tau^{-1/2}$. This behavior corresponds to a saddle point solution, Eq. (3.1). At longer times, for $10 \lesssim \tau \lesssim 100$, the time decay changes to $\tau^{-3/2}$. Such a behavior signals the dominant effect of soft reparametrization fluctuations around the saddle point, as described in Ref. [16]. At still longer times, $\tau \gtrsim 100$, the time decay of the correlation function is dominated by a first excited many-body state $|n = 1\rangle$ (we'll refer to it as "two-level" system), due to the discreteness of the energy spectrum in a finite size system. The crossover to the two-level regime at long times is quantified on the right panel of Fig. 3.1. In that panel, the dashed lines correspond to the calculation of the correlation functions taking into account the two

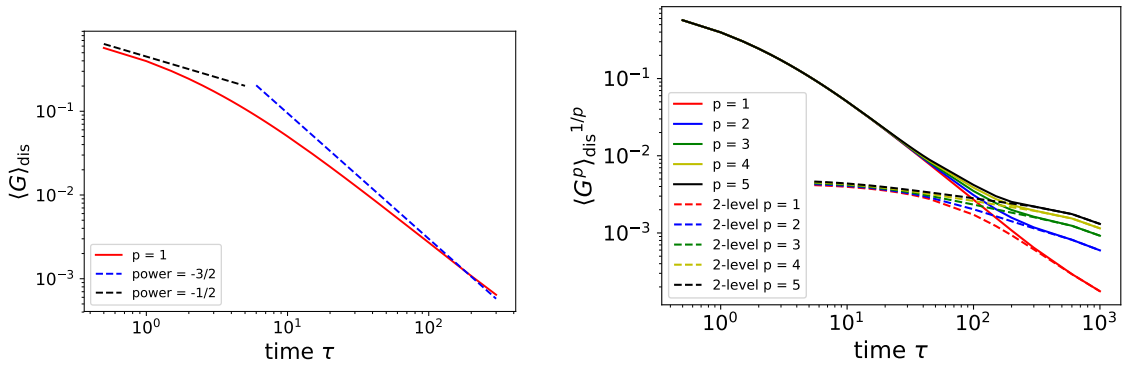

Figure 3.1: (a) Numerical results for $\langle G(\tau,0)\rangle_{\rm dis}$ at $N = 32$ averaged over 30 realizations (Log-Log plot). At short time, it decays with power $-1/2$, while at long time it decays with power $-3/2$. (b) Numerical results for $\langle G(\tau,0)^p\rangle_{\rm dis}^{1/p}$ in time domain (Log-Log plot). The dashed lines are Green's functions obtained by taking into account the contribution from the lowest two eigenstates only. Time is measured in units of $1/J$.

lowest energy levels, $|GS\rangle$ and $|n = 1\rangle$, only.

The right panel in Fig. 3.1 shows that the correlation functions $(\langle[G(\tau,0)]^p\rangle_{\rm dis})^{1/p}$, calculated for different p, coincide in a wide time range, which includes both mean-field and reparameterization dominated regimes. Comparing this behavior with the theoretical expectations, Eq. (3.17), we conclude that it is consistent *only* with the *replica-diagonal* structure of the saddle point. We present an additional independent support to this conclusion by considering site non-local correlation functions in the next section.

Eventually graphs for different p diverge on approaching the two-level system regime. This latter behavior may be quantitatively explained assuming some (independent) distribution functions for matrix elements $\langle GS|\chi_i|1\rangle$ and energy splitting $E_1 - E_{GS}$ (notice that since the ground-state and the excited state belong to different parity sectors, there is no repulsion between them). See appendix A.5 for more details on the two-level regime. To the best of our knowledge, it is not known how to incorporate two-level regime into the replica filed-theory discussed here (see Ref. [19] for an alternative approach). The situation is very different in SYK_2 model, where the corresponding filed-theory is rotationally invariant in the replica space, allowing for the treatment of RSB at the two-level energy scale [13, 40, 41, 42, 43].

3.2.3 Site non-local correlation functions

The existence of the replica off-diagonal solutions may be also detected by considering site non-local correlation functions of the type:

$$\mathcal{D}_{2p}(\tau) = \langle [G_{ij}(\tau,0)G_{ji}(\tau,0)]^p \rangle_{\rm dis} = \langle [\langle GS|\chi_i(\tau)\chi_j(0)|GS\rangle\langle GS|\chi_j(\tau)\chi_i(0)|GS\rangle]^p \rangle_{\rm dis}\,, \tag{3.19}$$

with $i \neq j$. The advantage of this object is that it vanishes, being calculated at the replica-diagonal saddle point (without account for massive fluctuations), but does *not* vanish, being calculated at the off-diagonal saddle point. To see this we rewrite it in the replica formalism as,

$$\begin{aligned}\mathcal{D}_{2p}(\tau) &= \left\langle \chi_i^{a_1}(\tau)\chi_j^{a_1}(0)\chi_j^{a_2}(\tau)\chi_i^{a_2}(0)...\chi_i^{a_{2p-1}}(\tau)\chi_j^{a_{2p-1}}(0)\chi_j^{a_{2p}}(\tau)\chi_i^{a_{2p}}(0)\right\rangle \\ &\approx \left\langle \chi_i^{a_1}(\tau)\chi_i^{a_2}(0)...\chi_i^{a_{2p-1}}(\tau)\chi_i^{a_{2p}}(0)\right\rangle\left\langle \chi_j^{a_1}(0)\chi_j^{a_2}(\tau)...\chi_j^{a_{2p-1}}(0)\chi_j^{a_{2p}}(\tau)\right\rangle, \end{aligned} \tag{3.20}$$

where in the second line we disregarded Gaussian fluctuations and used the site-locality of the saddle point correlation functions (both replica diagonal and off-diagonal ones). Since all replica indexes $a_1, \ldots, a_{2p}$ are distinct here, it is clear that the second line in Eq. (3.20) is zero on the diagonal saddle point. To estimate it in the replica non-diagonal saddle point we consider block-diagonal matrices $\mathbf{g}$ and $\boldsymbol{\sigma}$, consisting of n blocks each of the size $2p \times 2p$ along the main diagonal (see Fig. 3.2). In the replica-limit $n \to 0$, one remains with saddle point equations for a single $p \times p$ block of the matrix in Fig. 3.2. Here we perform explicit calculations for the case $p = 1$. Using the saddle point ansatz Eq. (3.1), we obtain the correlation function $\mathcal{D}_2$ in the form

$$\mathcal{D}_2(\tau) = \langle \chi_i^{a_1}(\tau)\chi_i^{a_2}(0)\rangle \, \langle \chi_j^{a_1}(0)\chi_j^{a_2}(\tau)\rangle = -\frac{g_{a_1a_2}^2}{(4\pi)^{1/2}}\frac{1}{|\tau|}, \tag{3.21}$$

where we use the saddle point matrix $\mathbf{g}$ consisting of 2×2 blocks. Replica non-diagonal solutions of Eqs. (2.58) for 2×2 blocks read

$$\mathbf{g} = \mathbf{1}_n \otimes \frac{1}{\sqrt{J}2^{1/4}} \begin{pmatrix} 1 & \pm i \\ \pm i & 1 \end{pmatrix}, \;\; \boldsymbol{\sigma} = \mathbf{1}_n \otimes \frac{1}{2^{3/4}} \begin{pmatrix} 1 & \mp i \\ \mp i & 1 \end{pmatrix}. \tag{3.22}$$

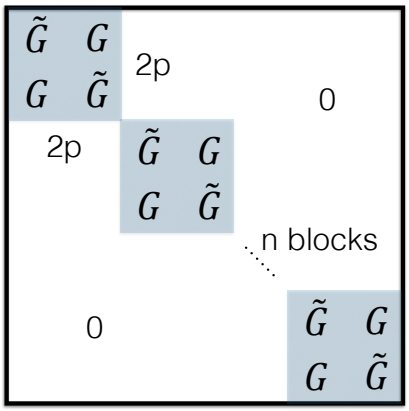

Figure 3.2: Structure of the saddle point matrix for calculation of correlation function $\mathcal{D}_{2p}$

Eq. (3.21) describes the behavior of the correlation function at short times, when the influence of reparameterization fluctuations is negligible. To obtain the correct time dependence at longer times, replica off-diagonal correlation function has to be averaged over the reparametrization fluctuations (see Appendix A.3 for details). Since the reparameterizations are locked according to Eq. (3.11), one integrates over a single reparameterization degree of freedom for the both replicas involved in $\mathcal{D}_2(\tau)$. This leads to:

$$D_2^{\text{off}-\text{diag}}(\tau) = \frac{1}{2\sqrt{2\pi}J|\tau|^{3/2}}. \tag{3.23}$$

We come back now to the replica diagonal scenario, which leads to vanishing result for the non-local functions (3.19), being calculated at the diagonal saddle point. However one can include massive (with the mass of order N) Gaussian fluctuations δG_{ab} and $\delta\Sigma_{ab}$ around the diagonal saddle point to find a non-zero result for the first line in Eq. (3.20) (see Appendix A.2 for detailed derivation). This leads to:

$$D_2^{\text{diag}}(\tau) = \frac{3}{4\pi 2^{10} JN^3}\frac{1}{|\tau|} \tag{3.24}$$

for $\tau < N/J$. Subsequent averaging over the reparameterization fluctuations around

the replica-diagonal saddle point with two independent (unlocked) reparameterization modes, one for each replica, results in:

$$D_2^{\rm diag}(\tau) = \frac{3}{4\pi 2^{10} J N^3} \frac{1}{|\tau|^3}. \tag{3.25}$$

Analytical calculations of the correlation function Eq. (3.20) for $p > 2$ result in the following general relation between the correlation functions for different powers p

$$\begin{aligned}
\left(\frac{\mathcal{D}_{2p}(\tau)}{(2p-1)!!}\right)^{1/p} &= \begin{cases} \frac{1}{2\sqrt{2\pi}J|\tau|}, & \tau < N/J \quad \text{replica off-diagonal ,} \\ \frac{3}{4\pi 2^{10} J N^3}\frac{1}{|\tau|}, & \tau < N/J \quad \text{replica diagonal.} \end{cases} \\
\left(\frac{\mathcal{D}_{2p}(\tau)}{(2p-1)!!}\right)^{1/p} &= \begin{cases} \frac{1}{2\sqrt{2\pi}J|\tau|^{3/2p}}, & \tau > N/J \quad \text{replica off-diagonal,} \\ \frac{3}{4\pi 2^{10} J N^3}\frac{1}{|\tau|^3}, & \tau > N/J \quad \text{replica diagonal .} \end{cases}
\end{aligned} \tag{3.26}$$

As one can see from Eqs. (3.21), (3.24), for short times the two above mentioned scenarios differ only in the scaling of the correlation function $\mathcal{D}_2(\tau)$ with the number of sites N, while for long times both the scaling with N as well as the predicted time dependence become different. Therefore, the time dependence *as well as the dependence on the total number of sites* N can be used do discriminate between Eqs. (3.23) and (3.24).

Results of numerical calculations of the dependence $\mathcal{D}_{2p}(\tau)$ are shown in Figs. 3.3 and 3.4. Figure 3.3 shows the time dependence of the correlation function $\mathcal{D}_{2p}(\tau)$ for different p, for our largest system, $N = 32$. First, one notices the non-monotonous dependence of the correlation functions on time. This short time behavior originates from the fact that equal time expectation $\langle \chi_i(0)\chi_j(0)\rangle = 0$ for $i \neq j$ for $N = 8, 16, 24, 32, \ldots$, which belong to the orthogonal symmetry class [17]. Indeed, from anticommutation of Majoranas one concludes that $\langle \chi_i \chi_j \rangle$ is pure imaginary. On the other hand, for orthogonal symmetry classes, there is a representation of Majorana operators with all matrix elements $\langle n|\chi_i|m\rangle$ being real. This contradiction enforces zero value for equal time expectation. The field theory does not resolve this fact. At longer time, $\tau \gtrsim 3/J$, the correlation functions decrease in time in a qualitative agreement with the field theory. However, while $p = 1$ function is consistent with Eqs. (3.24), (3.25), the $p \geq 2$ functions

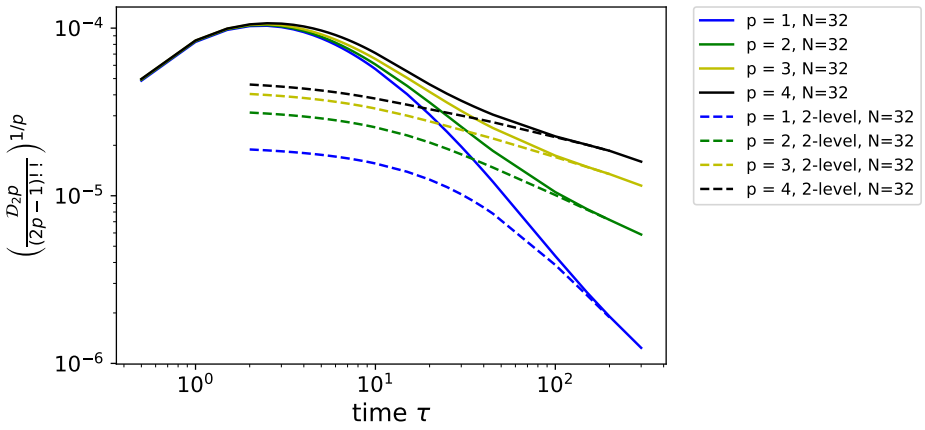

Figure 3.3: Log-Log plot of $\mathcal{D}_{2p}$ versus τ. The $p = 1$ graph is consistent with Eqs. (3.24), (3.25) between $5 \lesssim \tau \lesssim 100$. For $p \geq 2$ crossover to the two-level regime is too fast to deduce the time dependence expected from Eq. (3.26).

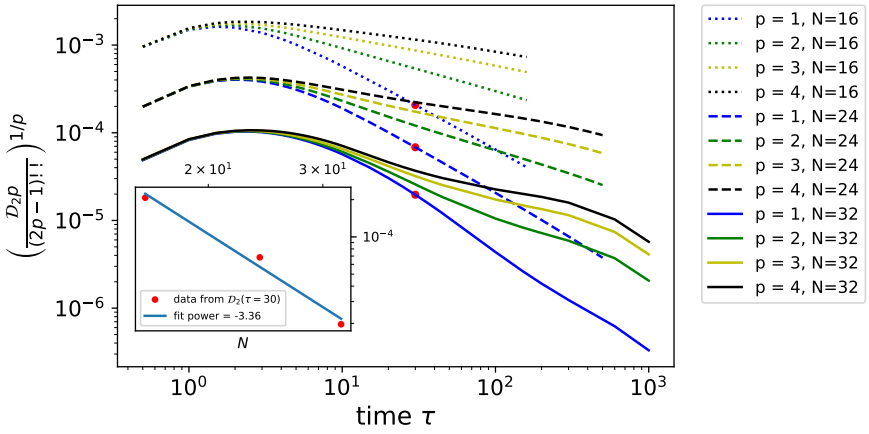

Figure 3.4: Log-Log plot of $\mathcal{D}_{2p}$ versus τ for $N = 16$ (dots), 24 (dashed) and 32 (solid), averaged over 50000, 5000 and 30 realizations respectively. Diminishing of the magnitude of correlation functions with N without the change of its time dependence confirms predictions of fluctuation expansion around the replica diagonal saddle point. Inset: Fit of the amplitude of the correlation function at $\tau = 30$ for different N. The best fit is achieved for the power -3.36, the fluctuation expansion predicts the power -3.

exhibit fast crossover to the two-level regime. We thus are not able to verify the time dependence of Eqs. (3.26) even for our largest system of $N = 32$ for $p \geq 2$.

We can, however, verify the N-dependence of Eqs. (3.26). Numerical results for the dependence of the correlation functions on the number of sites N are shown in Fig. 3.4. One can see that the correlations functions rapidly decrease with increasing N while keeping qualitatively the same time dependence. This is in accord with the predictions from the Gaussian fluctuation expansion around the replica-diagonal saddle point. The best fit, see inset in Fig. 3.4, for power law dependence on N is $N^{-3.36}$, which is close to the power N^{-3}, following from the Gaussian fluctuation expansion. In contrast, the replica off-diagonal saddle point predicts no suppression of the site off-diagonal correlation functions with N, Eq. (3.26). Once again we conclude that the numerics is consistent with the replica-diagonal theory and is inconsistent with the off-diagonal saddle points.

3.3 Conculsion for replica stucture

We have examined signatures of the replica off-diagonal saddle points in the field theory treatment of the SYK_4 model. We have argued that such off-diagonal elements affect the coset manifold $\mathcal{G}/H$ of reparameterization soft modes and thus change the expected long-time behavior of "mesoscopic" correlation functions. Comparing to numerically evaluated corresponding correlation functions for $N \leq 32$ SYK_4 model, we conclude that they do not show any evidence for replica off-diagonal saddle points. On the contrary, all correlation functions (both site local and non-local) are in a good agreement with the expectations stemming from the replica diagonal saddle point plus Gaussian fluctuations. The latter do include replica off-diagonal components, of course.

We conclude thus that we do not detect any evidence for replica off-diagonal saddle points, at least for time scales shorter than the inverse spacing between the ground-state and the first many-body excited state. At longer times the data is well described by statistics of the two-level system. We stress, though, that such two-level description is outside of the field theoretical treatment, we base our conclusions at. It remains to be seen if our conclusions can be reconciled with the results of Refs. [45, 46]. On the other hand, our findings are in line with no evidence for glassy behavior in the SYK model

reported in Ref. [39].

Does it mean that there is no room for replica symmetry breaking and replica off-diagonal structure in SYK-like models? In our opinion such conclusion is premature. One may investigate deformed models, such as eg. $SYK_4 + SYK_2$ [56, 57, 58]. In Chapter 5, we will discuss $SYK_4 + SYK_2$ model with similarities between level and eigenfunction statistics of such models to those of random regular graphs (RRG) [59, 60, 61] (see also [62, 63] for the related studies). In the case of RRG replica symmetry breaking was argued to be a proper framework to describe an observed phenomenology [61]. One is thus justified to expect that phenomenologically similar deformed SYK models may admit similar replica symmetry broken description. However, one should probably conclude that the *undeformed* SYK_4 model does *not* exhibit deviations from the replica diagonal and symmetric saddle point description.

Chapter 4

Superconductivity in strange metal

SYK model has received a great deal of attention in recent years as being an exactly solvable model with non-Fermi liquid properties [64, 65, 66, 67, 68, 58, 69]. Although the original model is zero-dimensional (0D) with all-to-all random interactions, it was soon generalized to include D-dimensional arrays of connected SYK grains [64, 70, 71, 72, 73, 68, 74, 75, 76, 77, 78]. Such models were shown to exhibit T-linear resistivity, making them attractive candidates for description of strongly correlated materials [79]. An account of quantum fluctuations in such arrays reveals [78] a quantum phase transition (QPT) between a gapless (thermal) insulator and the Fermi liquid at certain critical inter-grain coupling, see Fig. 4.1(b). In this picture the T-linear metallic phase appears as the quantum critical region [80] of the aforementioned QPT, which resemble the QCP scenario in high-Tc superconductivity see Fig. 4.1(a).

Success of the SYK model in describing the non-Fermi liquid state raises the question if superconductivity may be included in the same framework. A number of models were suggested with this goal in mind both in 0D [82, 83, 84, 85] and in the array [86, 87, 88] context. All of them found that the original SYK model must be upgraded to complex spin-full fermions with an extra mechanism of attraction, such as phonons [82, 83, 84], pair hopping [86], or special correlations between matrix elements [87, 88]. Such upgraded SYK-like models indeed exhibit superconducting correlations, which may

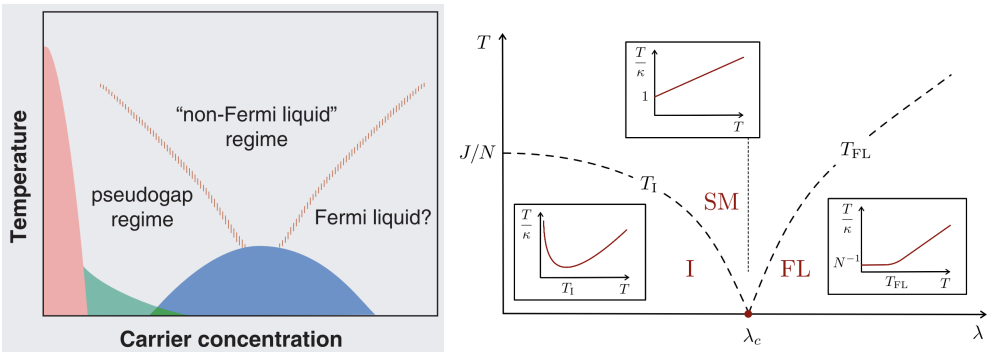

Figure 4.1: (a) Schematic phase diagram of high-temperature superconductors. The shaded blue area indicates the region in which superconducting long-range order occurs. A QCP may be buried due to the existence of superconducting dome. Taken from Ref. [81]. (b) Phase diagram of SYK array: T vs dimensionless hopping strength λ. There are three phases: insulator (I), strange metal (SM) and Fermi liquid (FL), separated by dashed crossover curves. Taken from Ref. [78]

be treated within the large N mean-field approach. Similarly to the Fermi liquid BCS mechanism, an infinitesimal attraction is sufficient to develop the superconductivity.

In this chapter, we will consider a 0D model where the attraction is provided by a negative U Hubbard term. In order to offer a taste of dealing with 0D superconductivity, we present the treatment of standard BSC type superconductivity in ultrasmall grains in Sec. 4.1. Then in the following sections, we demonstrate how superconductivity in SYK will deviate from the situation in Sec. 4.1, and the SYK superconductivity becomes a possible paradigm candidate for the high-Tc superconductivity.

4.1 BCS mean-field theory in ultrasmall grains

Before we touch the SYK superconductivity, let's first explore some key points in BCS superconductivity which built from normal metal in an ultrasmall grain. The study of superconductivity has mostly been based on the BCS Hamiltonian, which is formulated in momentum space, and relies heavily on translation symmetry. Translation symmetry is sometimes broken, for example by the presence of disorder or encounter zero dimensional system, and this renders the momentum-space formulation much less useful. In this section we introduce formalism that allows us to study BCS type pairing

and superconductivity in real space, which is suitable for 0D system.

We consider the attractive pair-hopping model with strength U on top of a normal metal, which is a BCS type mean-field theory:

$$H_{\mathrm{BCS}} = \sum_{i,\sigma}^{N} (\epsilon_i - \mu) c_{i\sigma}^{\dagger} c_{i\sigma} - U \sum_{ij}^{N} c_{i\uparrow}^{\dagger} c_{i\downarrow}^{\dagger} c_{j\downarrow} c_{j\uparrow}. \tag{4.1}$$

where ϵ_i's are the energy spectrum for the normal metal orbitals. To explore the fate of a Cooper pair under multiple scattering, let us consider the following four-point correlation function

$$C(\tau) = \frac{1}{N} \sum_{i} \langle c_{i\uparrow}^{\dagger}(\tau) c_{i\downarrow}^{\dagger}(\tau) c_{i\downarrow}(0) c_{i\uparrow}(0) \rangle \tag{4.2}$$

To calculate the correlation function, let us draw on the perturbative methods and solve it diagrammatically as shown in Fig.4.2: where the solid line in the diagram refers as

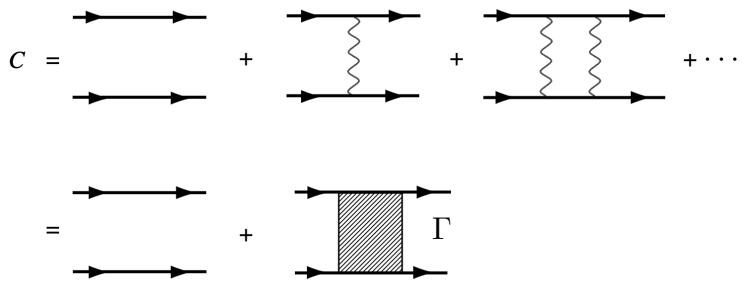

Figure 4.2: Two-particle propagator in the presence of attractive interaction U. The two Green function lines defining each rung of the ladder carry frequency ω and $-\omega$, respectively. The vertex of the propagator, defined through the second line, obeys the Bethe–Salpeter.

Green function, which defined in time-domain as $G_i(\tau) = \langle c_{i\sigma}^{\dagger}(\tau) c_{i\sigma}(0) \rangle$ and can be evaluated in frequency domain as

$$G_i(\omega) = \frac{1}{i\omega - (\epsilon_i - \mu)} \tag{4.3}$$

Write down the diagrammatic representation into formula, one get Bethe–Salpeter equation

$$\Gamma = U + U\left[\sum_i^N \int \frac{d\omega}{2\pi} \frac{1}{i\omega - (\epsilon_i - \mu)} \frac{1}{-i\omega - (\epsilon_i - \mu)}\right]\Gamma \tag{4.4}$$

$$= U + U\Gamma \sum_i \frac{1}{2|\epsilon_i - \mu|} \tag{4.5}$$

$$\simeq U + U\Gamma \int_{|\Delta|}^{\omega_D} \nu \frac{d\epsilon}{\epsilon} = U + U\Gamma\nu \ln\left(\frac{\omega_D}{|\Delta|}\right) \tag{4.6}$$

where we have used the fact that, the higher energy was cut by the range of pairing, i.e. Debye frequency ω_D, while singularity at low energy is regularized by temperature T or a energy gap $|\Delta|$. And $1/\nu$ is the typical level spacing between these two energy scale. Now one get the vertex of the propagator as

$$\Gamma \simeq \frac{U}{1 - U\nu \ln(\omega_D/|\Delta|)} \tag{4.7}$$

When the denominator of Γ goes to zero, the system would be unstable and transition to another state which is superconducting. Now the energy scale $|\Delta|$ can be translate as the superconducting gap, with relation

$$|\Delta| = \omega_D \exp\left[-\frac{1/\nu}{U}\right] \tag{4.8}$$

Thus for the BCS type superconductivity in ultrasmall grains, an arbitrarily weak attraction results in a finite superconducting order parameter, albeit an exponentially small one.

4.2 Overview the key results in SYK superconductivity

In the following sections, we consider a different 0D model with Hubbard interaction in SYK model. Contrary to the mechanisms mentioned in Sec. 4.1, the mean-field treatment completely fails to describe the SYK+Hubbard model even in the $N \to \infty$ limit. This is because the Hubbard term does not inhibit on-site phase fluctuations, which invalidate the mean-field approach. Such quantum phase fluctuations result in

an insulating *pseudogap* phase at $U < U_c$, where U_c is a critical attraction strength. For $U > U_c$ there is a superconducting "dome" on the U vs. temperature plane. The finite temperature transition in this regime is also fluctuation-dominated and does not conform to the mean-field description.

In view of the failure of the mean-field, one needs to develop alternative means, capable of treating strongly fluctuating phases. Fortunately, within the 0D framework this can be achieved. In the limit of large U we found that the model may be mapped onto a certain generalization of the exactly solvable Richardson model [89, 90, 91]. Its solution reveals a superconducting low temperature state with the first order transition, at $T_c \propto U^{-1}$, to a liquid of "preformed" incoherent pairs. The first order transition between a superconductor and a non-Fermi liquid has been already noticed in Refs. [92, 86]. It's possible that SYK+Hubbard and the associated Richardson models provide the simplest cartoon for this phenomenon.

In the opposite limit of a weak attraction, the phase fluctuations may be described by an effective model, which we call the *quantum Kuramoto* model. The classical Kuramoto model is a paradigm for synchronization of non-linear stochastic oscillators [93, 94, 95, 96, 97, 98, 99, 100, 101, 102, 103]. It's quantum counterpart provides a description of a QPT between the pseudogap state with unsynchronized phases and the phase-coherent superconductor. We found it remarkable that the SYK framework is capable to exhibit the pseudogap physics.

To verify validity of this theory we resort to an exact diagonalization of spin-1/2 SYK+Hubbard model. To detect superconductivity numerically in a finite size system, we employ the notion of the off-diagonal long-range order (ODLRO) [104, 105]. It allows for a sharp definition of the condensate fraction and its dependence on temperature and the attraction strength for a large, but finite N (number of sites). Numerical results are in a qualitative (and in cases where numerical coefficients may be evaluated, a quantitative) agreement with the theory.

4.3 Superconductivity models build from SYK

We consider 0D models, consisting of $N \gg 1$ orbitals (or sites), labeled as $i, j, \ldots = 1, 2, \ldots, N$. Each orbital may be occupied by a complex spin-1/2 fermion annihilated

with the operator $c_{i\sigma}$, where $\sigma = \downarrow, \uparrow$ is the spin index. In the spirit of the SYK model, we assume that all orbitals are exactly degenerate with the on-site energy taken to be zero. The orbitals interact through the four-fermion interaction with *real* spin-independent matrix elements. These interactions are summarized by the SYK part of the Hamiltonian:

$$H_{\text{SYK-complex}} = \frac{1}{2} \sum_{ijkl;\sigma\sigma'}^{N} J_{ij;kl} \left[c_{i\sigma}^{\dagger} c_{j\sigma'}^{\dagger} c_{k\sigma'} c_{l\sigma} + c_{l\sigma}^{\dagger} c_{k\sigma'}^{\dagger} c_{j\sigma'} c_{i\sigma} \right], \tag{4.9}$$

where $J_{ij;kl}$ is a real tensor with the following symmetry properties:

$$J_{ij;kl} = -J_{ji;kl} = -J_{ij;lk} = J_{lk;ji}. \tag{4.10}$$

We also demand that non-zero elements must have all four indexes i, j, k, l distinct. Up to these symmetries, the matrix elements $J_{ij;kl}$ are assumed to be real independent random variables, drawn from the Gaussian distribution with the zero mean, $\langle J_{ij;kl} \rangle = 0$, and the variance

$$\langle J_{ij;kl}^2 \rangle = J^2/(4N)^3. \tag{4.11}$$

We'll show below (both numerically and analytically) that the pure SYK Hamiltonian (4.9) does not lead to ODLRO [106]. For ODLRO to develop, one needs to supplement the SYK Hamiltonian with an attractive term, facilitating fermion pairing. One possibility is a site-local negative U Hubbard term:

$$H_{\text{Hub}} = -U \sum_{i}^{N} c_{i\uparrow}^{\dagger} c_{i\downarrow}^{\dagger} c_{i\downarrow} c_{i\uparrow} - \mu \sum_{i,\sigma}^{N} c_{i\sigma}^{\dagger} c_{i\sigma}. \tag{4.12}$$

Another option is all-to-all pair hopping [86]:

$$H_{\text{p-hop}} = -\frac{U}{N} \sum_{ij}^{N} c_{i\uparrow}^{\dagger} c_{i\downarrow}^{\dagger} c_{j\downarrow} c_{j\uparrow} - \mu \sum_{i,\sigma}^{N} c_{i\sigma}^{\dagger} c_{i\sigma}, \tag{4.13}$$

which annihilates a pair at an orbital j and creates at, in general, different orbital i. Both Hamiltonians contain a chemical potential to adjust the occupation fraction. The three Hamiltonians, written above, conserve particle number and are symmetric under the time-reversal transformations. States of these models are governed by temperature, T,

fermion occupation number, N_f, and the dimensionless parameter, U/J, characterizing the attraction strength.

In the absence of the SYK term the ground state of the pure Hubbard model, Eq. (4.12), consists of localized pairs and does not exhibit ODLRO. Its energy is obviously $-U$ per fermion pair and its degeneracy is given by the number of combinatorial possibilities of distributing a given number of pairs among N orbitals. Excited states are formed by breaking some of the pairs and creating single occupied orbitals with zero energy. As we show below, ODLRO may be established, mediated by the SYK interactions.

The pure pair-hopping Hamiltonian, Eq. (4.13), is somewhat different. It constitutes a limiting case of the Richardson model [89, 90, 91] (see section 4.6.1 and Appendix B.3 for details). The effective model in section 4.6.1 predicts a non-degenerate ground state with ODLRO separated by the gap, $\propto U$, from the first excited state, which is $(N-1)$-fold degenerate. We'll show that SYK interactions do not destroy ODLRO, but weaken it substantially if $U < J$.

Numerically we first block diagonalize the $2^{2N} \times 2^{2N}$ matrix Hamiltonian in the many-body space, using particle number conservation and other symmetries (e.g. particle-hole symmetry for the half-filled case). We then exactly diagonalize the relevant blocks to extract their spectrum and eigenfunctions.

4.4 Order parameter: off-diagonal long-range order

The standard definition of the superconductivity implies a finite anomalous expectation value, $\bar{\Delta}_i \propto \langle c^\dagger_{i\uparrow} c^\dagger_{i\downarrow} \rangle$. It is clear however, that for a finite size system with a particle conserving Hamiltonian such expectation value is bound to vanish. One thus needs another measure of the superconducting order. The corresponding concept of ODLRO is well known from, e.g., the theory of cold atom Bose condensates in optical or magnetic traps [105].

Let us define the bosonic pair creation operator as

$$b^\dagger_i = c^\dagger_{i\uparrow} c^\dagger_{i\downarrow}. \tag{4.14}$$

Since there can't be more than one such boson per orbital, we are dealing with the

hard-core bosonic particles. One then defines the reduced *single-particle* bosonic density matrix as

$$\rho_{ij} = \langle b_i^\dagger b_j \rangle, \tag{4.15}$$

where $\langle \ldots \rangle$ implies the exact many-body ground state (or thermal) expectation value. Defined this way, ρ_{ij}, is an $N \times N$ positive-definite matrix. Its trace is a total number of local pairs, which is less or equal than $N_f/2$ (we typically consider half-filled systems with $N_f = N$). One is interested in the spectrum of eigenvalues of ρ_{ij}: λ_α, where $\lambda_0 \geq \lambda_1 \geq ... \geq \lambda_{N-1} \geq 0$ and $\sum_{\alpha=0}^{N-1} \lambda_\alpha \leq N_f/2$. The absence of the pair condensate corresponds to all N eigenvalues λ_α being of order one, $O(1)$. On the other hand, the pair condensate corresponds to the largest eigenvalue λ_0 being $O(N)$, while the remaining $N-1$ eigenvalues being $O(1)$.

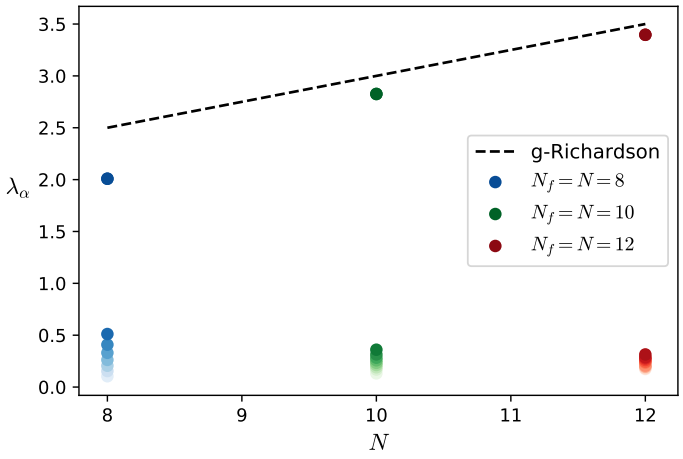

Figure 4.3: Spectrum of ρ_{ij}, i.e. λ_α vs. number of orbitals N for the ground state of SYK+Hubbard model with $U/J = 2$ and $N_f = N$. Dashed line is a result from generalized Richardson model (Section 4.6.1).

Figure 4.3 shows $T = 0$ spectrum of ρ_{ij} for SYK +Hubbard model with $U/J = 2$ for $N = N_f = 8, 10, 12$. One can clearly see the largest eigenvalue splits from the rest and approaches $N/4 + 1/2$. The remaining eigenvalues coalesce towards $\approx 1/4$. This behavior may be understood with the help of the generalized Richardson model, as explained in Section 4.6.1. The presence of the single eigenvalue with the $O(N)$

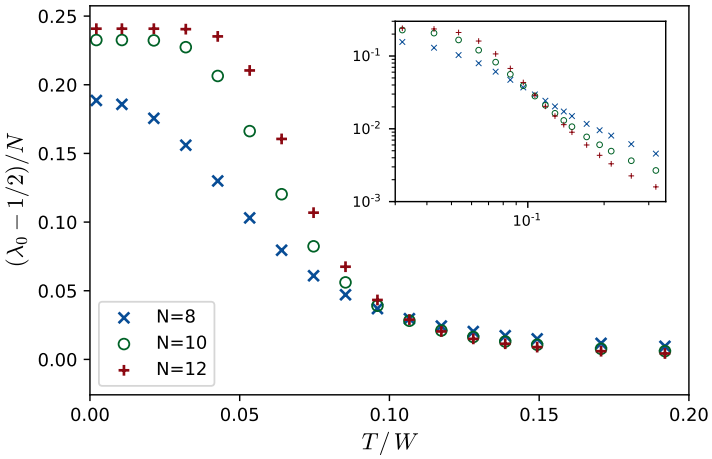

Figure 4.4: $(\lambda_0 - 1/2)/N$ vs. temperature of SYK+Hubbard model with $U/J = 2$. The temperature is normalized to $W = 3J^2/32U$ (Section 4.6.1). Inset: vicinity of the crossing point.

scaling is the hallmark of ODLRO [105]. Indeed, admitting a nonzero anomalous average $\bar{\Delta}_i \propto \langle c^\dagger_{i\uparrow} c^\dagger_{i\downarrow} \rangle$, one finds $\rho_{ij} \propto \bar{\Delta}_i \Delta_j$, where Δ_j is the complex conjugate of $\bar{\Delta}_j$. This is the rank-1 matrix with the single non-zero eigenvalue, given by its trace ($\propto N$).

Figure 4.4 shows temperature dependence of the condensate density, $(\lambda_0 - 1/2)/N$, (subtraction of $1/2$ is motivated by the expectation that, in the absence of ODLRO, all λ's approach $1/2$). One notices the approximate crossing point at $T_c \approx 0.1W$, where W is the energy scale of the Richardson model, $W = 3J^2/32U$, (see Eq. (4.20) in Section 4.6.1). Such crossing point indicates a phase transition in the $N \to \infty$ limit between phases with a finite and zero condensate density.

4.5 Mean-field treatment and its failure

4.5.1 Mean-field theory in SYK

To develop a large N mean-field treatment, one follows the standard route [6, 16] of averaging over the random SYK matrix elements $J_{ij;kl}$ and deriving the so-called $G\Sigma$ action. There is a peculiarity, though, associated with the matrix elements being real. It is coming from the fact that there are two distinct terms in the square bracket on

the right hand side of Eq. (4.9), see Appendix B.1. Upon averaging over the Gaussian distribution of $J_{ij;kl}$, one obtains two types of terms which are expressed through the normal and anomalous two-point fields:

$$G_{\tau,\tau'} = -\frac{1}{N}\sum_{i}^{N} c_{i\sigma}(\tau)c^{\dagger}_{i\sigma}(\tau');$$
$$F_{\tau,\tau'} = -\frac{1}{N}\sum_{i}^{N} c_{i\downarrow}(\tau)c_{i\uparrow}(\tau'), \tag{4.16}$$

The normal component is spin-diagonal and independent of the spin-projection. Here we have suppressed replica indices for brevity. The normal and anomalous components may be combined in the Nambu matrix field $\hat{G}_{\tau,\tau'}$. The definitions (4.16) are enforced by conjugate non-local fields, which may be also combined into the Nambu space matrix $\hat{\Sigma}_{\tau,\tau'}$, playing the role of the self-energy.

The Hubbard term, Eq. (4.12), may be decoupled in the Cooper channel with the help of the local fields $\Delta_i(\tau)$, leading to the effective action of the form:

$$\begin{aligned} S = \quad & \sum_{i}^{N}\int d\tau \left[\frac{|\Delta_i|^2}{U} - \frac{1}{2}\,\mathrm{Tr}\ln(\partial_\tau + \mu + \hat{\Sigma} + \hat{\Delta}_i)\right] \\ & - N\iint d\tau d\tau' \left[\hat{\Sigma}_{\tau,\tau'}\hat{G}_{\tau',\tau} + \frac{J^2}{64}\left(\bar{F}^2_{\tau\tau'}F^2_{\tau\tau'} + G^4_{\tau\tau'}\right)\right], \end{aligned} \tag{4.17}$$

where $\hat{\Delta}_i = \Delta_i\sigma_+ + \bar{\Delta}_i\sigma_-$ is the off-diagonal Nambu matrix. For the pair-hopping model, Eq. (4.13), one needs a single field $\Delta(\tau)$ to decouple it. One thus arrives at the same action (4.17) with the constraint $\Delta_i = \Delta$. In the latter case there is a large factor N in front of the entire action, justifying the mean-field saddle point approximation.

The mean-field equations, obtained upon variation of the action over the matrix fields $\hat{G}$, $\hat{\Sigma}$ as well as over Δ are specified in Appendix B.1. Their numerical analysis [106] shows that in the absence of attraction ($U = 0$ and thus $\Delta_i = 0$) the lowest free energy solution is purely normal, i.e. $F_{\tau,\tau'} = 0$, while $\hat{G}_{\tau,\tau'} \propto |\tau - \tau'|^{-1/2}$, same as in conventional complex-J SYK model.

One can investigate now stability of such non-superconducting SYK solution against a small attractive U perturbation. The corresponding self-consistency equation for Δ

takes the form $U^{-1} = \mathcal{C}(\Delta)$, where the Cooper channel polarization $\mathcal{C} = \int d\tau G_\tau^2$, with $G_\tau = G_{\tau,\tau'=0}$. In the normal phase of SYK, $G_\tau \propto (J\tau)^{-1/2}$, and therefore $\mathcal{C}$ is given by the logarithmic integral. In the IR limit, the integral of $\mathcal{C}$ is cut by either temperature or $|\Delta|$, leading to $U^{-1} \propto J^{-1} \ln(J/|\Delta|)$ and thus $|\Delta| \sim J e^{-\text{const}\cdot J/U}$ for $U \ll J$. Thus the mean-field treatment predicts that, similarly to BCS case, *an arbitrarily weak attraction* results in a finite superconducting order parameter, albeit an exponentially small one.

A detailed calculation, presented in Appendix B.1, leads to the following mean-field solution for the absolute value of the order parameter

$$|\Delta| \propto \begin{cases} J\, e^{-J\sqrt{\pi}/(8\sqrt{2}U)}; & U \ll J, \\ U/2; & J \ll U. \end{cases} \tag{4.18}$$

It is worth mentioning that the energy gap in the many-body spectrum scales as $|\Delta|^2/J$ for $U \ll J$ and as $|\Delta|$ for $U \gg J$, Appendix B.1.

As mentioned above, one expects the mean-field treatment to be accurate for the SYK+pair hopping model in $N \to \infty$ limit. It is not clear a priori if SYK+Hubbard is also accurately described by this theory. Indeed, in the latter case the order parameters, Δ_i, on individual orbitals fluctuate independently (first line in Eq. (4.17)) and such fluctuations are not necessarily decreasing as $N \to \infty$. To check this we perform finite-size exact diagonalization study, summarized below.

4.5.2 Exact Diagonalization

Figure 4.5 shows the exact diagonalization results for the SYK+pair hopping Hamiltonian, Eqs. (4.9), (4.13), for the half-filled $N = 12$ case – the largest size accessible in our simulations. The top panel shows ODLRO, defined as the difference between the largest and the second largest eigenvalues of ρ_{ij}, Eq. (4.15), as a function of U/J. The bottom panel shows the gap in the many-body spectrum, defined as the difference between the energies of the first excited and the ground-state, also as a function of U/J. At $U \gg J$ the ODLRO saturates to $N/4$, while the many-body gap approaches U - in agreement with the mean-field. Due to finite size effects, it is hard to draw definitive conclusions about small U behavior. Qualitatively it is also consistent with the mean-field expectations, Eq. (4.18).

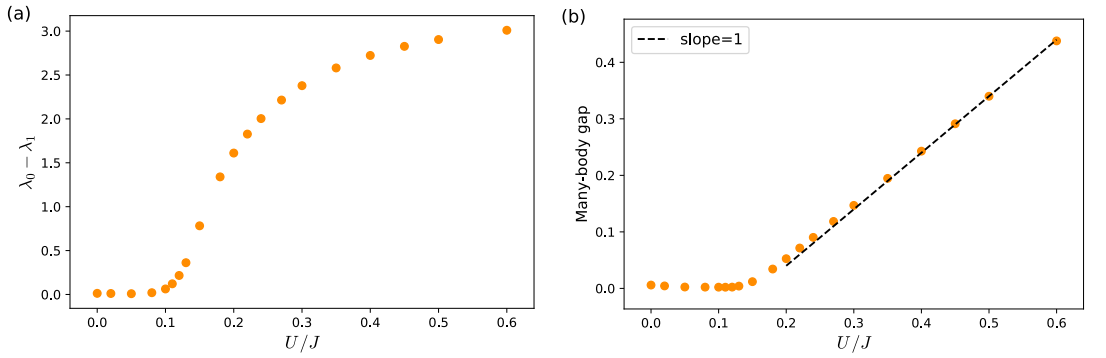

Figure 4.5: (a) ODLRO and (b) many-body energy gap in units of J vs. U/J for the SYK+pair-hopping model with $N_f = N = 12$.

This behavior should be contrasted with the results of the exact diagonalization of the SYK+Hubbard, Eqs. (4.9), (4.12), presented in Fig. 4.6. One notices a critical value $U_c \approx 0.24J$, below which there is not any evidence of neither ODLRO, nor the many-body gap (beyond a finite-size effect of the SYK model). As indicated in the inset, U_c does not decrease with increasing N and thus it's unlikely to be a finite-size artifact. Another marked difference is the behavior of the many-body gap at large U. Unlike the pair-hopping model, where the many-body gap increases with U, the Hubbard model exhibits a non-monotonic dependence of the gap with U, with the maximum gap reached at $U \approx 0.4J$. The finite-temperature behavior of the SYK+Hubbard model is illustrated in Fig. 4.7, where we present the color plot of the logarithm of ODLRO on the temperature vs. U/J plane. One notices the characteristic superconducting "dome" shape with a non-monotonic behavior of the critical temperature, where ODLRO is suppressed.

The presence of the critical interaction strength, U_c, and the non-monotonic behavior of the gap and T_c are contrary to the mean-field predictions, Eq. (4.18). We attribute both phenomena to the strong quantum fluctuations in the SYK+Hubbard model. To account for such large N, non-mean-field phenomenology, we investigate the SYK+Hubbard model in the two limiting cases of strong and weak attraction. In both cases we are able to account for the quantum fluctuations and show that they indeed explain the observed behavior.

In the case of the strong attraction this is achieved by mapping onto an exactly

solvable generalized Richardson model. It provides an asymptotically exact description of the low-energy part of the SYK+Hubbard model in the limit $U \gtrsim \sqrt{N}J/13$. In the opposite limit of the weak attraction we reduce the problem to a quantum version of the Kuramoto model. Its classical counterpart [93, 94, 95, 96, 97, 98, 99, 100, 101, 102, 103] provides a paradigm for synchronization of non-linear oscillators. We show that the quantum Kuramoto model provides description of the pseudogap phase for $U < U_c$ and the continuous superconducting QPT at $U = U_c$.

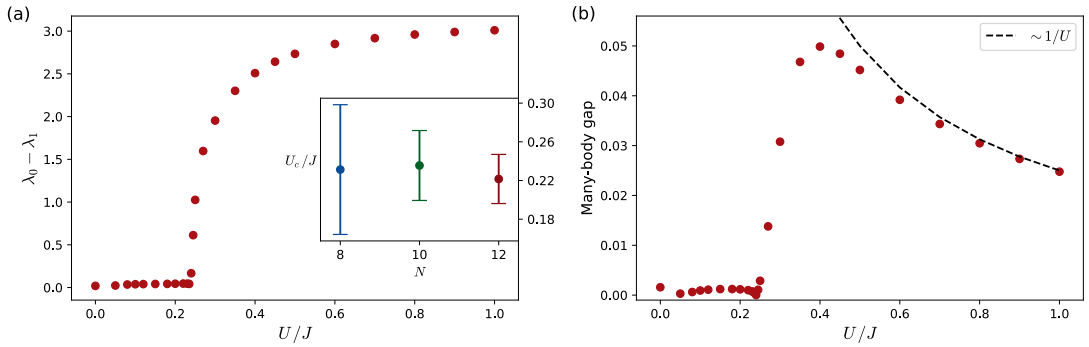

Figure 4.6: (a) ODLRO and (b) many-body gap vs. U/J for the SYK+Hubbard model with $N_f = N = 12$. Inset in (a): U_c vs. system size N. Error bars reflect statistical fluctuations.

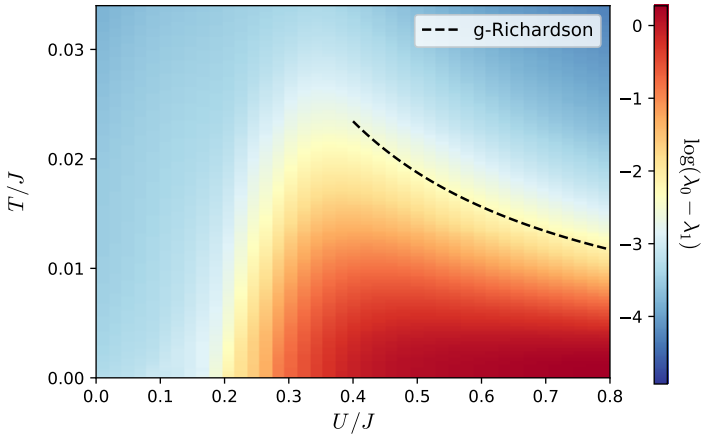

Figure 4.7: Superconducting "dome". Color plot of $\log(\lambda_0 - \lambda_1)$ for the SYK+Hubbard model with $N_f = N = 8$ on T vs. U/J phase plane. The dashed line is prediction for T_c for the generalized Richardson model, section 4.6.1.

4.6 Quantum fluctuations in SYK+Hubbard model

4.6.1 Generalized Richardson model

The many-body spectrum of the SYK+Hubbard model with $U = 2J$ and $N = 8$ is shown in Fig. 4.8 as a function of the fermion number, N_f. One notices strong alternation of the entire level sequence (and in particular the ground state energies) between even and odd fermion numbers. The low-energy part of the spectrum, which is not resolved in the main plot, is shown in the inset for even N_f. These low-energy bands are separated by the gap $\sim U$ from the rest of the spectrum. Number of many-body states in these low-energy bands is exactly $\binom{N}{N_f/2}$, i.e. the number of ways to place $N_f/2$ indistinguishable pairs over N orbitals. Therefore the low-energy bands are described by models of hard-core bosons, Eq. (4.14). In the absence of the SYK term, bosons are localized and all $\binom{N}{N_f/2}$ bosonic states are degenerate with the energy $-U$ per boson. The SYK term induces an effective bosonic hopping and thus leads to a formation of the low-energy bands.

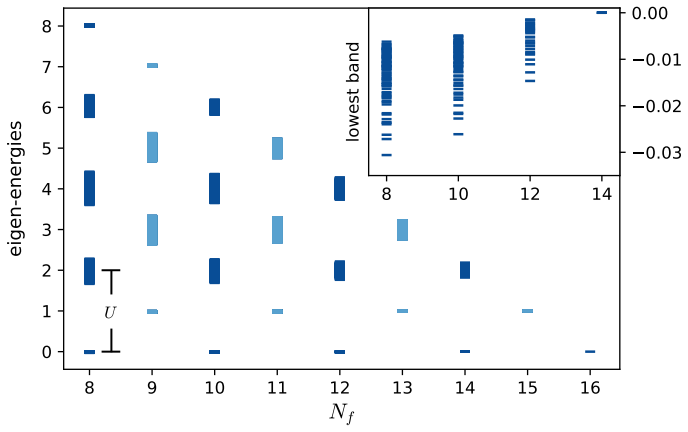

Figure 4.8: Many-body energy spectrum (in units of J) of SYK+Hubbard model vs. number of fermions N_f for $N = 8$ and $U = 2J$. Chemical potential, μ, is set $\mu = -U/2$ to preserve particle-hole symmetry between N_f and $2N - N_f$ sectors. The inset shows the lowest bands of the spectrum (right hand side of y-axis in units of J) for even N_f. Bandwidth for the lowest energy sector at half-filling is consistent with $NW/16 \simeq 0.023J$, predicted by the generalized Richardson solution, Eq. (4.23).

To gain an insight in the physics of the corresponding bosonic model, consider a state with $N_f/2$ hard-core bosons occupying a subset of N orbitals. Acting with a given term of the SYK Hamiltonian, (4.9), say $J_{ij;kl}$, on such a state produces a non-zero result only if orbitals k and l are occupied, while i and j are empty (or vice versa). It leads to a state with $N_f/2-2$ bosons and 2 broken pairs (i.e. 4 unpaired fermions on orbitals i,j,k,l). Such a state costs energy $2U$ and resides outside of the low-energy bosonic sector. From the point of view of an effective bosonic model, it is a virtual state, which ought to be integrated out. To bring the system back to the bosonic sector one has to act on it with *the same* SYK term, $J_{ij;kl}$. This either brings the system back to the initial state (generating an uninteresting on-site energy shift), or results into hopping of *two* bosons from the orbitals k,l to i,j. The latter option gives rise to the effective bosonic Hamiltonian:

$$H_{\rm b} = -\frac{6}{2U}\sum_{ijkl}^{N} J_{ij;kl}^2 \left[b_i^\dagger b_j^\dagger b_k b_l + b_l^\dagger b_k^\dagger b_j b_i\right], \tag{4.19}$$

where the factor of $6 = 2+4$ is coming from the opposite and same spin terms in the SYK Hamiltonian, correspondingly. There is also a one boson hopping term of the form $\sum_{jk} M_{jk} b_j^\dagger b_k$, where $M_{jk} \propto -\sum_{il}^{N} J_{ij;kl} J_{lj;ki}/U$. Since the two matrix elements here are uncorrelated, the corresponding sum includes N^2 sign alternating terms, implying for a typical matrix element $|M_{ij}| \sim \sqrt{N^2}J^2/(N^3U) = J^2/(N^2U)$. This makes one boson hopping insignificant at large N.

Hamiltonian (4.19) represents a version of the bosonic SYK model [36, 107]. Specifics of our model is that we work with *real* matrix elements $J_{ij;kl}$ and thus there is a *non-random* sign-definite part of the Hamiltonian (4.19), which we call a generalized Richardson model:

$$\begin{aligned} H_{\rm gR} &= -\frac{W}{N^3}\sum_{ijkl}^{N} b_i^\dagger b_j^\dagger b_k b_l \\ &= -\frac{W}{N^3}\Big[B_0^\dagger B_0^\dagger B_0 B_0 - 4B_0^\dagger \hat{N}_b B_0 + 2\hat{N}_b(\hat{N}_b-1)\Big], \end{aligned} \tag{4.20}$$

where $W = 3J^2/32U$ and all indexes i,j,k,l must be distinct. We introduced operator $B_0 = \sum_i^N b_i$ and the boson number operator $\hat{N}_b = \sum_i^N b_i^\dagger b_i$. Employing the

(anti)commutation relations for the hard-core bosons: $b_i^\dagger b_i + b_i b_i^\dagger = 1$ and $b_i^\dagger b_j - b_j b_i^\dagger = 0$ for $i \neq j$, one obtains

$$\begin{aligned} &[\hat{N}_b, B_0^\dagger] = B_0^\dagger; \quad [\hat{N}_b, B_0] = -B_0; \\ &[B_0^\dagger, B_0] = 2\hat{N}_b - N. \end{aligned} \tag{4.21}$$

These operators form the su(2) algebra upon identification $\hat{L}_+ = B_0^\dagger$, $\hat{L}_- = B_0$, $\hat{L}_z = \hat{N}_b - N/2$. One thus finds that: $B_0^\dagger B_0 = \hat{L}^2 - \hat{L}_z^2 + \hat{L}_z$. This observation allows one to solve the Richardson Model [89, 90, 91] with degenerate on-site energies, $H_{\rm R} = -\frac{W}{N} B_0^\dagger B_0$. Let us focus for simplicity on the half-filled model, with $N_b = N/2$ and thus $L_z = 0$. The spectrum of the half-filled Richardson model is thus given by $E_{\rm R}(L) = -WL(L+1)/N$, where the total angular momentum runs $L = 0, 1, \ldots, N/2$. The unique ground state corresponds to $L = N/2$. The degeneracies of the excited states are given by the multiplicity of the corresponding representations:

$$D(L) = \binom{N}{N/2 - L} - \binom{N}{N/2 - L - 1}, \tag{4.22}$$

with the total number of states: $\sum_{L=0}^{N/2-1} D(L) + 1 = \binom{N}{N/2}$, which is the Hilbert space dimensionality for the half-filled hard-core particles.

In the same way one finds the spectrum of the half-filled generalized Richardson model, Eq. (4.20), to be:

$$E_{\rm gR}(L) = -\frac{W}{N^3}[L(L+1) - (N-1)]^2 + \text{const}, \tag{4.23}$$

with the same set of degeneracies, Eq. (4.22). The many-body gap between the ground state, $L = N/2$, and the first excited band with $L = N/2 - 1$ and degeneracy $D(N/2 - 1) = N - 1$ is approaching $W/2$ at large N.

The ground state is $|GS\rangle \propto (B_0^\dagger)^{N/2}|0\rangle$. The corresponding single-particle density matrix ρ_{ij}, Eq. (4.15), has diagonal elements $\rho_{ii} = 1/2$ and off-diagonal ones $\rho_{ij} = \frac{1}{4}\frac{N-2}{N-1}$. Thus its largest eigenvalue is $\lambda_0 = N/4 + 1/2$ (dashed line in Fig. 4.3). The fact that it scales as N signals the presence of ODLRO in the ground state of the generalized Richardson model. The remaining $N - 1$ eigenvalues are degenerate at $\lambda_\alpha = \frac{1}{4}\frac{N}{N-1}$. These features are qualitatively consistent with the exact diagonalization results of

SYK+Hubbard shown in Fig. 4.3 for $U/J = 2$.

To describe the transition from the ODLRO to a normal state at an elevated temperature, one considers the partition function:

$$Z = \sum_{L=0}^{N/2} D(L) e^{-E_{\rm gR}(L)/T} \approx \int_0^{1/2} dl\, e^{-N f(l)/T}, \tag{4.24}$$

where we introduced $l = L/N$, substituting summation with the integration, and the free energy density, Fig. 4.9, is defined as $f(l) = \lim_{N\to\infty}(E_{\rm gR}(l) - T \ln D(l))/N$:

$$\begin{aligned} f(l) &= -W l^{\gamma} \\ &+ T\left[(1/2-l)\ln(1/2-l) + (1/2+l)\ln(1/2+l)\right], \end{aligned} \tag{4.25}$$

where $\gamma = 4$ for the generalized Richardson model.

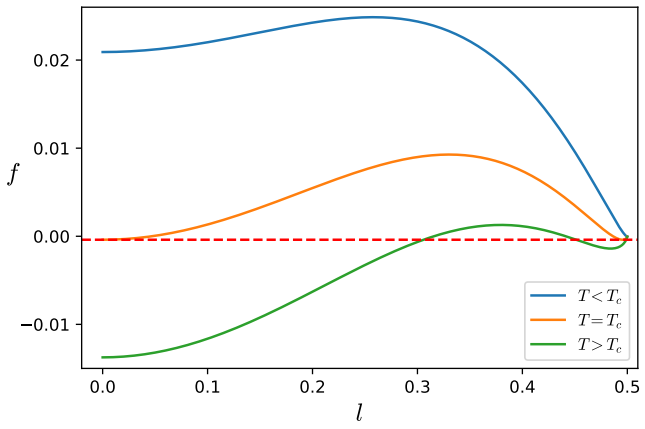

Figure 4.9: The free energy density of the generalized Richardson model, $f(l)$, Eq. (4.25), vs. scaled "angular momentum" $l = L/N$ for different temperatures.

In the large N limit, the integral in Eq. (4.24) is dominated by the minima of $f(l)$. The latter changes from being $l = 1/2$ at $T = 0$ to $l = 0$ at $T_c/W = 1/16 \ln 2 \approx 0.09$, where the model undergoes the first order transition to a state with no ODLRO. This behavior is illustrated in Fig. 4.10, which shows results of the exact diagonalization for the generalized bosonic Richardson model, Eq. (4.20). The crossing point at $T/W \approx 0.1$

marks the first order transition, were ODLRO jumps from 1/4 to zero in the $N \to \infty$ limit. This should be compared with the exact diagonalization of the SYK+Hubbard model shown in Fig. 4.4.

It is instructive to compare this behavior with that of the conventional Richardson model, $H_{\rm R} = -\frac{W}{N} B_0^\dagger B_0$, whose partition function is again given by Eqs. (4.24), (4.25) with $\gamma = 2$. The latter model may be seen to undergo a *continuous* phase transition at $T_c = W/2$. This model with $W = U$ is exactly the pure pair hopping model, Eq. (4.13).

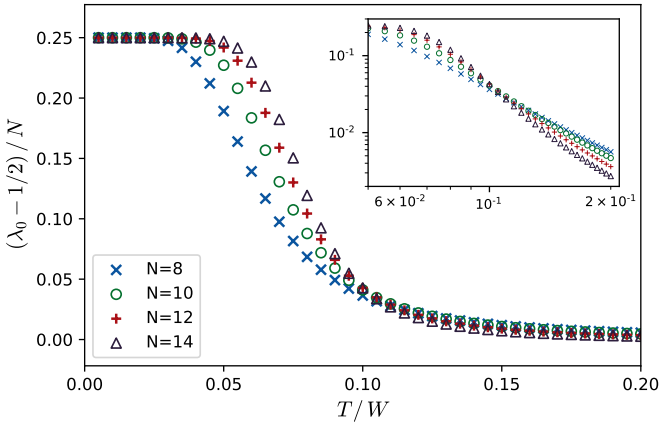

Figure 4.10: ODLRO vs. temperature for the generalized Richardson model, Eq. (4.20). Inset: vicinity of the crossing point. Compare with Fig. 4.4 for the SYK+Hubbard model.

One may worry if the generalized Richardson model, Eq. (4.20), is a reasonable approximation for the low-energy bosonic model (4.19). To answer this question one needs to examine the role of the random part of $J^2_{ij;kl}$ in Eq. (4.19). This random part removes degeneracies, Eq. (4.22), between excited states with $L < N/2$, transforming them into the bands. Let's focus on the lowest such band with $L = N/2 - 1$, consisting of $N - 1$ states. One can write an effective model for this band as $(N-1) \times (N-1)$ matrix Hamiltonian with the random elements h_{rs}. Their variance can be estimated from the fact that a matrix element h_{rs} is given by a sum of N^4 random sign terms each of the order W/N^3. As a result, $\langle h_{rs}^2 \rangle \sim N^4 (W/N^3)^2 = (W/N)^2$. The density of states of such random matrix is given by a semicircle with the bandwidth $\sqrt{N} W/N = W/\sqrt{N}$. Since the gap between the band and the ground-state scales as W, the latter remains

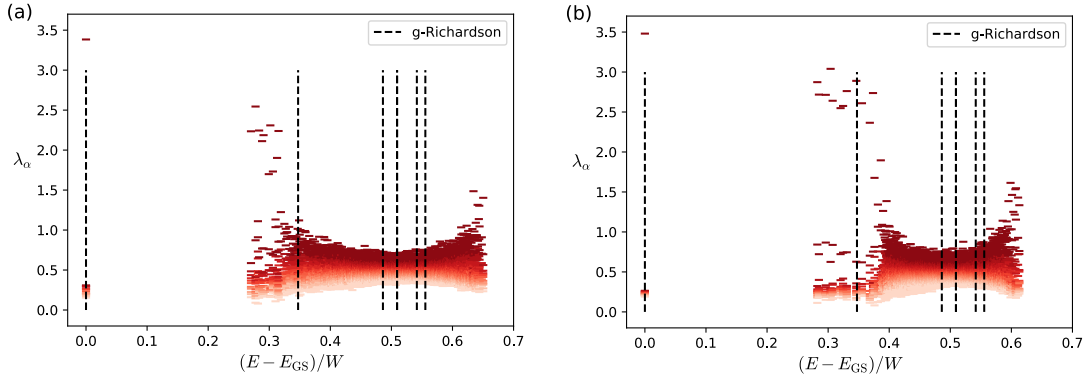

Figure 4.11: Spectra of $\langle n|b_i^\dagger b_j|n\rangle$ for each many-body state $|n\rangle$ vs. it's energy, $E-E_{\rm GS}$, for (a) SYK+Hubbard at half-filling and (b) effective low-energy bosonic theory with the Hamiltonian (4.19). Both (a) and (b) have the same $J_{ij;kl}$ realization in case $N=12$ with $U=2J$. Black dashed lines are energies of the generalized Richardson model, Eq. (4.23).

well separated as long as $N \gg 1$ even for the random model, Eq. (4.19), see Fig. 4.11.

We thus conclude that the generalized Richardson model, Eqs. (4.20)-(4.25), provides an accurate description of the low-energy sector of the SYK+Hubbard model for $U \gg J$. It predicts ODLRO at low temperature. The many-body gap and critical temperature both scale as J^2/U with the large ratio between the two, $8\ln 2 \approx 5.55$ (cf. with the BCS gap to T_c ratio of 3.53). An enhancement of this ratio is also known in the context of quantum critical models [108], holographic superconductors [109] and other SYK-like models [86, 82]. These features are qualitatively consistent with the exact diagonalization results for the moderate N SYK+Hubbard model. The single-particle fermionic excitations are separated by a larger gap $\sim U$. It is important to notice that the full bandwidth of the bosonic states is $NW/16 = 3NJ^2/512U$. The requirement for the Richardson model to be quantitatively accurate is $U > 3NJ^2/512U$, i.e. $U \gtrsim \sqrt{N}J/13$. This condition is satisfied for Figs. 4.3, 4.4 and 4.8.

4.6.2 Pseudogap and the quantum Kuramoto model

We turn now to the opposite limit of $U \ll J$, where there is no separation between bosonic and fermionic sectors. To describe this limit, we notice that the action (4.17)

exhibits a non-trivial saddle point with $|\Delta_i| = |\Delta| \propto Je^{-J\sqrt{\pi}/(8\sqrt{2}U)}$, Eq. (4.18). However, the phases, ϕ_i, of the local order parameters, $\Delta_i = |\Delta|e^{i\phi_i}$, are not fixed by the saddle point equations. They constitute thus the soft degrees of freedom, which are (almost) free to fluctuate. Such fluctuations are capable of destroying ODLRO, despite presence of the non-zero $|\Delta|$, even in the $N \to \infty$ limit.

The action which governs the low-energy dynamics of the local phases is given by:

$$S[\phi_i(\tau)] = \int d\tau \left[\frac{m}{2} \sum_i^N \dot{\phi}_i^2 - \frac{g}{N} \sum_{i<j}^N \cos(\phi_i - \phi_j) \right]. \tag{4.26}$$

The second term of this action is derived in details in Appendix B.2, where it is shown that the coupling constant $g = \overline{g_{ij}}$ is the average value of the off-diagonal Cooper susceptibility, $g_{ij}/N = |\Delta|^2 \partial^2 E_{\rm GS}/\partial\bar{\Delta}_i \partial\Delta_j$. It reflects the shift of the ground state energy, $E_{\rm GS}$, in response to an extra term in the Hamiltonian of the form $\bar{\Delta}_i c_{i\uparrow} c_{i\downarrow} + h.c.$. As shown in Appendix B.2, $g \sim |\Delta|^2/J$, with the mean-field pairing field $|\Delta|$ given by Eq. (4.18). The first term in Eq. (4.26) may be obtained by performing the local gauge transformation in the trace logarithm term in Eq. (4.17) with the unitary operator $\mathcal{U}_i = \exp\{i\phi_i\sigma_3/2\}$. The latter eliminates dynamic phases of the Δ_i, but brings the local chemical potential $\mu_i = \dot{\phi}_i/2$. The first term in Eq. (4.26) is the second order expansion of the action in such μ_i. As a result, the coupling constant, $m = \overline{m_i}$, is given by the average value of the local compressibility $m_i = -\partial^2 E_{\rm GS}/\partial\mu_i^2$, that is the susceptibility of the ground-state energy to a local chemical potential, entering the Hamiltonian as $-\mu_i c_{i\sigma}^\dagger c_{i\sigma}$. In the $|\Delta| = 0$ case it was evaluated in Ref. [[110]] and found to be $m \approx 1.04/J$. We do no expect it to be significantly affected by the presence of small $|\Delta|$.

The action (4.26) describes a quantum version of the celebrated classical Kuramoto model [93, 94, 95, 96, 97, 98, 99, 100, 101, 102, 103]. The latter was proposed [93] to describe synchronization of coupled non-linear oscillators. It's quantum version, Eq. (4.26), may be interpreted as N-body quantum mechanics of particles with mass m and coordinates ϕ_i, residing on the unit circle and interacting via all-to-all cos-potential. The synchronized phase of the classical Kuramoto model is analogous to a ϕ-localized ground state wavefunction of this quantum mechanics. Within the SYK+Hubbard

model such synchronized phase means globally phase-coherent superconductivity with ODLRO. Below we show that the synchronized phase of the quantum Kuramoto model, Eq. (4.26), emerges above some critical coupling $g > g_c$ (i.e. at $U > U_c$) as a continuous QPT.

Since the ground state is expected to be symmetric with respect to particle permutations, it may be thought of as a Bose condensate. Due to all-to-all nature of the interactions, the Bose condensation in the large N limit is accurately described by the Gross-Pitaevskii equation. In the present context it takes the non-local form:

$$-\frac{1}{2m}\frac{\partial^2\Psi(\phi)}{\partial\phi^2}-\frac{g}{N}\int_0^{2\pi}d\phi'\,|\Psi(\phi')|^2\cos(\phi'-\phi)\Psi(\phi)=\mu\Psi(\phi), \tag{4.27}$$

where the condensate wave-function is normalized as $\int_0^{2\pi}d\phi\,|\Psi(\phi)|^2=N$ and obeys the periodic boundary conditions, $\Psi(2\pi)=\Psi(0)$. Employing separability of the exponential potential, $e^{\pm i(\phi'-\phi)}$, one may reduce the non-linear equation (4.27) to the linear Mathieu equation:

$$-\frac{1}{2m}\frac{\partial^2\Psi(\phi)}{\partial\phi^2}-g\rho_1\cos(\phi)\Psi(\phi)=\mu\Psi(\phi), \tag{4.28}$$

supplemented with the self-consistency condition

$$\rho_1=\frac{1}{N}\int_0^{2\pi}d\phi'\,|\Psi(\phi')|^2\cos\phi', \tag{4.29}$$

where ρ_1 the first Fourier harmonics of the normalized condensate density, $|\Psi(\phi')|^2/N$. The strategy is to find a ground state wave-function of the Mathieu equation (4.28) for a given amplitude of the cos-potential, $g\rho_1$, and substitute it into the self-consistency condition (4.29) to find ρ_1. A trivial solution, $\rho_1=0$, with the uniform condensate, $\Psi=\sqrt{N/2\pi}$, and $\mu=0$ exists for any g. A non-trivial solution with $\mu<0$ requires $g>g_c$.

To find the non-trivial solution, one notices that the right hand side of Eq. (4.29) is an odd function of $g\rho_1$. Its behavior at small $g\rho_1$ may be found from the first order perturbation theory for the Mathieu equation (4.28), yielding the linear slope $2mg\rho_1$. On the other hand, at large $mg\rho_1\gg 1$ the ground state wave function of Eq. (4.28) is a

narrow Gaussian, centered at $\phi = 0$. This implies that the right hand side of Eq. (4.29) saturates to one for $mg\rho_1 \gg 1$. As a result, Eq. (4.29) is the standard mean-field equation for a second order transition with the order parameter ρ_1. It yields a finite order parameter $\rho_1 \propto \sqrt{g - g_c}$ for $g \gtrsim g_c$ with $g_c = 1/2m \approx 0.48J$, Fig. 4.12.

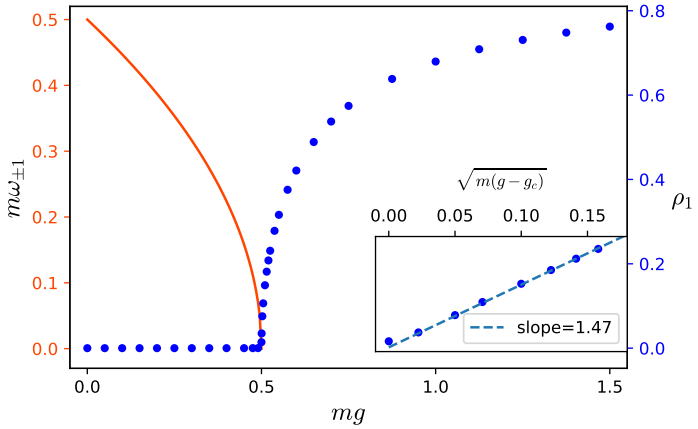

Figure 4.12: Numerical solution of Eqs. (4.28) and (4.29) for the order parameter, ρ_1, of the quantum Kuramoto model (dots). The solid line is the frequency of the lowest Bogoliubov mode with $l = \pm 1$ for $mg < 1/2$. Inset demonstrates $\rho_1 \propto \sqrt{g - g_c}$ scaling for $g > g_c$, which shares the scale of y-axis with outer (dots) plot.

An alternative way to determine g_c is to investigate a spectrum of linearized fluctuations on top of the uniform solution, $\Psi(\phi, t) = \sqrt{N/2\pi} + \sum_l \psi_l e^{il\phi - i\omega_l t}$, where $l = \pm 1, \pm 2, \ldots$ labels angular momentum components. Substituting this into the time-dependent Gross-Pitaevskii equation, Eq. (4.27) with $i\partial_t \Psi$ on the right hand side, and linearizing it with respect to ψ_l, one finds the spectrum:

$$\omega_{\pm 1} = \sqrt{\left(\frac{1}{2m}\right)^2 - \frac{g}{2m}}; \qquad \omega_{|l|\geq 2} = \frac{l^2}{2m}. \tag{4.30}$$

Therefore for $g > g_c = 1/2m$ the frequency of the $l = \pm 1$ components becomes imaginary, indicating instability towards a non-uniform condensate. This expression shows that the continuous QPT is indeed associated with the time-scale $\omega_{\pm 1}^{-1} \propto |g_c - g|^{-z\nu}$, which is divergent at the transition with the Gaussian exponent $z\nu = 1/2$.

We thus conclude that the quantum Kuramoto model exhibits the synchronized

phase for $mg > 1/2$, where the local phases, ϕ_i, are coalescing. In the large N limit this spells spontaneous breaking of the $U(1)$ symmetry. In terms of the SYK+Hubbard model these observations translate into formation of ODLRO for $U > U_c$, where, employing Eqs. (4.18) and (B.31), $U_c \approx J\sqrt{\pi}/(4\sqrt{2}\log C_2)$, see Appendix B.2. The quantum Kuramoto model synchronization transition is indeed seen in the exact diagonalization of the SYK+Hubbard model, Fig. 4.6, as the continuous QPT at $U = U_c$.

For $U < U_c$ the on-sites phases ϕ_i fluctuate freely and prevent formation of the global ODLRO. This phenomenon renders the mean-field treatment of Sec. 4.5 grossly inadequate for $U < U_c$ and leads to creation of the *pseudogap* phase. It does *not* exhibit neither ODLRO nor the many-body gap within a sector with a fixed N_f. On the other hand, there is still an even-odd alternation in the ground state energies of the sectors with successive N_f's. This phenomenon may be clearly seen in the $U > J$ case in Fig. 4.8. It seems to persist all the way down to $U < U_c$, though the statistical fluctuations make it hard to extract the it's quantitative value. This means that there is a gap in the *single-particle* density of states (indeed, the latter requires transitions between states with N_f and $N_f - 1$ particles). Therefore from the transport perspective, the pseudogap state is characterized as a narrow gap insulator. Correspondingly the Kuramoto QPT should be termed an insulator–superconductor one.

The line $2\pi T \approx \omega_{\pm 1}$, Eq. (4.30), spells the boundary of the quantum critical regime. If $2\pi T < \omega_{\pm 1}$, the quantum Kuramoto phase fluctuations, governed by $\langle e^{i\phi_i(\tau)} e^{-i\phi_i(0)} \rangle = e^{-\omega_{\pm 1}|\tau|}$, are averaged out to zero. This leads thus to the familiar SYK non Fermi liquid fermionic correlations. However, for $\omega_{\pm 1} < 2\pi T \lesssim |\Delta|$ the imaginary time circle is too short to completely wash out the superconducting correlations. This creates an interesting quantum critical scenario, where superconducting correlations show up as a finite temperature effect.

4.7 Conclusion for the SYK superconductivity

Following the earlier studies [82, 83, 84, 85, 86, 87, 88], we found that the spin-full version of the SYK model with extra attractive interactions may exhibit ODLRO and superconductivity. Furthermore we found that details of this extra attraction are crucially important in dictating the global phase diagram of the model. The previous

studies focused on an effective all-to-all attraction, which conform to the large N mean-field treatment. The pair hopping interaction calls for superconducting instability of the non-Fermi liquid groundstate at an arbitrarily weak attraction. This is indeed the case for the SYK+pair hopping model briefly considered here.

Our main finding is that a local attraction, such as on-site negative U Hubbard term, leads to a qualitatively different scenario of the superconducting transition. In this case the physics is dictated by quantum fluctuations of local phases. They destroy ODLRO in a sizable part of the phase diagram, confining the superconductivity to a dome-like region, Fig. 4.7. In particular, they lead to the pseudogap phase at small U and the continuous QPT to the superconducting phase at $U = U_c$. These features are described by the quantum version of the celebrated Kuramoto model. At strong attraction, the local nature of the attractive interactions is also of crucial importance, resulting in $T_c \sim U^{-1}$ scaling of the transition temperature. This limit is mapped on the Richardson-like model with two-boson hopping. Its exact solution predicts the first order transition at $T = T_c$ from ODLRO state into a bosonic insulating state. The latter consists of fermions, paired with the binding energy $U \gg T_c$, forming a gas of incoherent bosons. Fermionic transport in this state is suppressed as $e^{-U/T}$.

The natural question is if the superconducting version of the SYK model admits a holographic interpretation. We have presented some thoughts in these direction in Appendix B.4. There we discuss a possible holographic interpretation of the fluctuation-dominated SYK + Hubbard superconductivity in terms of the "bulk" description.

We list now some of the open questions raised by our study: (i) What are fermionic correlation functions in the pseudogap phase at $U < U_c$? The naive answer is that they are the same as in the non-Fermi liquid SYK model. Yet, contrary to SYK, fermions interact with the dynamical phases as $|\Delta|e^{i\phi_i(\tau)}c_{i\downarrow}c_{i\uparrow} + h.c.$, where the phases, $\phi_i(\tau)$, are governed by the Kuramoto quantum mechanics, Eq. (4.26). Close to the QPT this dynamics becomes increasingly slow, Eq. (4.30), and may significantly alter the fermionic correlation functions.

(ii) What are the implications of our 0D treatment for the array geometry? In particular, is the dome-like phase diagram, Fig. 4.7, applicable to arrays and how it depends on the coupling (hopping) strength between the dots in the array?

(iii) Is there an interaction and an interplay between the phases, governed by the

Kuramoto and the reparametrization modes [6, 16], governed by the Schwarzian action? The latter modes are described by the Liouville quantum mechanics [16], which predicts metal-insulator crossover at the energy scale J/N. For a finite N this energy scale may compete with the many-body gap $|\Delta|^2/J$, possibly affecting the insulator-superconductor QPT [78].

(iv) An interesting generalization is a model with a weak time reversal symmetry breaking parameter. In the Richardson model such generalization leads to the Russian Doll (RD) model, Appendix B.3, which is known to be integrable. One may expect that deformed in this manner the large U generalized Richardson is also integrable. SYK corresponds to the completely degenerate local Richardson parameters, $\epsilon_i = 0$, which means that holographically all flavor branes are sitting on the top of each other in the IR and the $SU(N)$ symmetry is classically unbroken. Generic values of ϵ_i correspond to displacements of flavor branes in the radial coordinate in the holographic treatment of Richardson or RD models. It would be interesting to elucidate the role of non-vanishing local parameters, ϵ_i, in the generalized Richardson model.

(v) The quantum Kuramoto mechanism of the condensate formation could fit within a more general framework. In particular, an intermediate pseudogap phase is believed to exist in the thermal QCD below the deconfinement phase transition, where the local phases of the chiral condensate are disordered. The synchronization of the chiral phases leading to formation of the homogeneous chiral condensate may occur in a Kuramoto-like way. Indeed as shown above, at the $1/N$ order the near-horizon gravity (RG) dynamics induces the Kuramoto potential for phases of the local Cooper pairs. Formation of the chiral condensate in the holographic QCD, being also a near-horizon effect, may thus lead to a non-abelian generalization of the Kuramoto potential for the exciton pairs.

Chapter 5

Many-body localization and quantum optimization

In this chapter, we will go back to the glassiness side of the disordered system. In Chapter 3, we argue that the SYK resembles as metal (even through a strange one) rather than glass. Due to the feature of strongest scrambling (short time) and thermalization (long time) in SYK type models, one may even imagine that if we have a glass material to start with, once we add the SYK type scrambling effect, the glass may somehow be "melted". In Sec. 5.1, we will demonstrate how this melting effect could happen in Hilbert space (rather than the real space). In addition, we will associate this effect as a type of Anderson (de-)localization in many-body system (MBL).

Anderson localization was first proposed by Anderson 1958 for single particle disordered electronic system [3]. A moving particle which can spread out the whole system in clean system, might be trapped around certain impurities if the disorder strength is strong enough. The phase of localization could be established, if the ergodicity of the movement of particles is destroyed. About 40 years later, people realize, even though the original proposal of localization was established in single particle picture, with the existence of interaction (which is more realistic), the localization phase is still stabilized. One of the typical example is the Ising type spin-glass. With both strong disorder and interaction, the system has plenty of meta-stable states. In practically, if one cools down a liquid very fast down to extremely low temperature, the system will have very little

chance to goes to the true ground state, but some meta-stable. We will demonstrate a spin-glass system in Sec. 5.2, its field theory and so on.

Except the interesting nature of glassy system as a MBL phase, people also find important application of the glassy system. People find that many realistic optimization problems, could be mapped to a glassiness Hamiltonian. That is to say, if one wants to find the lowest cost to do a certain realistic job, it turn out to be finding the ground state of the corresponding Hamiltonian. Unluckily, most treasurer job people wants to achieve, map to a Hamiltonian has a glass phase at low temperature, which means find the ground state (GS) of the Hamiltonian is certainly a very hard job. The how hard typically is? It is NP hard, which means you typically need exponentially long time in its systems size to find the GS. With the greedy to find the optimal solution with its shortest time, people thinks to "melt" the glass even at zero temperature, and utilize the "melting" feature to find the GS. This idea turn out to be the quantum annealing, a specific type of quantum computing which aiming to find the (at least approximate) GS state and GS energy with quantum adiabatic/diabatic evolution. This will be the main topic in Sec. 5.3.

5.1 Many-body localization in Hilbert space for deformed SYK model

As discussed in previous chapters, we understand that the many-body random matrix with 4-point interacted Majorana fermions, i.e. SYK_4 which has form

$$H_{\mathrm{SYK}_4} = \sum_{i<j<k<l} J_{ijkl}\, \chi_i\chi_j\chi_k\chi_l, \quad \text{with } \langle J_{ijkl}^2\rangle = J^2/N^3 \tag{5.1}$$

is maximally chaotic and obey many-body Wigner-Dyson statistics Fig. 2.2. Family of SYK model basically share the same property of maximally chaotic as SYK_4 except for SYK_2 [14], which consist only 2-point interaction. People may wondering that, albeit SYK_2 by definition is a random matrix with its spectrum follows Wigner-Dyson statistics, it is naturally non-chaotic. Truth be told that, the single particle spectrum of SYK_2 follows Wigner-Dyson statistics, while its many-body eigen-state, which build from the Slater determinate of the single-body eigen-states, obeys Poisson distribution.

This also could be understood that, these disordered single particle spectrum, is nothing but the Fermi-liquid (or gas actually) type excitations and the system is fully integrable. To be specific, the SYK_2 has Hamiltonian

$$H_{\mathrm{SYK}_2} = i \sum_{1<i<j<N} K_{ij}\chi_i\chi_j \quad \text{with } \langle K_{ij}^2\rangle = K^2/N \tag{5.2}$$

(be careful with the i in front of summation is the imaginary unit). The many-body spectrum of SYK_2 can be constructed by single particle states which is the eigenstates of K_{ij}, shows it integrable nature. Now we have a nature question to ask: if we have both SYK_4 and SYK_2, should we have chaotic system or integrable system?

The answer depend on the relative strength between SYK_4 and SYK_2, and one defined the full Hamiltonian as

$$H_{\text{SYK-deformed}} = \sum_{i<j<k<l} J_{ijkl}\chi_i\chi_j\chi_k\chi_l + u\sum_{i<j} i\,K_{ij}\chi_i\chi_j \tag{5.3}$$

We want to investigate chaotic-integrable transition when tuning the relative strength u. This can be analyzed by checking level statics, OTOC [57] and spectrum form[49, 56]). In this section, we would present the view that this chaotic-integrable transition maybe understood as many-body localization [111, 112, 113], and the MBL should happen in the many-body Fock space of this deformed SYK model. Summarize in words, we view this zero dimensional SYK_4+SYK_2 as an Anderson model in Fock space [111]. and SYK_2 as non-interacting H_0 spanned the Hilbert space, and SYK_4 as interaction part V to mixing the states in the Hilbert space.

To be more specific on the MBL in Hilbert space, we should start from non-interacting system H_0, and view eigenstates of SYK_2 to be building sites of Fock space. Once choose a site (i.e. a state of SYK_2) as a initial location of the system without V, the system will stay at this state forever, and this is the notion of localization at certain site (or state). Then turn on the interaction term V, states of SYK_2 no longer be the eigenstates of the full Hamiltonian $H = H_0 + u\,V$, but start to hop on other sites and sooner become some linear combination of states of SYK_2. It can be view as states willing to spread out on the many-body Fock space lattice due to interaction term V coming from SYK_4. By tuning relative strength between SYK_4 and SYK_2, one may

expect that if u is small, the system would prefer to be localized at original SYK_2 state. While at large u would make the eigen-state of the deformed system sitting on all Fock space sites with equal probability, which reflect chaotic nature of SYK_4.

Due to particle number parity, the matrix of Hamiltonian splits to two block which do not talk to each other. And we will only focus on one of the block which has dimension $D = 2^{N/2-1}$. The eigenstates of SYK_2 is denoted as $|\mu\rangle$, with μ labeled from 1 to D. The eigenstates of the full Hamiltonian $H_{\text{SYK-deformed}}$, is labeled by its eigen-energy with notation $|E\rangle$. Here we use E as scaled energy compare to GS, i.e. $E \to E/|E_{\mathrm{GS}}|$ (e.g. GS in the scaled form has $E = -1$.). The overlap between $|\mu\rangle$ and $|E\rangle$, i.e. $\psi_E(\mu) = \langle\mu|E\rangle$ should be viewed as wavefunction which is the configuration of spreading on SYK_2 lattice. We now can investigate how wavefunction $\psi_E(\mu)$ look like, by using the inverse participation ratio (IPR). IPR is a standard signature to distinguish extend/localized state and we present the result in the following section.

5.1.1 IPR and proper scaling

By exact diagonalizing the full Hamiltonian 5.3 with certain parity, one can directly calculate the IPR by the wavefuntion $\psi_E(\mu)$ as following

$$\mathrm{IPR}(E) = \sum_{\mu=1}^{D} |\psi_E(\mu)|^4 \tag{5.4}$$

where we normalized $\sum_{\mu=1}^{D} |\psi_E(\mu)|^2 = 1$. And we understand that for fully localized state, only one site is occupied, with IPR = 1, while for fully delocalized state, every site is occupied equally, with IPR $= 1/D$, i.e.

$$\mathrm{IPR} = \begin{cases} 1 & \text{wavefunction fully localized} \\ 1/D & \text{wavefunction fully delocalized} \end{cases} \tag{5.5}$$

In Fig. 5.1(a), we plot IPR as function of total energy E when fixing relative strength u. The ground state of the system is always fully localized with IPR= 1. When increasing the energy from GS to the center of band, the IPR decrease and has strong system size dependence. Larger the system size, smaller the IPR, may indicate a extend phase

around the center of band. In addition to the discorded averaged value of IPR, we also investigate the distribution function of IPR as shown in Fig. 5.1(b). It has three different types of distribution denoted in red, blue and purple, refers to different total energy E corresponding to ground state (GS, $E = -1$), crossover region (Crossover, $E = -0.6$) and center of band (Center, $E = 0$), respectively. Distribution of IPR for GS is peaked at 1 with narrow width, which means wavefunction is almost fully localized only at one site; Distribution of IPR for center of band is peaked just above zero, with average of IPR close to $1/D$, which means wavefunction is spread out for the whole Fock space lattice. For distribution of IPR around the crossover region, one may identify two separate peaks, which indicating the wavefunction may be contributed by two parts: there is one specific site that wavefunction strongly (with finite large probability but smaller than 1) localized on, while rest of sites are spreaded with equal probability. This may indicate a coexist region at crossover.

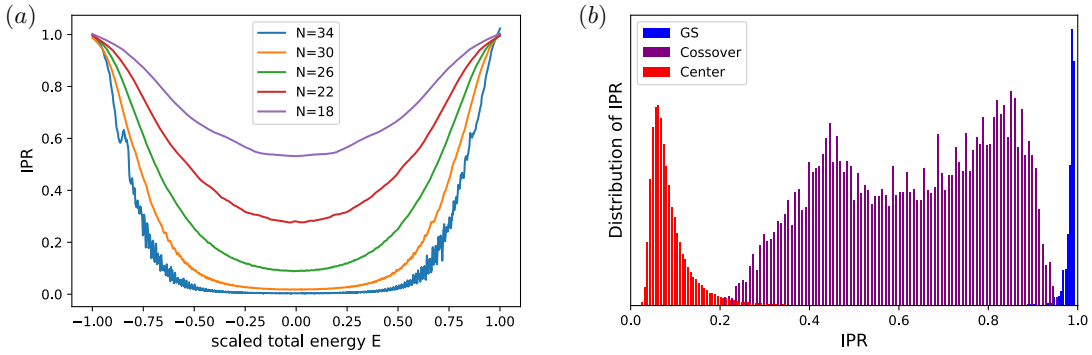

Figure 5.1: (a) IPR vs scaled total energy for different $N = 18, 22, 26, 30, 34$ (GUE) with fixing $u = 5$. (b) Distribution function of IPR when fixing energy around ground state(blue), crossover region (purple) and center of band (red) with different realizations at $N = 26$.

All these features seemingly indicate that there may be a mobility edge E_c separate extended/localized phase at certain u. But as shown in Fig. 5.1(a), no crossing point to identify mobility edge E_c as one change different system size. This may indicate two different scenarios (i) the system only exhibit crossover as IPR always smoothly decreasing from 1 to $1/D$ at even infinite N. (ii) the system exhibit a MBL transition, not for fixed u, but for a properly scaled u with system size. In order to investigate the

probability for scenario (ii), i.e. a transition exists, we want to have some method to pin point the "transition point". We may distinguish extended/localized states at finite N by calculating the width of the distribution of IPR, i.e. the second moment of IPR $\sigma^2_{\mathrm{IPR}} = \langle \mathrm{IPR}^2 \rangle_{\mathrm{dis}} - \langle \mathrm{IPR} \rangle^2_{\mathrm{dis}}$, where $\langle \cdots \rangle_{\mathrm{dis}}$ refers to average over different realizations. Fig. 5.2(a) shows, there are two maximum value of σ_{IPR} which indicate a mobility edge E_c separate localized and extended states. This means for a system size N, at relative strength u, $|E| > E_c$ is localized phase while $|E| < E_c$ is de-localized phase. We also notice, for fixed u with different system size N, the peak in the fluctuate σ_{IPR} are locate in different E_c. We rescaled the relative strength u with system size N to be $\tilde{u}(N)$ as

$$\tilde{u}(N) = W(u)/W(2D), \tag{5.6}$$

where $W(u)$ is Lambert W function defined as $W(u) = v$ with $u = ve^v$. With this scaled relative strength $\tilde{u}(N)$, one can collapse all the mobility edge E_c on a single 'critical' curve with different system size, see Fig. 5.2(b). On the phase diagram of $\tilde{u}(N)$ vs E, this curve is nothing but the separation of the localized states (upper left of the 'critical' curve) and the delocalized states (lower right of 'critical' curve). This result also coincide with the analytical result in reference [114], where they find in the center of the band (which means u is large), $u_c \sim \exp(N/2)$ which means $\tilde{u_c} \sim \log(u_c)/N$, just the asymptotic form at large u of proper scaling $\tilde{u}(N)$ as we used.

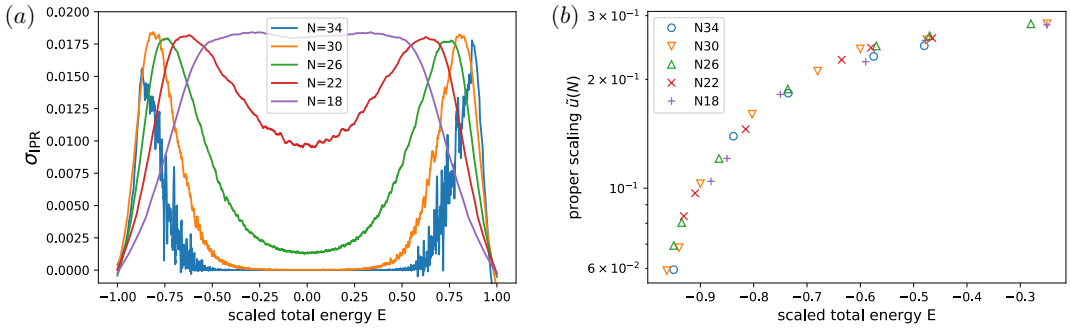

Figure 5.2: (a) σ_{IPR} has two peeks at certain energy, which refer to transition points from localized phase to extended phase. (b) All transition points collide on single line with proper scaling function $\tilde{u}(N)$. Lower than the critical line is extended phase, while upper part is localized phase.

As consequence, when we use this proper scaling of u of N, plotting IPR vs $\tilde{u}(N)$ will have a crossing point for different system sizes as shown in Fig. 5.3(a). These IPR curves get sharper when enlarge system size, which indicate phase transition rather than crossover from localized states to extended states when tuning u.On the other hand, one can use the same scaling to deal with level statistics. Calculating nearest neighbor energy gap ratio [113]

$$r_\mu = \max\left\{\frac{\Delta E_\mu}{\Delta E_{\mu+1}}, \frac{\Delta E_{\mu+1}}{\Delta E_\mu}\right\} \tag{5.7}$$

where $\Delta E_\mu = E_\mu - E_{\mu-1}$. Plot r vs properly scaled $\tilde{u}$, there is also a crossing point for different N, no matter what total energy E the state stay in, as shown in Fig. 5.3(b).

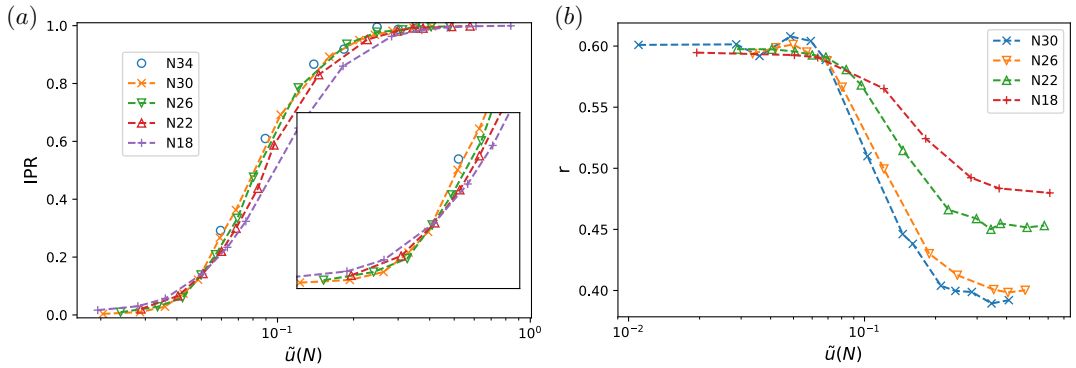

Figure 5.3: (a) IPR vs proper scaling $\tilde{u}(N)$ have one single crossing point when fixing E. This plot shows the case for $E = -0.93$. Insert: clear version of crossing. (b) r vs proper scaling $\tilde{u}(N)$ have one single crossing point. Case for E=-0.88.

5.1.2 Phase diagram and non-ergodic extended phase

By using properly scaled relative strength $\tilde{u}$, we find the curves of IPR vs $\tilde{u}$ as well as r vs $\tilde{u}$ cross at one single point with different system sizes which indicate a phase transition. For physical meaning of each, we say IPR crossing point separate extended states and localized states (i.e. delocalization-localization transition), while r curve crossing point separate chaotic states and integrable states (i.e. chaotic-integrable transition). But as shown in Fig. 5.4, these two critical curves match with each other, which enrich the regimes of the full phase diagram. Above the blue curve (dots), the states are

in the localized phase. Below the red curve (dots), the states are extended which understood by IPR will eventually decrease to zero when have large enough N and level statistics is Wigner-Dyson means chaotic. This region we called ergodic, in the sense the wavefunction spread out the total Fock space.

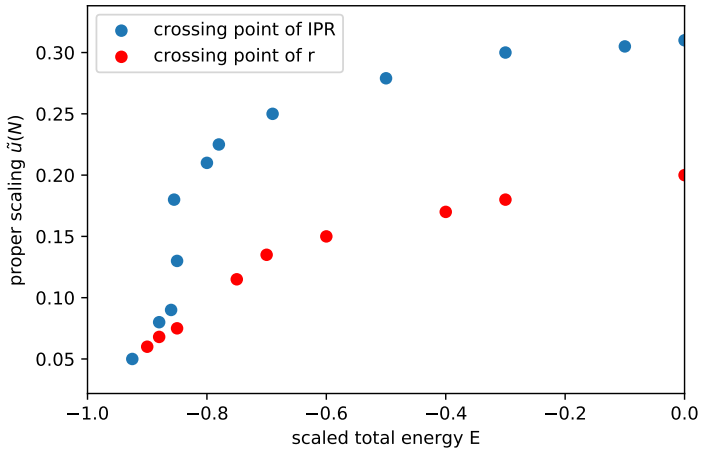

Figure 5.4: Phase diagram of this deformed SYK model. Blue dots separate localized and extend phase. Red dots separate integrable and chaotic phase. Between these two colored lines is the non-ergodic extend phase.

The new region between two phase transition curves as would be explained, could be called as non-ergodic extend region. In order to verify the property of the states in this region, we pick a specific state inside this non-ergodic extend phase with different system size N, see Fig. 5.5. The IPR of this state getting down when enlarge N which means extensiveness since we expect IPR eventually go down to zero. While its level statistics is Poisson type, where level repulsion becomes weak when increasing N.

At this stage, we may understand the existence of non-ergodic extended phase in following way. As suggested in reference [111], the structure of the many-body Fock space may resemble a Cayley tree. So transition we discussed in the deformed SYK model may be view as single particle Anderson transition on the Cayley tree. In reference [62, 115], people find fractal behavior of eigenstates for Anderson model on RRG and Cayley tree, which is the indication of the non-ergodic extended states. In the simple Cayley tree picture, if one choose to have a state occupied on one of the branches of the tree, this state could spread out for a finite friction of the whole lattice space which

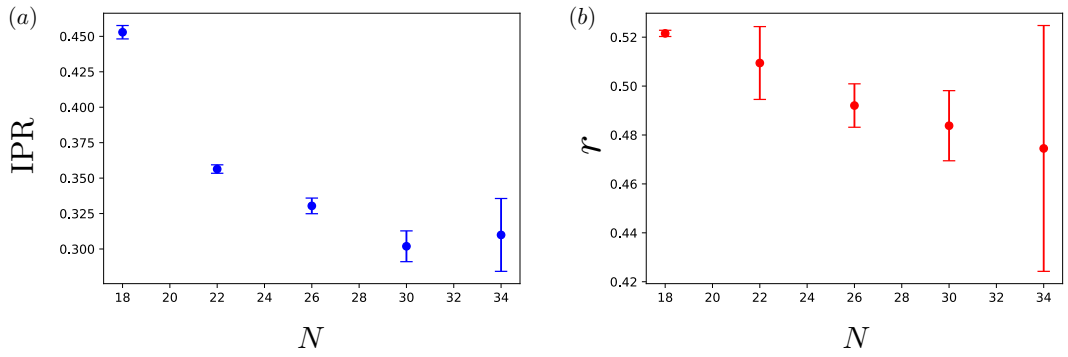

Figure 5.5: (a) Verify IPR property of state in non-ergodic extend phase, IPR goes down with larger N means extended. (b) Verify r property of state in non-ergodic extend phase, r goes down with larger N means non-ergodic.

is extended. While, choosing two states occupied two different branches, these two do not overlap sufficiently with each other, which indicating no level repulsion between them even if these two states may closed in energy space. As a consequence, there is no contradiction between non-ergodic and extended phase.

5.2 Many-body delocalization in spin-glass

In this section, we will discuss the many-body delocalization transition in spin-glass systems. We understand that a glass system has exponentially many meta-stable states, and has high possibility to stuck at one of them when they are prepared in experiment, which refers to be a many-body localized state. To be concrete, let's consider a spin-glass model with all to all interaction among different sites with Hamiltonian

$$H_{\mathrm{SK}} = \sum_{ij}^{N} J_{ij}\sigma_i^z\sigma_j^z, \tag{5.8}$$

where J_{ij} are random interaction $\langle J_{ij}^2\rangle = J/N$. With scaling $\langle J_{ij}^2\rangle \sim 1/N$, the low energy states have their energies proportional to N (even though typical states energy is proportional to $\sqrt{N}$), and we define the scaled energy $\epsilon = E/(NJ)$. One can find

that the density of states for the spin-glass model follows Gaussian distribution:

$$\mathrm{DOS}(\epsilon) \propto \exp\left[-\frac{(E/J)^2}{N}\right] = \exp[-\epsilon^2]. \tag{5.9}$$

This model have become paradigms for the mean-field theory of spin glasses, with its name Sherrington-Kirkpatrick (SK) model [4]. At high temperature, the system has paramagnetic phase since the polarization of the spins are proportional to the external field. While at low temperature, the free-energy landscape in spin-configuration is non-concave function, and have many local minimums in energy space which represent meta-stable states. The vertical line in Fig. 5.6(a) refers to the thermal transition at $T = 0.6J$.

Quantum fluctuations could be imposed on the SK model, which is the magnetic field in the x-direction. One define the quantum SK model as

$$H_{\text{Q-SK}} = \sum_{ij}^{N} J_{ij}\sigma_i^z\sigma_j^z - B_x\sum_{i}^{N}\sigma_i^x. \tag{5.10}$$

At large enough $B_x \gg J$, the GS of the system is fully polarized at x-direction, and all eigen-states is ordered in energy by the Hamming distance from the GS (Here Hamming distance means the number of spin-flips compare two states.). This is a paramagnetic phase at large B_x. People found out that $B_x \simeq J$, there is a quantum phase transition separate glassiness GS and the paramagnetic GS. The horizontal line ($T = 0$) in Fig. 5.6(a) refers to the quantum phase transition. Fig. 5.6 comes from Ref. [116], and Γ in plot is equivalent to the B_x/J in our definition.

Similar to the deformed SYK model in Sec. 5.1, the quantum SK model also has a mobility edge when one tunes the interaction strength B_x. People can translate between the finite energy to finite temperature, and Fig. 5.6(b) shows the mobility edge. In order to understand the meaning in the Fig. 5.6, we need some understanding in ergodic, nonergodic, and MBL eigenstates in the quantum SK model.

In order to distinguish these phases, one need concern the off-diagonal matrix elements of local operators. Schematically, denote by $\hat{A}$ an operator that can flip $\mathcal{O}(1)$ spins at a time (e.g. $\hat{A} = \sigma_x$). Consider any two eigenstates of the Quantum SK model, $|\psi\rangle$ and $|\phi\rangle$ with relatively close energies $N(\epsilon \pm \delta\epsilon/2)$, and evaluate the overlap $\langle\phi|\sigma|\psi\rangle$

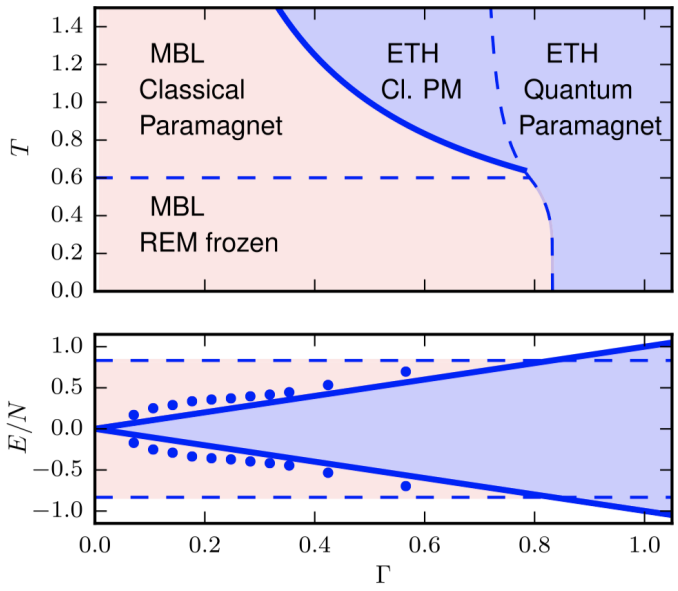

Figure 5.6: (a) The canonical phase diagram of the spin-glass in $B_x - T$ plane. (b) The microcanonical phase diagram in the $B_x - \epsilon$ plane. Taken from Ref. [116], and $\Gamma = B_x/J$.

- Ergodic phase: This is the situation that eigenstate thermalization hypothesis (ETH) works. This indicate the overlap follows

$$\langle \phi|\sigma|\psi\rangle \sim \frac{\mathcal{A}(\epsilon, \delta\epsilon)}{\sqrt{\mathcal{D}(\epsilon)}} \tag{5.11}$$

  where $\mathcal{D}(\epsilon)$ is the number of states around ϵ which is a exponentially large value, and $\mathcal{A}(\epsilon, \delta\epsilon)$ is just a smooth function depend on energy with $\mathcal{O}(1)$ value.

- Non-ergodic phase: This is the situation that many meta-stable states appear at the energy ϵ. We understand for each meta-stable state, there are $\mathcal{O}(1)$ spin-flipped states associated with it. One meta-stable state with its neighbor in Hamming distance form a valley in free-energy landscape, and the bottom of the valley is this meta-stable state which correspond to the local minimum. If we choose two

eigenstates of the Quantum SK from the same valley, one find

$$\langle \phi^{(v)} | \sigma | \psi^{(v)} \rangle \sim \frac{\mathcal{A}^{(v)}(\epsilon, \delta\epsilon)}{\sqrt{\mathcal{D}^{(v)}(\epsilon)}} \tag{5.12}$$

where the superscript (v) means the state is chosen in valley (v), and $\mathcal{D}^{(v)}(\epsilon)$ is the number of state around ϵ inside valley (v). So it is resemble a ETH subsystem. If we choose two eigenstates from two different valley (v) and (v'), one find

$$\langle \phi^{(v')} | \sigma | \psi^{(v)} \rangle \ll \frac{1}{\sqrt{\mathcal{D}(\epsilon)}} \tag{5.13}$$

The overlap is heavily suppressed compared to ETH. So the overlap can be used to characterize different phases of localization.

One can try to understand how many-body delocalization happens at finite energy ϵ with certain B_x, which will lead to the notion of mobility edge. Start from a localized state $|\alpha\rangle$, which is the eigenstate of the classical SK (i.e. Hamiltonian (5.8)). We understand that a state $|\alpha\rangle$ delocalize itself, is equivalent to say that there are states could "resonant" to $|\alpha\rangle$. This resonance can be characterized by the overlap between two states $|\alpha\rangle$ and $|\beta\rangle$ after the flipping effect was include, i.e. $\langle\beta|\psi_\alpha\rangle$, where $|\psi_\alpha\rangle$ is the perturbed $|\alpha\rangle$ under small B_x. So we one can use forward scattering approximation (namely only lowest order perturbation is include) at small B_x:

$$\langle \beta | \psi_\alpha \rangle \approx (B_x)^d \sum_{\mathcal{P}} \prod_{\gamma \in \mathcal{P}} \frac{1}{E_\alpha - E_\gamma} \tag{5.14}$$

where $\mathcal{P}$ denote a possible path that flip $|\alpha\rangle$ to $|\beta\rangle$ with d times, where d is the Hamming distance between $|\alpha\rangle$ and $|\beta\rangle$. And γ states are the intermediate states who has Hamming distance $d_\gamma < d$ that support along d times flipping, and there should have $\mathcal{M} = \sum_{d_\gamma=1}^{d} \binom{N}{d_\gamma}$ of these γ states. Then the energy window of $|E_\alpha - E_\gamma| \sim \sqrt{N}\sqrt{\log \mathcal{M}} \ll NJ|\epsilon|$, where $NJ\epsilon$ is the energy of state $|\alpha\rangle$. So the typical value of

weight for each flip is $(B_x/J)/(N|\epsilon|)$, and we have $d!$ paths to choose, which gives

$$\langle\beta|\psi_\alpha\rangle \approx d! \left(\frac{B_x}{NJ|\epsilon|}\right)^d \tag{5.15}$$

$$\simeq \exp\left[d\log\left(\frac{d}{N}\frac{B_x/J}{|\epsilon|}\right)\right] \tag{5.16}$$

We understand that when de-localization transition happened, every states (including the $|\beta\rangle$) should be resonated, even with the furthest Hamming distance compare to $|\alpha\rangle$. At this point $d \simeq N$ and $\langle\beta|\psi_\alpha\rangle$ is no longer exponentially small. This indicate we have a critical energy $\epsilon_c \simeq B_x/J$, if $|\epsilon| < \epsilon_c$, the state at this scaled energy ϵ is delocalized, as shown in Fig. 5.6(b). We also notice that this mobility edge do not have any scaling with systems size which contrary to the situation we discussed in deformed SYK in Sec. 5.1.

5.3 Quantum optimization in glassy system

There are many daily life problems which we want to pay least cost when finished them. Many of them locate in the category of combinatorial optimization problems and are equivalent as finding the ground state of corresponding spin-glass Hamiltonian, e.g. the traveling salesman problem. Let's demostrate the example of the traveling salesman, who would sales his goods to N cities and wish to minimize his cost on airplane tickets. Assume that the price of the tickets between city i and city j is J_{ij}, and he will choose to go to city in the order of $c_1 \to c_2 \to ...c_{N-1} \to c_N$ and eventually come back $c_{N+1} = c_1$. So the total cost on his tickets is

$$H_{\text{tickets}} = \sum_{\alpha}^{N} J_{c_\alpha, c_{\alpha+1}} \tag{5.17}$$

Now we want to choose the best order to pass through these cities, to minimize H_{tickets}. Actually this optimization problem can be directly mapped to a random Ising model

with introduce of bit spin:

$$n_{i,\alpha} = \begin{cases} 1 & \text{goes to city } i \text{ at the } \alpha \text{ step} \\ 0 & \text{doesn't go to city } i \text{ at the } \alpha \text{ step} \end{cases} \tag{5.18}$$

Since the salesman would pass through the cities only once, we have $\sum_{\alpha}^{N} n_{i,\alpha} = 1$ for all i. While at each step, he can only pass through one city, i.e. $\sum_{i}^{N} n_{i,\alpha} = 1$ for all α. Now we have

$$H_{\text{tickets}} = \sum_{\alpha}^{N} \sum_{ij}^{N} J_{ij} n_{i,\alpha} n_{i,\alpha} \tag{5.19}$$

This is a disordered spin model (although the spin here is defined in bit as $0, 1$ rather than standard ± 1) with N different species. So now the question comes to finding the ground state of the spin-glass Hamiltonian. Generically, there are different types of optimization problems and these corresponds to different spin-glass models. Sherrington-Kirkpatrick model with Hamiltonian Eq. (5.8), as a canonical example of spin-glass, was taken to be used a benchmark test in many experiments. And the SK model (rather than traveling salesman Hamiltonian Eq. (5.19)) would be used in the main text of our discussion of quantum optimization in Sec. 5.3.2.

In this chapter, we would like to discuss how to find the ground state of such problems. But the life is not easy, since the Hamiltonian of these combinatorial optimization typically has a glass phase, which will lead to a false GS when one tries to minimize the cost/energy. A standard method to find GS is to do simulated (thermal) annealing, namely starting from a random high energy state, one lower the energy of the state by local flipping the spin. This method will inevitably lead to a local minimum state of the problem rather than global minimum. And these local minimum typically have very high energy barrier, which would be hard to hop from one local minimum to another in a decent time (rather than forever).

In order to make the system hop from one local minimum to another, people introduce the quantum fluctuation to do the job and quantum annealing as well as the quantum adiabatic computing was invented. The idea behind the quantum annealing is that, when one adding quantum fluctuation and destroy the glass phase, it is very easy

to find the GS outside the glass phase. And at the same time, the GS in and out-side the glass phase should be adiabatically connected. So if one can found the GS out-side the glass phase and adiabatically evolve the quantum system back to its classical limit, one will eventually find the GS solution of your optimization problem.

5.3.1 Quantum annealing and its bottleneck

The idea of optimizing by adiabatic quantum evolution seems to be a good idea, since the GS of the system are always connected together and once one find GS in one regime will lead to discover on other side of the regimes. But unfortunately, for large enough system size, when system encounter a phase transition, there is always a gap associate with it. Landau-Zener formula tells us, if you want to stick on the instantaneous GS when turn off the quantum fluctuation, one better to maintain the rate of turning-off/changing parameter to be smaller than the order of energy level spacing. In other words, a small gap between the GS and first excited state, will lead a long time annealing to maintain the notion of adiabaticity. Typically NP-hard optimization problems will always have exponentially small gaps in quantum annealing set-up, and one need exponentially long time to finish the anneal protocol.

For the Sherrington-Kirkpatrick model we discussed in Sec. 5.2, there is a quantum phase transition when one increase the x-direction magnetic field. And at the quantum phase transition point, a gap show up between the instantaneous GS and first excitation state. Truth be told that this quantum phase transition is second order (i.e. QCP), and everything is scaling invariant at that transition point, so does the gap. As a consequence, the gap is power law smallness, rather than exponentially small, seem to leave a room for adiabatic quantum annealing. But as it has been pointed out in Ref. [117, 118, 119] that, for these SK types of spin-glass with conventional "forward" protocol, though exist a QCP type gap, there could be many other anti-crossings between the lowest two levels and at the same time these minimal gap is near the end of annealing, which leads to a exponentially small gap to spoil adiabatic quantum annealing. Because of these unpleasant exponentially small gaps in the conventional "forward" protocol, people are questioning the efficiency of quantum annealing. Therefore, it stimulates the interests to construct other types of quantum annealing protocol. Among many types of them, a diabatic annealing protocol with multiple cycles is gradually

popular these days, where the system is approaching GS cycle by cycle with a relatively faster rate of dialing parameters than adiabatic annealing [120, 121, 122]. And this types of annealing protocol would be the main topic in this chapter.

Due to the iteration nature of the protocol we are interested in, the initial trial state of each iteration comes from the previous iteration, and it should be a classical bit-sting type state, i.e. diagonal in the computational basis. A quantum annealing protocol, if starting from a bit-sting type state and end up with (typically) another bit-sting type state which was first proposed and tested in Ref. [123], are name after Ref. [124, 125] as "reverse annealing". The term "reverse annealing" may be somewhat misleading: it is not the reverse type of the conventional quantum annealing. Also it is not necessary for the system ends up to its initial Hamiltonian as if it reverses the time at the middle of the conventional forward annealing process. One may use an additional initial Hamiltonian to set the initial state as certain bit-string eigenstate of the problem Hamiltonian. There are refined proposals [126] and detailed experiments [127] since then.

Theoretical and numerical studies of reverse annealing was heavily discussed in [120, 121, 122] with ferromagnetic p-spin model as the problem Hamiltonian. In Ref. [120, 121], they studied two types of reverse annealing protocol: (a) adiabatic reverse annealing with an initializing Hamiltonian and (b) iterative diabatic reverse annealing without an initializing Hamiltonian. In protocol (a), with "good" choice of initial state and trajectory of annealing , the annealing process may skip exponentially small gaps which should be existent due to first order phase transition. The better guess of the initial trial state is, the larger the parameter space is to circumvent first order phase transition (It is like transition from liquid-water to gas-water, one can bypass the first order phase line and forbid the exponentially small gap.). This observation is encouraging in adiabatic quantum computing, but the existence of a absence of the first order transition is observed only in non-disordered model. In protocol (b), without the initializing Hamiltonian, they investigate if diabatic annealing process can scatter the state from high energy to low energy with the help of Landau-Zener effect within few iterations. The result are discouraging in the sense that the overlap between the annealing state (typically a superposition of many eigenstates of the problem Hamiltonian) and the GS of the problem Hamiltonian, did not significantly increasing after few iterations. While in

Ref. [122], with same protocol (b) but adding relaxation effect, i.e. couple to reservoir, the system can drop from high energy eigenstate to GS in single iteration drastically. The temperature lowering effect is enhanced with the existence of quantum fluctuation.

These studies [120, 121, 122] are the benchmark tests for crossing/bypass *few* exponential small gaps in QA. However, in realistic NP-hard problems, which are equivalent to spin-glass type models, the enhancement shown by these tests could fail. First, the exponentially small gaps maybe unavoidable due to anti-crossing between states with large hamming distances in the localization phase [117] and at the same time there maybe exponentially many of them [118]. Second, the relaxation with reservoir is limited by the non-convex landscape structure of spin-glass and the state will be trapped at some local minimum. (Moreover, in these benchmark tests, the transition between states can be reduced to a much smaller subspace of Hilbert space by the symmetry of toy model, which is not the case in generic spin-glass models.) Whether the promised enhancement exists is an open question for spin-glass. Therefore, we would want to study a more realistic scenario and take advantages of iterated diabatic annealing with initializing Hamiltonian.

5.3.2 Diabatic Iterative Quantum Annealing

To be concrete in the discussion of the quantum annealing protocol, let's formulate the optimization problem. One start with a so-called problem Hamiltonian which need to be optimized. We choose Sherrington-Kirkpatrick (SK) model as problem Hamiltonian, with the form

$$H_{\text{prob.}} = \sum_{ij}^{N} J_{ij}\sigma_i^z\sigma_j^z, \tag{5.20}$$

where N is the number of qubits. All eigenstates of the problem Hamiltonian are polarized in z-direction, i.e. diagonal in computational basis. Define the state α has configuration $\{s_i^\alpha\}$ with energy E_α. One wants to search the minimum of energy among E_α among all α's.

In standard QA, one add quantum fluctuation $H_{\text{q-fluct}} = \sum \sigma_i^x$ mixing these states by adding magnetic field in x-direction. So the full Hamiltonian for standard QA is

$$H(t) = H_{\text{prob.}} + B_x(t)H_{\text{q-fluct}}. \tag{5.21}$$

When B_x is large, the GS is melt by the many-body delocalization at B_x^c, which is a equal superposition of all bit string states [116, 128]. And this is the initial place where standard QA is start from, i.e. $B_x(t)/J \gtrsim 1$ (numerical value may need to be larger than 2). The annealing protocol is to decrease the B_x, and around the quantum phase transition point B_x^c, the instantaneous GS will suddenly changed from delocalized state to a specific bit string state, which could be the GS of the pure problem Hamiltonian. The probability distribution to go back to the states of pure Hamiltonian is fixed, and the probability of going back to the exact GS could be exponentially small, due to exponentially small gaps at small B_x. This means you may need exponentially many trails to repeat your protocol, without systemically improvement.

Now one could introduce iterative version of the QA, aiming to improve your annealing result after each iteration. One can start from a bit string state from simulated annealing as a first trail, which is one of the local minimums of the problem Hamiltonian. We want design a quantum annealing protocol, that after one iteration, the resulting state is still a local minimum of the problem Hamiltonian with a lowered energy (with a high probability). This may be achieved by introduce a reference state, where itself is the initial state of the protocol. It should also involved in the Hamiltonian, so that the system may remember this state all the way along the protocol and decide to pick a new state which energy is lower than the reference state.

To be specific, we choose a reference state, with spin configuration $\{s_i^r\}$. And a reference Hamiltonian

$$H_{\text{refer}} = -\sum_i s_i^r \sigma_i^z, \tag{5.22}$$

The full Hamiltonian for a given reference state, is controlled by the parameter B_x and B_z as following,

$$H_{\text{full}}(t) = H_{\text{SK}} + B_z(t) H_{\text{refer}} + B_x(t) H_{\text{q-fluct}}, \tag{5.23}$$

Now we introduce the protocol of the iterative annealing:

- Stage 1: Programming the quantum annealer with Hamiltonian of Eq. (5.23) by picking a reference configuration. The reference configuration should come from the stimulating annealer, which offers a random local minimum of the problem Hamiltonian. Fixing $B_x = 0$, while increasing the B_z from 0 to $B_z > B_z^{\text{bdy}}$

(accurate definition of B_z^{bdy} will come up later, for now it is a order 1 number in unit of J). We understand that there should be a energy scale B_z^{bdy} to separate the system from spin-glass phase and a paramagnetic phase which is polarized by reference Hamiltonian in z-direction.

- Stage 2: After crossing the B_z^{bdy}, we increase the B_x. Due to the fact that we are in paramagnetic phase, increasing B_x will not lead the system outside this phase, but make the instantaneous GS consist with not only reference component but also other bit string states. During this process, the instantaneous GS is separate with other instantaneous excited state in energy space (i.e. a gapped phase). So the system will safely stay in the instantaneous GS, as long as the changing rate of the magnetic field is not comparable to the magnetic field itself. Now we stop at certain B_x, so the ratio between the magnetic field is $\chi = B_x/B_z$ at some order one ratio. And we will specify the best ratio later.

- Stage 3: Decreasing B_z and B_x with the fixed ratio/slope χ. We will cross a "phase boundary" which separate the spin glass phase and the paramagnetic phase. The gap size at the phase boundary and the shape of the phase boundary will strongly depend on the χ and the energy of the reference state one may choose. Fig. 5.7 shows the schematic diagram of protocol lines of the first three stages on top of the phase diagram. During stage 3, unlike stage 2, we may meet many small gaps on and inside the phase boundary. With proper speed (discuss later), we may comes to a state which superposited by bit-string states mostly come from the state with energy is lower than the reference state and few come from the states higher than the reference state.

- Stage 4: Now we sit in the position $B_x = B_z = 0$ with a wavefuntion. Do the measurement and the wavefuction will collapse on one of the bit-string of the pure problem Hamiltonian. We can cool down this state to its associated local minimum by stimulate annealing (e.g. gradient descent in a classical computer). So we got a new bit-string state which is a local minimum of the problem Hamiltonian. Now, if this new state has higher energy compare to original reference state, we would choose to forget the new result and repeat the protocol with our previous reference state. Or if the new local minimum state have lower energy, we would choose this

new state as our new reference state and do the cycle again. We will argue later, the chance to lower the energy after one cycle is order one (more likely to be $\sim 50\%$ rather than exponentially small), if we properly choose the annealing slope χ.

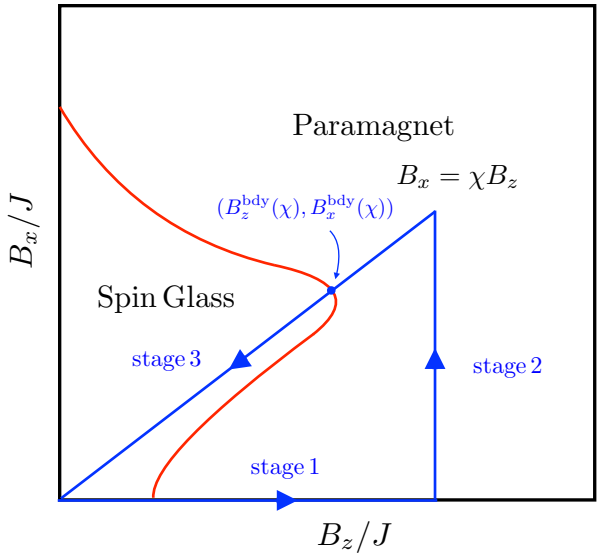

Figure 5.7: Schematic phase diagram of $H = H_{\rm prob.} + B_z H_{\rm refer} + B_x H_{\rm q-fluct}$ for a specific reference state. The reference state is chosen in side one of the local minimum of the pure problem Hamiltonian. (Red curve) Possible phase boundary. (Blue lines) Stage 1,2,3 of the annealing protocol discussed in the main text

Now come back to the problem of choosing proper χ, that it can basically satisfy following conditions:

- 1. The gap should be large enough at the phase boundary, that means the wave-function will maintain at instantaneous eigen-GS just across the phase boundary from outside, even with a comparatively fast annealing speed. We need the χ large enough, so that the $B_x = B_x^{\rm bdy}(\chi)$ at the crossing between the protocol line at stage 3 and the phase boundary is large ($\sim \mathcal{O}(1)J$). This indicate we want χ as large as possible.

- 2. We want the instantaneous eigen-GS around the phase boundary, mostly consist/superposited with the bit-string state have lower energy (of the pure problem

Hamiltonian). We understand that when $\chi \to \infty$, the protocol goes as the standard quantum annealing, and the instantaneous eigen-GS is equal superposition with all bit-string state, no matter its energy is higher or lower than the reference state. On the other hand, we know when $\chi \to 0$, the eigen-GS around the phase boundary will only mix the state that is lower than the reference state (detail later). This indicate χ should not be too large.

These two point indicate that, there might be a best choice of χ, that can trade off these two contrary request. To understand this more, we should have some semi-quantitative method to approach the problem at intermediate χ.

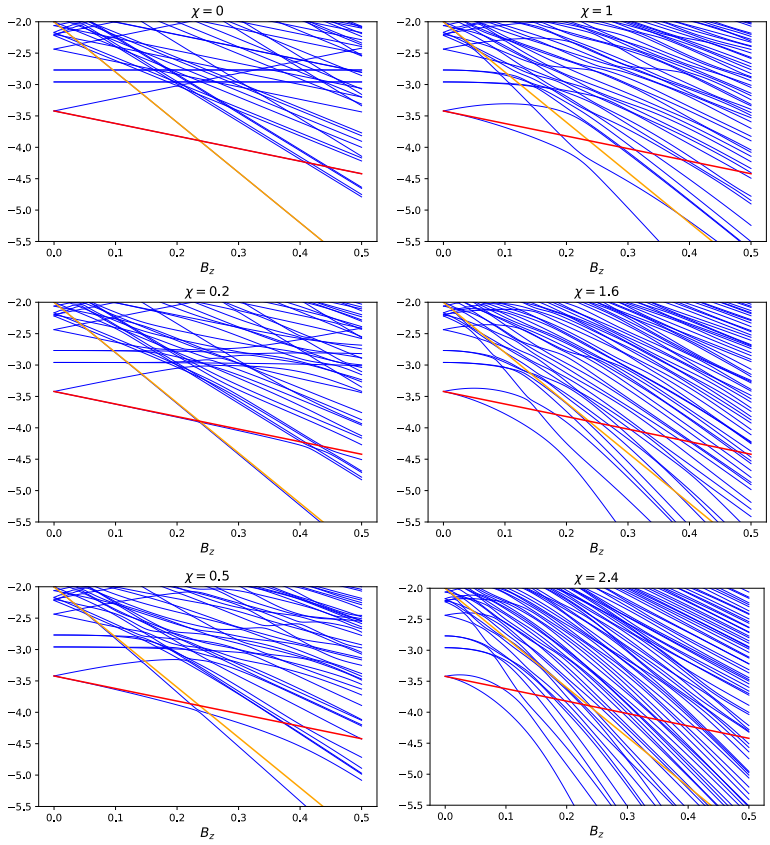

Figure 5.8: Exact diagonalization results for: ($\chi = 0$) Zeeman lines: energy spectrum of $H_{\mathrm{SK}} + B_z H_{\mathrm{refer}}$ vs. B_z. ($\chi = 0.2, 0.5, 1, 1.6, 2.4$) Adding finite transverse field B_x. Energy spectrum of $H_{\mathrm{SK}} + B_z H_{\mathrm{refer}} + B_x H_{\mathrm{q-fluct}}$ vs. B_z, where $B_x = \chi B_z$.

When $\chi \ll 1$, we understand that the off-diagonal mixing from B_x is small. So the energy spectrum will mainly controlled by the Zeeman splitting. Depending on how far away the state compare to reference state in Hamming distance, their behavior are different. Let's assume we have a bit-string state α has spin configuration $\{s_i^\alpha\}$ and energy $E_\alpha = \epsilon_\alpha NJ$. This bit-string state has Hamming distance $d_\alpha = (N - \sum_i s_i^\alpha s_i^r)/2$ compare to reference state. The energy shift (i.e. the renormalizaed energy) as a function of B_z for state α is $\tilde{\epsilon}_\alpha = \epsilon_\alpha - (1 - 2d_\alpha/N)B_z/J$ and for reference state $\tilde{\epsilon}_r = \epsilon_r - B_z/J$. We called this energy denpendence of B_z as Zeeman lines. See Fig. 5.8 for the spectrum at small χ (The plots comes from exact diagonalization of Eq. (5.23) for small N). It is clear that reference Zeeman line has the largest slope to decrease the energy with respect to B_z, so it will cross all other Zeeman lines has lower energies compare to ϵ_r at $B_z = 0$ and have no touch to the lines with higher energies. We can define the crossing point between the reference Zeeman line and α Zeeman lines as $(B_{z,\alpha}^{\text{cross}}, B_{x,\alpha}^{\text{cross}})$. Now for different α states, one can find the largest value of $B_{z,\alpha}^{\text{cross}}$ among all α's, and this crossing point will become the phase boundary for this χ, i.e. defining $B_z^{\text{bdy}} = \text{Max}_\alpha(B_{z,\alpha}^{\text{cross}})$. So when $B_z > B_z^{\text{bdy}}$, the reference state Zeeman line becomes to the instantaneous GS at the paramagnetic phase.

With very small $B_{x,\alpha}^{\text{cross}} = \chi B_{z,\alpha}^{\text{cross}}$ at the crossing point, the gap between the reference Zeeman line and state α Zeeman line is

$$\Delta_\alpha \propto (B_{x,\alpha}^{\text{cross}}/J)^{d_\alpha}, \tag{5.24}$$

where the crossing point between reference state and α happens at

$$B_{z,\alpha}^{\text{cross}} = \frac{\epsilon_r - \epsilon_\alpha}{1 - 2d_\alpha/N} \text{ and } B_{x,\alpha}^{\text{cross}} = \chi B_{z,\alpha}^{\text{cross}}. \tag{5.25}$$

Due to the fact that $d_\alpha \propto N$ for state α not inside local minimum which associated with reference state, the gap one meet when annealing from paramagnetic phase to spin glass (stage 3) will be exponentially small. If one can tolerant with the exponentially long time $T_{\text{anneal}} \propto 1/\Delta^2$, then one can 100% sure after one iteration, the result state will have lower energy compare to the reference state.

Let's now comes to intermediate χ, to analysis how the energy spectrum may look like (i.e. how the Zeeman lines picture at $\chi \ll 1$ changes at $\chi \sim 1$). We understand that,

when $\chi \sim 1$, the off-diagonal B_x will come into play with two roles. (a) If one choose two state associate with two different local minimums, the large Hamming distance between the two different local minimums will lead exponentially small gaps. This is the effect we discussed in $\chi \ll 1$ regime. Let's neglect this effect for a moment. (b) If two states are associated in the same local minimum, we know that them only have $\mathcal{O}(1)$ spin flip between them, so the level repulsion is strong. Let's assume we focus on the local minimum among these close states and investigate how the energy curves looks like as a function of B_x and B_z, without mixing effect from state at other local minimum (i.e. effect (a)). We understand that this local minimum will be kicked downward by its nearby state when increasing B_x, with the form $E_{\text{loc. min}} = NJ\left[1 - \sqrt{1 + (B_x/J)^2}\right]$. Here we assume the local minimum state has energy J separated from one spin flip states, in principle there should be a order 1 number differ from different local minimum. This formula tells us that, when B_x is large, these local minimums are the states have the largest slope $\simeq -N$ around $B_x/J \sim 1$, which will eventually become the instantaneous low energy part in the paramagnetic phase. We may also decorate the formula with local minimum dependence. Some of the local minimum valley have stronger level repulsion and some are weak. This can be characterized in single parameter l_α, where α label the local minimum states. The l_α characterize the typical energy separation between local minimum with its nearby spin-flip states as $l_\alpha J$, i.e. the local density of states around α state is proportional to $1/l_\alpha$. Now the local minimum dependence version of level repulsion effect could be:

$$E^{\alpha}_{\text{loc. min}} = NJ\left[l_\alpha - \sqrt{l_\alpha^2 + (B_x/J)^2}\right] \tag{5.26}$$

We can now put back the Zeeman effect of the B_z, this is the diagonal effect which shift the energy of the local minimum state α, with slope $s_\alpha = -(1 - 2d_\alpha/N)$. With this effect, we have the full local minimum curve (again without mixing effect between different local minimums) as:

$$\tilde{\epsilon}_\alpha = \epsilon_\alpha + \left[l_\alpha - \sqrt{(l_\alpha + s_\alpha B_z/J)^2 + (B_x/J)^2}\right], \tag{5.27}$$

where $\tilde{\epsilon}_\alpha = E^{\alpha}_{\text{loc. min}}/(NJ)$ is the scale renormalizaed energy, and ϵ_α are the scaled energy for the local minimum α of the pure problem whose distribution is chosen as in

Ref. [129, 130].

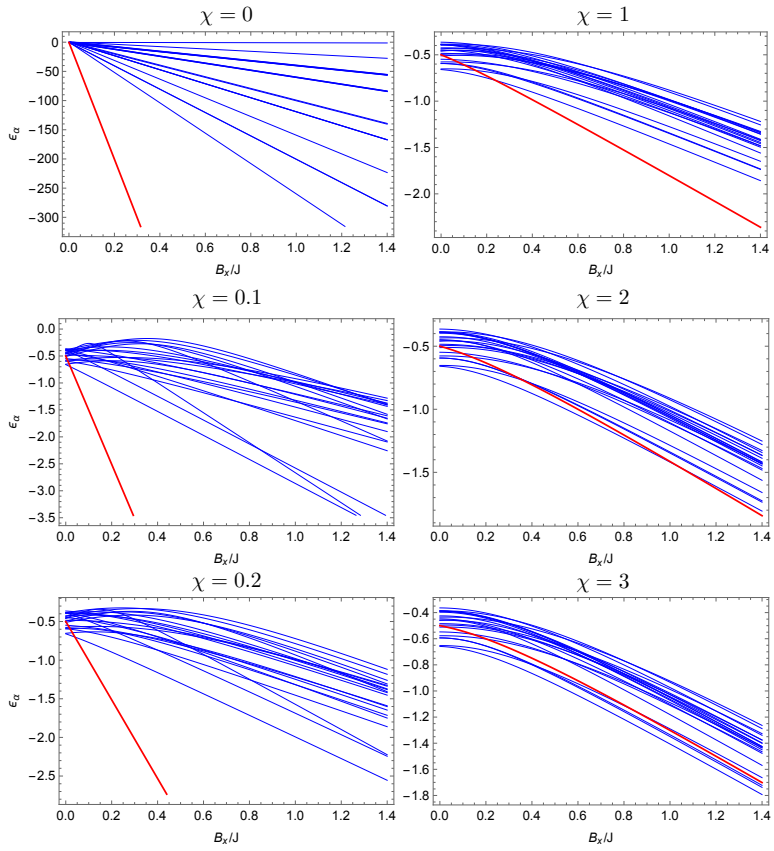

Figure 5.9: Spectrum of local minimums constructed according to Eq. (5.27). (χ = 0, 0.1, 0.2, 1) Small χ regime, the largest crossing point of B_x/J between reference state and other states are smaller than 1. The gap induced by the crossing point is exponentially small. ($\chi = 2$) The largest crossing B_x/J is around 1, so the energy spectrum where $B_x/J > 1$ is not reliably predicted by Eq. (5.27), power law smallness of gap start to develop. ($\chi = 3$) Many higher energy state could curve down below the reference curve.

Fig. 5.9 demonstrate the scaled energy spectrum of local minimums α from Eq.(5.27) with random generation of s_α and l_α for small system size. Red curve is the reference state curve $\tilde{\epsilon}_r$, with largest slope at small χ. At small χ regime, the reference curve will always become the GS after $B_x > B_{x,\alpha}^{\text{cross}}$, for all α. Here $B_{x,\alpha}^{\text{cross}}$ is defined by the crossing

point of reference energy curve and α state energy curve, i.e. $\tilde{\epsilon}_r(B^{\text{cross}}_{x,\alpha}) = \tilde{\epsilon}_\alpha(B^{\text{cross}}_{x,\alpha})$.

When χ is increasing, the $B^{\text{cross}}_{x,\alpha}$ is also increasing. Until $\text{Max}(B^{\text{cross}}_{x,\alpha})$ is approaching J, every gap induced between two curves should be exponentially small, if one put back the mixing effect for different local minimums at this stage. With this small gap, One can still identify/trace who is the reference state and who is α state, even with the mixing effect for different local minimums. In this regime of χ, we can simulate larger system size and identify the phase boundary $B^{\text{bdy}}_x = \text{Max}_\alpha(B^{\text{cross}}_{x,\alpha})$. Fig. 5.10 shows the phase boundary curve $(B^{\text{bdy}}_z(\chi), B^{\text{bdy}}_x(\chi))$ for different reference energy. One can found a critical $\chi_c \simeq 3.6$ (black dashed line), that if one do the annealing with $\chi < \chi_c$, one will always meet an exponentially small gap at the phase boundary, which comes from the crossing point of reference and α local minimum spectrum curves.

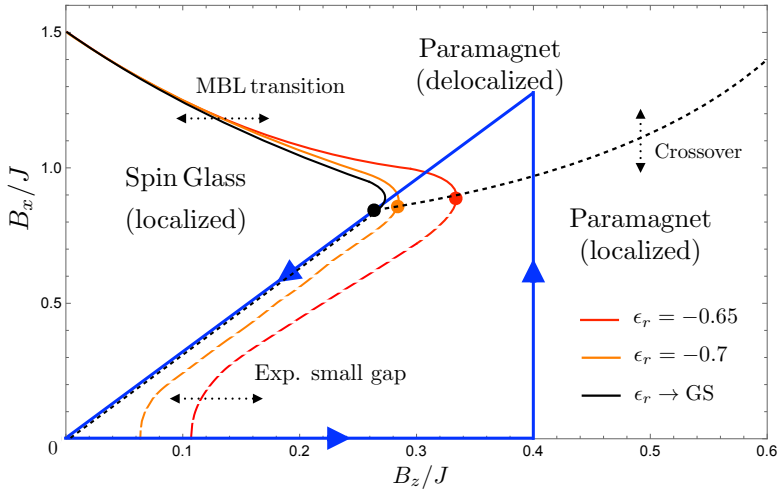

Figure 5.10: Phase diagram of full Hamiltonian (5.23) with different reference state. There are three different region: spin glass, paramagnet (delocalized) and paramagnet (localized). Different color (red, orange and black) are phase boundaries for certain reference state with gradually lowered energy. For the phase boundary for a specific reference energy, it has dashed portion and solid portion separated by a big solid dot. The dashed portion of the phase boundary has exponentially small gap while the solid portion refers to the many-body localization transition.

Then what happens if we choose $\chi > \chi_c$? If we follow the Eq. (5.27), it tells that (exponentially) many local minimum curves will come to cross the reference curve at $B_x \simeq J$. This may totally change the picture of $\chi > \chi_c$ case comparing to the

exponentially small gap between two local minimum curves bypassing B_x^{bdy} for $\chi < \chi_c$ case. And this is the story associated with the concept of many-body localization transition from $B_x \gtrsim B_x^{\text{bdy}}$ to $B_x \lesssim B_x^{\text{bdy}}$ at intermediate χ.

Two local minimums will typically have exponentially small hopping between each other because of the Hamming distance between them are proportional to N. For single particle system, it may means the system may always be in localized state, and two local minimums interchange their order of energy due to renormalization (i.e. Eq. (5.27)), and open an exponentially small gap. This is not the case in the many-body systems, where a competing exponential small energy level space may induce a de-localized phase as shown following. An effective low energy theory for the local minimums could be built:

$$H_{r,\alpha\,\text{block}} = \begin{pmatrix} \tilde{E}_r & t_{r\alpha} \\ t_{r\alpha} & \tilde{E}_\alpha \end{pmatrix} \tag{5.28}$$

where $t_{r\alpha}$ is the effective hopping between r and α state, and be calculated according to Forward Scattering Approximation:

$$t_{r\alpha} = B_x \sum_{\gamma \in \text{Path}} \prod_{i=1}^{d_{r\alpha}} \frac{B_x}{|\tilde{E}_r - \tilde{E}_{\gamma_i}|} \tag{5.29}$$

There will be a phase transition happens when increase B_x, so that $t_{r\alpha}$ exceed the exponentially small level spacing $|\tilde{E}_r - \tilde{E}_\alpha|$. For a given χ, there is exist a $B_x^{\text{bdy}}(\chi)$, when $B_x > B_x^{\text{bdy}}(\chi)$, the instantaneous eigen-GS no longer be the localized state, but mixing all the α local minimum, whose renormalized energies are exponentially closed. This is a many-body delocalization state in paramagnetic phase, with its form

$$|\text{GS}(B_x > B_x^{\text{bdy}})\rangle \propto \widetilde{|r\rangle} + \sum_\alpha \widetilde{|\alpha\rangle} \tag{5.30}$$

where $\widetilde{|r\rangle}$ and $\widetilde{|\alpha\rangle}$ are renormalized state due to nearest neighbor level repulsion. So when one get $|\text{GS}(B_x > B_x^{\text{bdy}})\rangle$ at the end of the stage 2 of the algorithm, and start to decrease B_x and B_z with ratio χ, the system will pick one of the local minimum α once cross the phase boundary $(B_z^{\text{bdy}}(\chi), B_x^{\text{bdy}}(\chi))$. This is the many-body localization transition at $\chi > \chi_c$.

The many-body localization transition now will introduce a power law smallness of gap when crossing B_x^{bdy} due to the divergence of correlation length, i.e. $\Delta \propto 1/\xi^z \sim 1/N^z$, where z is the dynamical dimension. But at the same time, the state with energy ϵ_α higher than the reference state energy ϵ_r will have develop high probability to curve down around the reference curve at $B_x/J \simeq 1$, which will be one of the ingredient of the delocalized state in $|\text{GS}(B_x > B_x^{\text{bdy}})\rangle$. That means when annealing at stage 3 of our protocol, by passing the B_x^{bdy} from paramagnetic phase, the system would have chance to stuck at state α where $\epsilon_\alpha > \epsilon_r$. So when doing measurement at stage 4, one may pick a bit string that increase the energy compare to ϵ_r. This is a bad signal to do annealing.

To quantify how bad it would be at certain $\chi > \chi_c$, we need to count the number of states that curve down below reference curve at $B_x/J \simeq 1$ for those α that $\epsilon_\alpha > \epsilon_r$ (refer as $\mathcal{N}_>$). To compare with the number of states that originally (i.e. at $B_x = 0$) below the ϵ_r which always contribute the instantaneous GS at $B_x \gtrsim B_x^{\text{bdy}}$ (refer as $\mathcal{N}_<$). Now the instantaneous GS at $B_x/J \simeq 1$ should be superposited by $\mathcal{N}_<$ states and $\mathcal{N}_>$ states more or less equally. So the probability to scatter to the higher energy bit-string when annealing at stage 3 around the phase boundary is $\mathcal{N}_>/(\mathcal{N}_> + \mathcal{N}_<)$. Fig. 5.11 shows how $\mathcal{N}_>/\mathcal{N}_<$ depend on χ, with different reference energy ϵ_r, simulated by using Eq. (5.27). It shows that only when $\chi > \chi_c \simeq 3.6$, the higher energy start to curve down below the reference curve. And it also demonstrate that lower the reference energy ϵ_r, faster the ratio $\mathcal{N}_>/\mathcal{N}_<$ will grow to a fairly large value that too many higher energy state comes to scramble the instantaneous GS at $B_x/J \simeq 1$. We suspect the ratio could be exponentially growing as

$$\frac{\mathcal{N}_>}{\mathcal{N}_<} \propto \exp\left[\frac{(\chi - \chi_c)^\gamma}{(\epsilon_r - \epsilon_{\text{GS}})^\delta}\right], \tag{5.31}$$

where $\gamma > 0$ and $\delta > 0$ are scaling exponents and ϵ_{GS} is the true GS energy of the pure problem Hamiltonian.This indicate, if one do not want ruin out the annealing because of too many (exponentially many) higher energy superposited in the instantaneous GS, one need to maintain $\chi - \chi_c < (\epsilon_r - \epsilon_{\text{GS}})^{\delta/\gamma}$, See Fig. 5.10 for the dashed red, blue and orange line.

On the other hand, when $\chi - \chi_c > (\epsilon_r - \epsilon_{\text{GS}})^{\delta/\gamma}$, the instantaneous GS will mix exponentially many local minimums without energy preference, and will fully delocalized

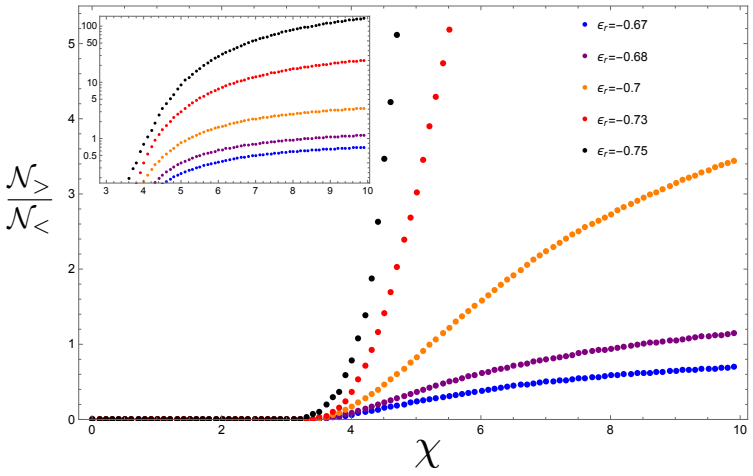

Figure 5.11: Ratio of higher energy states mixed in the instantaneous GS at $B_x/J = 1$, as a function of annealing slope χ, with different reference energy. No matter what reference energy is, they all start to develop non-zero ratio at $\chi_c = 0.36$. Smaller the reference energy, fast the ratio grows to order 1 (50% chance to lower the energy after one cycle of annealing). (Insert) Logarithmic scale in vertical axis.

in bit string basis. So in this regime, we can simply adapt the phase boundary from the MBL transition boundary curves [131, 132]. And at this point, the system do not care where your reference you choose at stage 1 of the protocol. So no matter what ϵ_r is, the phase boundary for $\chi - \chi_c > (\epsilon_r - \epsilon_{\rm GS})^{\delta/\gamma}$ are the same, See Fig. 5.10 transition lines upper. So we may argue that we have a best region of χ for iterative quantum annealing:

$$\chi_c < \chi_{\rm best} < \chi_c + (\epsilon_r - \epsilon_{\rm GS})^{\delta/\gamma} \tag{5.32}$$

Inside this region of χ, we know that the gap is no longer exponentially small due to the mixing of different local minimum curves at $B_x/J \simeq 1$. While at the same time, the instantaneous GS would only contain $\sim$ 50% higher energy bit-string and the chance to increase the energy after the annealing is $\sim$ 50%. See Fig. 5.10, the solid lines for each color (i.e. each reference energy) are the "bad" phase boundary. If one choose a slope that cross the "bad" phase boundary, the annealing result is not good. The slope without solid line phase boundary crossing in Fig. 5.10 are the slope $\chi_c < \chi_{\rm best} < \chi_c + (\epsilon_r - \epsilon_{\rm GS})^{\delta/\gamma}$. Smaller the reference energy, smaller room for χ that we can choose.

We can estimate the annealing time for lowering the energy after one iteration. Set $\epsilon = \epsilon_r - \epsilon_{\rm GS}$ as the accuracy one demand for the quantum annealing. The gap at the phase boundary is power law small around $\chi \gtrsim \chi_c$, i.e. $\Delta \propto (\chi - \chi_c)^\theta / N^\beta$. So the annealing time for one iteration is

$$T_{\rm anneal} \propto 1/\Delta^2 = \frac{N^{2\beta}}{\epsilon^{2\delta\theta/\gamma}}. \tag{5.33}$$

We need power law long time to do one iteration to make sure we have better bit-string result compare to previous result.

To conclude this section, we propose a four-stages iterative annealing protocol with reference Hamiltonian to do the quantum optimization. Compare to the standard "forward" annealing with uncontrolled output due to localization effect between different valleys, the iterative quantum optimization algorithm could have good control of lowering energy of the output with high probability, as long as the annealing loop has a suitable slope as we argued. The output of the full protocol (many-iteration) could be as close as the true GS with accuracy ϵ, within only a power-law annealing time.

Chapter 6

Conclusion

In this thesis, we addressed few toy models which are beneficial to investigate different phases in strongly interacting disordered systems.

For the original SYK model, We investigate existence of replica off-diagonal solutions in the field-theoretical description. To this end we evaluate a set of local and non-local dynamic correlation functions in the long time limit. We argue that the structure of the soft- mode Schwarzian action is qualitatively different in replica-diagonal vs. replica-off-diagonal scenarios, leading to distinct long-time predictions for the correlation functions. We then evaluate the corresponding correlation functions numerically and compare the simulations with analytical predictions of replica-diagonal and replica-off-diagonal calculations. We conclude that all our numerical results are in a quantitative agreement with the theory based on the replica-diagonal saddle point plus Schwarzian and massive Gaussian fluctuations (the latter do contain replica off-diagonal components). This seems to exclude any contributions from replica-off-diagonal saddle points, at least on the time scales shorter than the inverse many-body level spacing.

With the knowledge of the dominance of the replica-diagonal saddle points, we understand that the SYK model could emerged as a paradigm of the non-Fermi liquid behavior. We investigate a possibility of having a superconducting off-diagonal long-range order and a pseudogap phase within the SYK framework. We found that ODLRO may be established in spin-1/2 version of the model with the time-reversal invariance and an extra attractive interaction. If the latter is taken as the on-site negative U Hubbard term, it leads to the pseudogap phase at $U < U_c$ dominated by quantum

fluctuations of local phases. These fluctuations are described by a quantum version of the Kuramoto model, traditionally employed to illustrate synchronization of classical non-linear oscillators. In the opposite limit of large U, the SYK+Hubbard model is approaching a certain generalization of the integrable Richardson model. We present exact diagonalization studies, along with analytic solutions of the aforementioned limiting cases. We also discuss possible holographic interpretations of the model, ODLRO and the pseudogap.

When investigating a deformed model composed with both SYK_4 and SYK_2, we found two transition which are associated with each other while conceptually different. By calculating IPR, one can indicate a delocalization-localization transition boundary with properly scaled relative strength $\tilde{u}(N)$ in the notion of MBL in Hilbert space. Use the same scaling of $\tilde{u}(N)$, one also can figure out the boundary of chaotic-integrable transition. In single particle situation, these are the two concept, and share the same phase boundary. While in many-body case, these two separate with existence of non-ergodic extended phase in between. What we can learn from it is that two extensive states in Hilbert space are not necessarily have level repulsion with each, as demonstrated in the single particle hopping on Cayley tree lattice.

For the application side of the disordered systems, we discuss the possible non-standard quantum annealing protocol that could be more efficient compare to conventional forward quantum annealing. One may introduce an iterative version of the QA, aiming to improve the annealing result after each iteration in reasonable time. We argue that a triangle loop on $B_z - B_x$ phase plane with a initializing Hamiltonian generated by a reference state could be the preferable protocol to use. The reference state would maintain its properties along the first crossing through the phase boundary, and scatter to a lower energy state at the second touch to the phase boundary due the many-body delocalization-localization transition. We argue the slope of the triangle loop $B_z - B_x$ phase plane is limited, and one may find a optimal value of the loop. At that certain slope, the many-body delocalization-localization will open a power-law gap which save the annealing time, and at the same time, the many-body delocalization-localization should not mix too much higher energy states so that the reference state has high probability to scatter down in energy. As a consequence, the output bit-string state of the full protocol (many-iteration) could be as close as the true GS within accuracy ϵ, with

only a power-law annealing time.

References

[1] In Charles E. Porter, editor, *Statistical theories of spectra: fluctuations*. Academic Press, New York, 1965.

[2] Freeman J. Dyson. Statistical theory of the energy levels of complex systems. *J. Math. Phys.*, 3(1):140–156, 1962.

[3] Philip W. Anderson. Absence of diffusion in certain random lattices. *Phys. Rev.*, 109(5):1492, 1958.

[4] David Sherrington and Scott Kirkpatrick. Solvable model of a spin-glass. *Phys. Rev. Lett.*, 35(26):1792, 1975.

[5] Subir Sachdev and Jinwu Ye. Gapless spin-fluid ground state in a random quantum Heisenberg magnet. *Phys. Rev. Lett.*, 70(21):3339, 1993.

[6] Alexei Kitaev. A simple model of quantum holography. `http://online.kitp.ucsb.edu/online/entangled15/kitaev/` and `http://online.kitp.ucsb.edu/online/entangled15/kitaev2/`, 7 April 2015 and 27 May 2015.

[7] Tadashi Kadowaki and Hidetoshi Nishimori. Quantum annealing in the transverse ising model. *Phys. Rev. E*, 58(5):5355, 1998.

[8] Hanteng Wang, D. Bagrets, A. L. Chudnovskiy, and A. Kamenev. On the replica structure of Sachdev-Ye-Kitaev model. *J. High Energy Phys.*, 09(2019):057, 2019.

[9] Hanteng Wang, A. L. Chudnovskiy, Alexander Gorsky, and Alex Kamenev. Sachdev-Ye-Kitaev superconductivity: Quantum Kuramoto and generalized Richardson models. *Phys. Rev. Research*, 2(3):033025, 2020.

[10] Eugene P. Wigner. Characteristic vectors of bordered matrices with infinite dimensions. *Ann. Math.*, 62(3), 1955.

[11] O. Bohigas, R. U. Haq, and A. Pandey. Nuclear data for science and technology. *Reidel, Dordrecht*, page 809, 1983.

[12] Y. Y. Atas, E. Bogomolny, O. Giraud, and G. Roux. Distribution of the ratio of consecutive level spacings in random matrix ensembles. *Phys. Rev. Lett.*, 110(8):084101, 2013.

[13] Alex Kamenev and Marc Mézard. Wigner-Dyson statistics from the replica method. *J. Phys. A: Math. Gen.*, 32(24):4373, 1999.

[14] Juan Maldacena and Douglas Stanford. Remarks on the Sachdev-Ye-Kitaev model. *Phys. Rev. D*, 94(10):106002, 2016.

[15] Joseph Polchinski and Vladimir Rosenhaus. The spectrum in the Sachdev-Ye-Kitaev model. *J. High Energy Phys.*, 04:001, 2016.

[16] Dmitry Bagrets, Alexander Altland, and Alex Kamenev. Sachdev–Ye–Kitaev model as Liouville quantum mechanics. *Nucl. Phys. B*, 911:191–205, 2016.

[17] Yi-Zhuang You, Andreas W. W. Ludwig, and Cenke Xu. Sachdev-Ye-Kitaev model and thermalization on the boundary of many-body localized fermionic symmetry-protected topological states. *Phys. Rev. B*, 95(11):115150, 2017.

[18] Antonio M. García-García and Jacobus J. M. Verbaarschot. Spectral and thermodynamic properties of the Sachdev-Ye-Kitaev model. *Phys. Rev. D*, 94(12):126010, 2016.

[19] Alexander Altland and Dmitry Bagrets. Quantum ergodicity in the SYK model. *Nucl. Phys. B*, 930:45–68, 2018.

[20] Hrant Gharibyan, Masanori Hanada, Stephen H Shenker, and Masaki Tezuka. Onset of random matrix behavior in scrambling systems. *J. High Energy Phys.*, 07:124, 2018.

[21] Stephen H. Shenker and Douglas Stanford. Black holes and the butterfly effect. *J. High Energy Phys.*, 03(2014):67, 2014.

[22] Juan Maldacena, Stephen H Shenker, and Douglas Stanford. A bound on chaos. *J. High Energy Phys.*, 08:106, 2016.

[23] Subir Sachdev. Strange metals and the AdS/CFT correspondence. *Journal of Statistical Mechanics: Theory and Experiment*, 2010(11):P11022, 2010.

[24] Subir Sachdev. Bekenstein-Hawking Entropy and Strange Metals. *Phys. Rev. X*, 5(4):041025, 2015.

[25] Julius Engelsöy, Thomas G Mertens, and Herman Verlinde. An investigation of AdS_2 backreaction and holography. *J. High Energy Phys.*, 07:139, 2016.

[26] Douglas Stanford and Edward Witten. Fermionic localization of the Schwarzian theory. *J. High Energy Phys.*, 10:008, 2017.

[27] Thomas G. Mertens. The Schwarzian theory — origins. *J. High Energy Phys.*, 05:036, 2018.

[28] Juan Maldacena, Douglas Stanford, and Zhenbin Yang. Conformal symmetry and its breaking in two-dimensional nearly anti-de Sitter space. *Prog. Theor. Exp. Phys.*, 2016:12C104, 2016.

[29] Juan Maldacena and Douglas Stanford. Remarks on the Sachdev-Ye-Kitaev model. *Phys. Rev. D*, 94(10):106002, 2016.

[30] Dmitry Bagrets, Alexander Altland, and Alex Kamenev. Power-law out of time order correlation functions in the SYK model. *Nucl. Phys. B*, 921:727–752, 2017.

[31] Antonio M. García-García and Jacobus J. M. Verbaarschot. Analytical Spectral Density of the Sachdev-Ye-Kitaev Model at finite N. *Phys. Rev. D*, 96:066012, 2017.

[32] Samuel Frederick Edwards and Phil W Anderson. Theory of spin glasses. *J. Phys. F: Met. Phys.*, 5(5):965, 1975.

[33] Giorgio Parisi. Order parameter for spin-glasses. *Phys. Rev. Lett.*, 50(24):1946, 1983.

[34] Marc Mézard, Giorgio Parisi, and Miguel Virasoro. *Spin glass theory and beyond: An Introduction to the Replica Method and Its Applications*, volume 9. World Scientific Publishing Company, 1987.

[35] Antoine Georges, Olivier Parcollet, and Subir Sachdev. Quantum fluctuations of a nearly critical Heisenberg spin glass. *Phys. Rev. B*, 63(13):134406, 2001.

[36] Wenbo Fu and Subir Sachdev. Numerical study of fermion and boson models with infinite-range random interactions. *Phys. Rev. B*, 94(3):035135, 2016.

[37] Jinwu Ye. Two indices Sachdev-Ye-Kitaev model. 2018, arXiv:1809.06667.

[38] Yong-Hui Qi, Yunseok Seo, Sang-Jin Sin, and Geunho Song. Correlation functions in Schwarzian liquid. *Phys. Rev. D*, 99(6):066001, 2019.

[39] Guy Gur-Ari, Raghu Mahajan, and Abolhassan Vaezi. Does the SYK model have a spin glass phase? *J. High Energy Phys.*, 11:070, 2018.

[40] Alex Kamenev and Marc Mézard. Level correlations in disordered metals: the replica σ model. *Phys. Rev. B*, 60(6):3944, 1999.

[41] Igor V. Yurkevich and Igor V. Lerner. Nonperturbative results for level correlations from the replica nonlinear σ model. *Phys. Rev. B*, 60(6):3955, 1999.

[42] Shinsuke M. Nishigaki and Alex Kamenev. Replica treatment of non-Hermitian disordered Hamiltonians. *J. Phys. A: Math. Gen.*, 35(21):4571, 2002.

[43] Eugene Kanzieper. Replica field theories, Painlevé transcendents, and exact correlation functions. *Phys. Rev. Lett.*, 89(25):250201, 2002.

[44] A. V. Andreev and B. L. Altshuler. Spectral statistics beyond random matrix theory. *Phys. Rev. Lett.*, 75(5):902, 1995.

[45] Phil Saad, Stephen H Shenker, and Douglas Stanford. A semiclassical ramp in SYK and in gravity. 2018, arXiv:1806.06840.

[46] Irina Aref'eva, Mikhail Khramtsov, Maria Tikhanovskaya, and Igor Volovich. Replica-nondiagonal solutions in the SYK model. *J. High Energy Phys.*, 2019(7):1–59, 2019.

[47] Boris L'vovich Altshuler, Patrick A Lee, and W Richard Webb, editors. *Mesoscopic Phenomena in Solids*, volume 30 of *Modern Problems in Condensed Matter Sciences*. Elsevier, 1991.

[48] Ahmed Almheiri and Joseph Polchinski. Models of AdS_2 backreaction and holography. *J. High Energy Phys.*, 11:014, 2015.

[49] Jordan S Cotler, Guy Gur-Ari, Masanori Hanada, Joseph Polchinski, Phil Saad, Stephen H Shenker, Douglas Stanford, Alexandre Streicher, and Masaki Tezuka. Black holes and random matrices. *Journal of High Energy Physics*, 2017(5):118, 2017.

[50] David J. Gross and Vladimir Rosenhaus. The bulk dual of SYK: cubic couplings. *J. High Energy Phys.*, 05:092, 2017.

[51] Sean A Hartnoll, Andrew Lucas, and Subir Sachdev. *Holographic quantum matter*. MIT press, 2018, arXiv:1612.07324.

[52] Kristan Jensen. Chaos in AdS_2 holography. *Phys. Rev. Lett*, 117(11):111601, 2016.

[53] Antal Jevicki and Kenta Suzuki. Bi-local holography in the SYK model: perturbations. *J. High Energy Phys.*, 11:046, 2016.

[54] Alexei Kitaev and S Josephine Suh. The soft mode in the Sachdev-Ye-Kitaev model and its gravity dual. *J. High Energy Phys.*, 05:183, 2018.

[55] Daniel Harlow and Daniel Jafferis. The Factorization Problem in Jackiw-Teitelboim Gravity. 2018, arXiv:1804.01081.

[56] Tomoki Nosaka, Dario Rosa, and Junggi Yoon. The thouless time for mass-deformed syk. *J. High Energy Phys.*, 2018(9):1–40, 2018.

[57] Antonio M. García-García, Bruno Loureiro, Aurelio Romero-Bermúdez, and Masaki Tezuka. Chaotic-Integrable Transition in the Sachdev-Ye-Kitaev Model. *Phys. Rev. Lett.*, 120(24):241603, 2018.

[58] A. V. Lunkin, K. S. Tikhonov, and M. V. Feigel'man. Sachdev-Ye-Kitaev Model with Quadratic Perturbations: The Route to a Non-Fermi Liquid. *Phys. Rev. Lett.*, 121:236601, 2018.

[59] B. L. Altshuler, E. Cuevas, L. B. Ioffe, and V. E. Kravtsov. Nonergodic phases in strongly disordered random regular graphs. *Phys. Rev. Lett*, 117(15):156601, 2016.

[60] B. L. Altshuler, L. B. Ioffe, and V. E. Kravtsov. Multifractal states in self-consistent theory of localization: analytical solution. 2016, arXiv:1610.00758.

[61] V. E. Kravtsov, B. L. Altshuler, and L. B. Ioffe. Non-ergodic delocalized phase in Anderson model on Bethe lattice and regular graph. *Ann. Phys.*, 389:148 – 191, 2018.

[62] K. S. Tikhonov and A. D. Mirlin. Fractality of wave functions on a cayley tree: Difference between tree and locally treelike graph without boundary. *Phys. Rev. B*, 94:184203, Nov 2016.

[63] KS Tikhonov and AD Mirlin. Statistics of eigenstates near the localization transition on random regular graphs. *Phys. Rev. B*, 99(2):024202, 2019, arXiv:1810.11444.

[64] Xue-Yang Song, Chao-Ming Jian, and Leon Balents. Strongly Correlated Metal Built from Sachdev-Ye-Kitaev Models. *Phys. Rev. Lett.*, 119(21):216601, 2017.

[65] Richard A Davison, Wenbo Fu, Antoine Georges, Yingfei Gu, Kristan Jensen, and Subir Sachdev. Thermoelectric transport in disordered metals without quasiparticles: The Sachdev-Ye-Kitaev models and holography. *Phys. Rev. B*, 95(15):155131, 2017.

[66] Sumilan Banerjee and Ehud Altman. Solvable model for a dynamical quantum phase transition from fast to slow scrambling. *Phys. Rev. B*, 95(13):134302, 2017.

[67] Aavishkar A Patel, John McGreevy, Daniel P Arovas, and Subir Sachdev. Magnetotransport in a Model of a Disordered Strange Metal. *Phys. Rev. X*, 8(2):021049, 2018.

[68] Debanjan Chowdhury, Yochai Werman, Erez Berg, and T Senthil. Translationally Invariant Non-Fermi-Liquid Metals with Critical Fermi Surfaces: Solvable Models. *Phys. Rev. X*, 8(3):031024, 2018.

[69] Alexander Altland, Dmitry Bagrets, and Alex Kamenev. Sachdev-Ye-Kitaev Non-Fermi-Liquid Correlations in Nanoscopic Quantum Transport. *Phys. Rev. Lett.*, 123:226801, 2019.

[70] Yingfei Gu, Xiao-Liang Qi, and Douglas Stanford. Local criticality, diffusion and chaos in generalized Sachdev-Ye-Kitaev models. *Journal of High Energy Physics*, 2017(5):125, 2017.

[71] Chao-Ming Jian, Zhen Bi, and Cenke Xu. Model for continuous thermal metal to insulator transition. *Phys. Rev. B*, 96:115122, Sep 2017.

[72] Shao-Kai Jian and Hong Yao. Solvable Sachdev-Ye-Kitaev Models in Higher Dimensions: From Diffusion to Many-Body Localization. *Phys. Rev. Lett.*, 119:206602, Nov 2017.

[73] Pengfei Zhang. Dispersive Sachdev-Ye-Kitaev model: Band structure and quantum chaos. *Phys. Rev. B*, 96(20):205138, 2017.

[74] Shao-Kai Jian, Zhuo-Yu Xian, and Hong Yao. Quantum criticality and duality in the Sachdev-Ye-Kitaev/AdS_2 chain. *Phys. Rev. B*, 97(20):205141, 2018.

[75] Arijit Haldar, Sumilan Banerjee, and Vijay B. Shenoy. Higher-dimensional Sachdev-Ye-Kitaev non-Fermi liquids at Lifshitz transitions. *Phys. Rev. B*, 97:241106(R), Jun 2018.

[76] Pengfei Zhang and Hui Zhai. Topological Sachdev-Ye-Kitaev model. *Phys. Rev. B*, 97(20):201112, 2018, arXiv:1803.01411.

[77] Xiao-Chuan Wu, Chao-Ming Jian, and Cenke Xu. Lattice models for non-Fermi liquids with tunable transport scalings. *Phys. Rev. B*, 100(7):075101, 2019.

[78] Alexander Altland, Dmitry Bagrets, and Alex Kamenev. Quantum Criticality of Granular Sachdev-Ye-Kitaev Matter. *Phys. Rev. Lett.*, 123:106601, 2019.

[79] M Gurvitch and A. T. Fiory. Resistivity of $La_{1.825}Sr_{0.175}CuO_4$ and $YBa_2Cu_3O_7$ to 1100 K: absence of saturation and its implications. *Phys. Rev. Lett.*, 59(12):1337, 1987.

[80] Subir Sachdev. *Quantum Phase Transitions*. Cambridge University Press, Cambridge, U.K., 2011.

[81] J. Orenstein and A. J. Millis. Advances in the physics of high-temperature superconductivity. *Science*, 288(5465):468–474, 2000.

[82] Ilya Esterlis and Jörg Schmalian. Cooper pairing of incoherent electrons: an electron-phonon version of the Sachdev-Ye-Kitaev model. *Phys. Rev. B*, 100:115132, 2019.

[83] Daniel Hauck, Markus J Klug, Ilya Esterlis, and Jörg Schmalian. Eliashberg equations for an electron-phonon version of the Sachdev-Ye-Kitaev model: Pair Breaking in non-Fermi liquid superconductors. *Ann. Phys.*, 417:168120, 2020.

[84] Yuxuan Wang. Solvable Strong-Coupling Quantum-Dot Model with a Non-Fermi-Liquid Pairing Transition. *Phys. Rev. Lett.*, 124:017002, 2020.

[85] Y Cheipesh, A. I. Pavlov, V Scopelliti, J Tworzydło, and N. V. Gnezdilov. Reentrant superconductivity in a quantum dot coupled to a Sachdev-Ye-Kitaev metal. *Phys. Rev. B*, 100:220506(R), 2019.

[86] Aavishkar A Patel, Michael J Lawler, and Eun-Ah Kim. Coherent Superconductivity with a Large Gap Ratio from Incoherent Metals. *Phys. Rev. Lett.*, 121:187001, 2018.

[87] Debanjan Chowdhury and Erez Berg. Intrinsic superconducting instabilities of a solvable model for an incoherent metal. *Phys. Rev. Research*, 2:013301, 2020.

[88] Debanjan Chowdhury and Erez Berg. The unreasonable effectiveness of Eliashberg theory for pairing of non-Fermi liquids. *Ann. Phys.*, 417:168125, 2020.

[89] R W Richardson. A restricted class of exact eigenstates of the pairing-force Hamiltonian. *Phys. Lett.*, 3:277–279, 1963.

[90] Jan Von Delft and Fabian Braun. Superconductivity in ultrasmall grains: introduction to Richardson's exact solution. In I. O. Kulik and R. Ellialtioglu, editors, *Quantum Mesoscopic Phenomena and Mesoscopic Devices in Microelectronics*, page 361. Kluwer, Dordrecht, 2000.

[91] J. Dukelsky, S. Pittel, and G. Sierra. Colloquium: Exactly solvable Richardson-Gaudin models for many-body quantum systems. *Rev. Mod. Phys.*, 76:643, 2004.

[92] Andrey V Chubukov, Alexander M Finkel'stein, Robert Haslinger, and Dirk K Morr. First-Order Superconducting Transition near a Ferromagnetic Quantum Critical Point. *Phys. Rev. Lett.*, 90:077002, 2003.

[93] Yoshiki Kuramoto. Self-entrainment of a population of coupled non-linear oscillators. In H. Araki, editor, *International Symposium on Mathematical Problems in Theoretical Physics*, page 420. Springer, New York, 1975.

[94] Hiroaki Daido. Quasientrainment and slow relaxation in a population of oscillators with random and frustrated interactions. *Phys. Rev. Lett.*, 68:1073, 1992.

[95] Kurt Wiesenfeld, Pere Colet, and Steven H Strogatz. Frequency locking in Josephson arrays: Connection with the Kuramoto model. *Phys. Rev. E*, 57:1563, 1998.

[96] Steven H Strogatz. From Kuramoto to Crawford: exploring the onset of synchronization in populations of coupled oscillators. *Physica (Amsterdam)*, 143D(1-4):1–20, 2000.

[97] Juan A Acebrón, Luis L Bonilla, Conrad J Pérez Vicente, Félix Ritort, and Renato Spigler. The Kuramoto model: A simple paradigm for synchronization phenomena. *Rev. Mod. Phys.*, 77:137, 2005.

[98] Alex Arenas, Albert Díaz-Guilera, and Conrad J Pérez-Vicente. Synchronization processes in complex networks. *Physica (Amsterdam)*, 224D(1-2):27–34, 2006.

[99] Jesús Gómez-Gardeñes, Yamir Moreno, and Alex Arenas. Synchronizability determined by coupling strengths and topology on complex networks. *Phys. Rev. E*, 75(6):066106, 2007.

[100] Florian Dörfler, Michael Chertkov, and Francesco Bullo. Synchronization in complex oscillator networks and smart grids. *Proc. Natl. Acad. Sci. U.S.A.*, 110(6):2005–2010, 2013.

[101] Stefano Boccaletti, Ginestra Bianconi, Regino Criado, Charo I Del Genio, Jesús Gómez-Gardenes, Miguel Romance, Irene Sendina-Nadal, Zhen Wang, and Massimiliano Zanin. The structure and dynamics of multilayer networks. *Phys. Rep.*, 544(1):1–122, 2014.

[102] Dirk Witthaut, Sandro Wimberger, Raffaella Burioni, and Marc Timme. Classical synchronization indicates persistent entanglement in isolated quantum systems. *Nat. Commun.*, 8(1):14829, 2017.

[103] Raissa M D'Souza, Jesus Gómez-Gardeñes, Jan Nagler, and Alex Arenas. Explosive phenomena in complex networks. *Adv. Phys.*, 68(3):123–223, 2019.

[104] Chen-Ning Yang. Concept of Off-Diagonal Long-Range Order and the Quantum Phases of Liquid He and of Superconductors. *Rev. Mod. Phys.*, 34:694, 1962.

[105] Anthony J Leggett. Bose-Einstein condensation in the alkali gases: Some fundamental concepts. *Rev. Mod. Phys.*, 73:307, 2001.

[106] A Milekhin, G Tarnopolsky, A Kamenev, and I Klebanov, unpublished.

[107] C. L. Baldwin and B. Swingle. Quenched vs Annealed: Glassiness from SK to SYK. *Phys. Rev. X*, 10(3):031026, 2020.

[108] Yi-Ming Wu, Artem Abanov, and Andrey V. Chubukov. Pairing in quantum critical systems: Transition temperature, pairing gap, and their ratio. *Phys. Rev. B*, 99(1):014502, 2019.

[109] Sean A Hartnoll, Christopher P Herzog, and Gary T Horowitz. Building a Holographic Superconductor. *Phys. Rev. Lett.*, 101:031601, 2008.

[110] Yingfei Gu, Alexei Kitaev, Subir Sachdev, and Grigory Tarnopolsky. Notes on the complex Sachdev-Ye-Kitaev model. *J. High Energy Phys.*, 02(2020):157, 2020.

[111] Boris L Altshuler, Yuval Gefen, Alex Kamenev, and Leonid S Levitov. Quasiparticle lifetime in a finite system: A nonperturbative approach. *Phys. Rev. Lett.*, 78:2803, 1997, arXiv:cond-mat/9609132.

[112] Denis M Basko, Igor L Aleiner, and Boris L Altshuler. Metal–insulator transition in a weakly interacting many-electron system with localized single-particle states. *Ann. Phys.*, 321(5):1126–1205, 2006, arXiv:cond-mat/0506617.

[113] Vadim Oganesyan and David A Huse. Localization of interacting fermions at high temperature. *Phys. Rev. B*, 75:155111, 2007, arXiv:cond-mat/0610854.

[114] T Micklitz, Felipe Monteiro, and Alexander Altland. Nonergodic Extended States in the Sachdev-Ye-Kitaev Model. *Phys. Rev. Lett.*, 123(12):125701, 2019.

[115] K. S. Tikhonov and A. D. Mirlin. Statistics of eigenstates near the localization transition on random regular graphs. 2018, arXiv:1810.11444.

[116] Christopher R Laumann, A Pal, and A Scardicchio. Many-body mobility edge in a mean-field quantum spin glass. *Phys. Rev. Lett.*, 113(20):200405, 2014.

[117] Mohammad HS Amin and Vicki Choi. First-order quantum phase transition in adiabatic quantum computation. *Phys. Rev. A*, 80(6):062326, 2009.

[118] Boris Altshuler, Hari Krovi, and Jérémie Roland. Anderson localization makes adiabatic quantum optimization fail. *Proc. Natl. Acad. Sci. U.S.A.*, 107(28):12446–12450, 2010.

[119] Sergey Knysh. Zero-temperature quantum annealing bottlenecks in the spin-glass phase. *Nat. Commun.*, 7:12370, 2016.

[120] Masaki Ohkuwa, Hidetoshi Nishimori, and Daniel A Lidar. Reverse annealing for the fully connected p-spin model. *Phys. Rev. A*, 98(2):022314, 2018.

[121] Yu Yamashiro, Masaki Ohkuwa, Hidetoshi Nishimori, and Daniel A Lidar. Dynamics of reverse annealing for the fully connected p-spin model. *Phys. Rev. A*, 100(5):052321, 2019.

[122] Gianluca Passarelli, Ka-Wa Yip, Daniel A Lidar, Hidetoshi Nishimori, and Procolo Lucignano. Reverse quantum annealing of the p-spin model with relaxation. *Phys. Rev. A*, 101(2):022331, 2020.

[123] Alejandro Perdomo-Ortiz, Salvador E Venegas-Andraca, and Alan Aspuru-Guzik. A study of heuristic guesses for adiabatic quantum computation. *Quantum Inf. Proc.*, 10(1):33–52, 2011.

[124] Vasil S Denchev, Masoud Mohseni, and Hartmut Neven. Quantum assisted optimization. `https://patentimages.storage.googleapis.com/96/42/7c/ee519ba91acaf1/WO2017189052A1.pdf`, 2017. International Patent Application WO 2017/189052 A1.

[125] D-Wave Systems. Reverse quantum annealing for local refinement of solutions. `https://www.dwavesys.com/sites/default/files/14-1018A-A_Reverse_Quantum_Annealing_for_Local_Refinement_of_Solutions.pdf`, 2017. D-Wave White Paper Series, Tech. Rep. 14-1018A-A.

[126] Nicholas Chancellor. Modernizing quantum annealing using local searches. *New J. Phys.*, 19(2):023024, 2017.

[127] Andrew D King et al. Observation of topological phenomena in a programmable lattice of 1,800 qubits. *Nature*, 560(7719):456–460, 2018.

[128] C. L. Baldwin, C. R. Laumann, A. Pal, and A. Scardicchio. Clustering of Nonergodic Eigenstates in Quantum Spin Glasses. *Phys. Rev. Lett.*, 118(12):127201, 2017.

[129] Andrea Crisanti, Luca Leuzzi, Giorgio Parisi, and Tommaso Rizzo. Complexity in the Sherrington-Kirkpatrick model in the annealed approximation. *Phys. Rev. B*, 68(17):174401, 2003.

[130] Andrea Cavagna, Irene Giardina, and Giorgio Parisi. Numerical Study of Metastable States in Ising Spin Glasses. *Phys. Rev. Lett.*, 92(12):120603, 2004.

[131] A. P. Young. Stability of the quantum Sherrington-Kirkpatrick spin glass model. *Phys. Rev. E*, 96(3):032112, 2017.

[132] Sudip Mukherjee, Sabyasachi Nag, and Arti Garg. Many-body localization-delocalization transition in the quantum Sherrington-Kirkpatrick model. *Phys. Rev. B*, 97:144202, 2018, arXiv:1712.00204.

[133] M. C. Cambiaggio, A. M. F. Rivas, and M. Saraceno. Integrability of the pairing Hamiltonian. *Nucl. Phys. A*, 624:157, 1997.

[134] Manuel Asorey, Fernando Falceto, and German Sierra. Chern-Simons theory and BCS superconductivity. *Nucl. Phys. B*, 622:593–614, 2002.

[135] Andre LeClair, Jose Maria Roman, and German Sierra. Russian doll renormalization group and superconductivity. *Phys. Rev. B*, 69:020505(R), 2004.

[136] Clare Dunning and Jon Links. Integrability of the Russian doll BCS model. *Nucl. Phys. B*, 702:481–494, 2004.

[137] K. M. Bulycheva and A. S. Gorsky. Limit cycles in renormalization group dynamics. *Phys. Usp.*, 57:171–182, 2014.

[138] Claude Dimo and Alexandre Faribault. Quadratic operator relations and Bethe equations for spin-1/2 Richardson–Gaudin models. *J. Phys. A*, 51:325202, 2018.

[139] Mitsutoshi Fujita, Sarah Harrison, Andreas Karch, Rene Meyer, and Natalie M. Paquette. Towards a Holographic Bose-Hubbard Model. *J. High Energy Phys.*, 04(2015):068, 2015.

[140] Mitsutoshi Fujita, René Meyer, Sumiran Pujari, and Masaki Tezuka. Effective Hopping in Holographic Bose and Fermi Hubbard Models. *J. High Energy Phys.*, 01(2019):045, 2019.

[141] Tadakatsu Sakai and Shigeki Sugimoto. Low energy hadron physics in holographic QCD. *Prog. Theor. Phys.*, 113:843–882, 2005.

[142] Dominik Nickel and Dam T. Son. Deconstructing holographic liquids. *New J. Phys.*, 13:075010, 2011.

[143] D. T. Son and M. A. Stephanov. QCD and dimensional deconstruction. *Phys. Rev. D*, 69:065020, 2004.

[144] Edward Witten. Baryons and branes in anti-de Sitter space. *J. High Energy Phys.*, 07(1998):006, 1998.

[145] Thomas C. Kraan and Pierre van Baal. Periodic instantons with nontrivial holonomy. *Nucl. Phys. B*, 533:627–659, 1998.

[146] Yong-Liang Ma and Mannque Rho. Pseudoconformal structure in dense baryonic matter. *Phys. Rev. D*, 99(1):014034, 2019.

[147] Tatsuma Nishioka, Shinsei Ryu, and Tadashi Takayanagi. Holographic Superconductor/Insulator Transition at Zero Temperature. *J. High Energy Phys.*, 03(2010):131, 2010.

[148] Pranjal Nayak, Ashish Shukla, Ronak M. Soni, Sandip P. Trivedi, and V. Vishal. On the Dynamics of Near-Extremal Black Holes. *J. High Energy Phys.*, 09(2018):048, 2018.

Appendix A

Replica structure in SYK: technical details

A.1 Replica non-diagonal saddle point solutions.

In this section we provide detailed form of the replica non-diagonal solutions of saddle point Eqs. (2.58). Consider the $n \times n$ matrix $\mathbf{g}$ with all diagonal elements equal $\tilde{g}$, and all off-diagonal elements equal g

$$g_{ab} = \tilde{g}\delta_{ab} + g(1 - \delta_{ab}), \tag{A.1}$$

Substituting the ansatz Eq. (A.1) into saddle point Eqs. (2.58), we obtain

$$\tilde{g}^4 + (n-1)g^4 = 1, \tag{A.2}$$

$$\tilde{g}^3 g + g^3 \tilde{g} + (n-2)g^4 = 0. \tag{A.3}$$

Introducing the variable $z = \tilde{g}/g$ we obtain from Eq. (A.3)

$$z^3 + z + (n-2) = 0. \tag{A.4}$$

In the replica-limit $n \to 0$, equation for z can be written as

$$(z-1)(z^2 + z + 2) = 0 \tag{A.5}$$

The solution $z = 1$ means $\tilde{g} = g$, which cannot satisfy Eq. (A.2). The solutions of equation $z^2 + z + 2 = 0$,

$$z = \frac{-1 \pm i\sqrt{7}}{2}, \tag{A.6}$$

result in the nontrivial replica non-diagonal saddle-points that are discussed below. For $z = \frac{-1+i\sqrt{7}}{2}$, we obtain

$$g^4 = -\frac{1}{4} e^{i \arctan(3\sqrt{7})}, \ \tilde{g}^4 = e^{-i \arctan\left(\frac{3\sqrt{7}}{31}\right)}, \tag{A.7}$$

while $z = \frac{-1-i\sqrt{7}}{2}$ results in the complex conjugated expressions. It follows, that there are four pairs of mutually complex conjugated solutions with nontrivial replica-off-diagonal part, $g \neq 0$.

To determine the relevance of the found saddle point solutions, we compare the values of the saddle-point action at the replica-diagonal and at the replica-off-diagonal saddle points. For the calculation of Tr ln term at replica-off-diagonal saddle point we use the following formula

$$\begin{aligned} &\mathrm{Tr} \ln \Sigma^{ab}_{\tau\tau'} = \ln \det \left[\hat{\sigma}\right] + n \mathrm{Tr} \ln \left(\Sigma_{\tau,\tau'}\right) \\ &= \ln \left\{ \tilde{\sigma}^n \left(1 - \frac{\sigma}{\tilde{\sigma}}\right)^{n-1} \left[1 + (n-1)\frac{\sigma}{\tilde{\sigma}}\right] \right\} + n \mathrm{Tr} \ln \left(\Sigma_{\tau,\tau'}\right). \end{aligned} \tag{A.8}$$

where $\tilde{\sigma}$ and σ denote the diagonal and off-diagonal elements of the replica-matrix $\hat{\sigma}$ for the self-energy, and $\Sigma_{\tau,\tau'}$ denotes the replica-diagonal solution as specified in Eqs. (2.57), (2.58), (3.1). Performing the replica limit $n \to 0$ in Eq. (A.8), the action for the replica-off-diagonal saddle point can be written as

$$\begin{aligned} -S_{\mathrm{RND}} = \frac{Nn}{2} \Bigg\{ &\ln(J^{3/2}\tilde{g}^3) + \ln\left(1 - \frac{1}{z^3}\right) + \\ &\frac{1}{z^3 - 1} + \frac{3}{4} J^2 \tilde{g}^4 \left(1 - \frac{1}{z^4}\right) + \mathrm{Tr} \ln \left(\Sigma_{\tau,\tau'}\right) \Bigg\}. \end{aligned} \tag{A.9}$$

Note that $\frac{3}{4} J^2 \tilde{g}^4 (1 - 1/z^4) = 3/4$ for both values of z from Eq. (A.6) and all possible solutions in Eq. (A.7), as well as for the replica diagonal saddle point $\tilde{g} = 1/\sqrt{J}$, $g = 0$. Therefore, the difference between the action at the replica-diagonal and at the

the replica-non-diagonal saddle points comes from the logarithmic terms only. It is given by

$$-\left(S_{\mathrm{RND}}-S_{\mathrm{RD}}\right)=\frac{Nn}{2}\left\{3\ln(\sqrt{J}\tilde{g})+\ln\left(1-\frac{1}{z^3}\right)+\frac{1}{z^3-1}\right\}. \tag{A.10}$$

The real part of Eq. (A.10) equals $-(S_{\mathrm{RND}}-S_{\mathrm{RD}})=0.0284\frac{Nn}{2}$ for all solutions listed in Eq. (A.7). Since it is positive, the replica-non-diagonal saddle points give the dominant contributions to the replicated partition function $\langle Z^n\rangle = e^{-S}$. The difference $-(S_{\mathrm{RND}}-S_{\mathrm{RD}})$ for possible solutions from Eq. (A.7) is summarized in the table below

z	$J^2\tilde{g}$	$J^2 g$	$-(S_{\mathrm{RSB}}-S_{\mathrm{RS}})$
$\frac{-1+i\sqrt{7}}{2}$	$0.99804-0.06262i$	$-0.29093-0.64448i$	$0.02843+1.66411i\pm i\frac{3\pi}{2}$
$\frac{-1+i\sqrt{7}}{2}$	$0.06262+0.998034i$	$0.64448-0.29093i$	$0.02842+0.87871i\pm i\frac{3\pi}{2}$
$\frac{-1+i\sqrt{7}}{2}$	$-0.99804+0.06262i$	$0.29093+0.64448i$	$0.02843+2.44951i\pm i\frac{3\pi}{2}$
$\frac{-1+i\sqrt{7}}{2}$	$-0.06262-0.99804i$	$-0.64448+0.29093i$	$0.02843-0.69209i\pm i\frac{3\pi}{2}$

The values for $z=\frac{-1-i\sqrt{7}}{2}$ are complex conjugated to the corresponding values given in the table.

In conclusion of this section, we consider another possible structure of the non-diagonal saddle point matrix $\mathbf{g}$, consisting of n blocks of the size $p\times p$ along the main diagonal, the structure of each $p\times p$ block being given by Eq. (A.1). In that case, Eqs. (2.58) result in the following equations for the matrix elements

$$\tilde{g}^4+(p-1)g^4=1, \tag{A.11}$$

$$\tilde{g}^3 g+g^3\tilde{g}+(p-2)g^4=0. \tag{A.12}$$

From Eq. (A.3) we obtain for $z=\tilde{g}/g$

$$z^3+z+(p-2)=0. \tag{A.13}$$

In general, there are three solutions for z. However, only two mutually complex conjugated solutions are consistent with Eq. (A.2). Each solution fixes unambiguously the values of $\tilde{g}^4$ and g^4, thus resulting in four possible (generally complex) values of $\tilde{g}$ and

g. In particular, for $p = 2$ we obtain

$$z = 0, \;\; or \;\; z = \pm i. \tag{A.14}$$

The solution $z = 0$ results in the completely replica off-diagonal matrix $\mathbf{g}$, which clearly contradicts numerical results in Sec. **??**. From the solution $z = i$ it follows $\tilde{g} = ig$. Substituting this relation in Eq. (A.2) for $p = 2$, we obtain, as one possible solution, the matrix $\mathbf{g}$ as given in Eq. (3.22).

A.2 Fluctuation expansion around the replica-diagonal saddle point

To obtain the action for massive fluctuations around the replica diagonal saddle point, we adopt the ansatz

$$G^{ab}_{\tau\tau'} = G(\tau - \tau')\delta_{ab} + \delta G^{ab}_{\tau\tau'}, \tag{A.15}$$

$$\Sigma^{ab}_{\tau\tau'} = \Sigma(\tau - \tau')\delta_{ab} + \delta \Sigma^{ab}_{\tau\tau'}, \tag{A.16}$$

where $G(\tau - \tau')$ and $\Sigma(\tau - \tau')$ denote the traditional replica-diagonal saddle point solutions. Substituting Eqs. (A.15), (A.16) into the action Eq. (2.55) and performing the expansion in $\delta\Sigma$ and δG, we obtain the action for the fluctuations around the the replica-diagonal saddle point, which can be represented as a sum of the actions for different replicas,

$$-\delta S[\delta\Sigma, \delta G] = -\sum_{a,b=1}^{n} \delta S^{ab}[\delta\Sigma^{ab}, \delta G^{ab}], \tag{A.17}$$

where

$$\delta S^{aa}[\delta\Sigma^{aa}, \delta G^{aa}] = \frac{N}{2}\left\{\frac{1}{2}\mathrm{Tr}\left[G\delta\Sigma^{aa}G\delta\Sigma^{aa}\right] - \int d\tau d\tau' \delta\Sigma^{aa}_{\tau'\tau}\delta G^{aa}_{\tau\tau'} - \right.$$
$$\left.\frac{1}{4}J^2\int d\tau d\tau' \left[6G^2(\tau-\tau')\left(\delta G^{aa}_{\tau\tau'}\right)^2 + 4G(\tau-\tau')\left(\delta G^{aa}_{\tau\tau'}\right)^3 + \left(\delta G^{aa}_{\tau\tau'}\right)^4\right]\right\} \tag{A.18}$$

$$\delta S^{ab}[\delta\Sigma^{ab},\delta G^{ab}]=\frac{N}{2}\left\{\frac{1}{2}\mathrm{Tr}\left[G\delta\Sigma^{ab}G\delta\Sigma^{ba}\right]-\int d\tau d\tau'\delta\Sigma^{ba}_{\tau'\tau}\delta G^{ab}_{\tau\tau'}-\frac{1}{4}J^2\left(\delta G^{ab}_{\tau\tau'}\right)^4\right\}. \tag{A.19}$$

Let us derive the generating functional for the correlation functions containing off-diagonal fluctuations $\delta\Sigma^{ab}$. To this end we extend the action Eq. (A.19) with source terms for $\delta\Sigma$ and δG

$$-S_{\mathrm{source}}=\frac{N}{2}\int d\tau d\tau'\left\{j^{ba}_{\tau'\tau}\delta G^{ab}_{\tau\tau'}+\delta\Sigma^{ba}_{\tau'\tau}h^{ab}_{\tau\tau'}\right\} \tag{A.20}$$

The quadratic part of the action $-S=-\delta S^{ab}[\delta\Sigma^{ab},\delta G^{ab}]-S_{\mathrm{source}}$ can be represented in the matrix form

$$\begin{aligned}-\delta S^{ab}_{(2)}&=\frac{1}{2}(h^{ab}_{\tau\tau'},j^{ab}_{\tau\tau'})\cdot\begin{pmatrix}\delta\Sigma^{ba}_{\tau',\tau}\\ \delta G^{ba}_{\tau'\tau}\end{pmatrix}-\\ &\frac{N}{4}\left(\delta\Sigma^{ab}_{\tau_1,\tau_2},\delta G^{ab}_{\tau_1,\tau_2}\right)\begin{pmatrix}\mathcal{K}^{\tau_2,\tau_3}_{\tau_1,\tau_4} & -\delta_{\tau_1,\tau_4}\delta_{\tau_2,\tau_3}\\ -\delta_{\tau_1,\tau_4}\delta_{\tau_2,\tau_3} & 0\end{pmatrix}\begin{pmatrix}\delta\Sigma^{ba}_{\tau_3,\tau_4}\\ \delta G^{ba}_{\tau_3\tau_4}\end{pmatrix}\end{aligned} \tag{A.21}$$

Using the symmetry of the fermionic Green functions with respect to exchange of arguments

$$\delta G^{ab}_{\tau_1,\tau_2}=-\delta G^{ba}_{\tau_2,\tau_1},\ \ \delta\Sigma^{ab}_{\tau_1,\tau_2}=-\delta\Sigma^{ba}_{\tau_2,\tau_1} \tag{A.22}$$

we rewrite the quadratic action in the form

$$\begin{aligned}-\delta S^{ab}_{(2)}&=\frac{N}{4}\left(\delta\Sigma^{ab}_{\tau_1,\tau_2},\delta G^{ab}_{\tau_1,\tau_2}\right)\begin{pmatrix}\mathcal{K}^{\tau_2,\tau_4}_{\tau_1,\tau_3} & -\delta_{\tau_1,\tau_3}\delta_{\tau_2,\tau_4}\\ -\delta_{\tau_1,\tau_3}\delta_{\tau_2,\tau_4} & 0\end{pmatrix}\begin{pmatrix}\delta\Sigma^{ab}_{\tau_3\tau_4}\\ \delta G^{ab}_{\tau_3\tau_4}\end{pmatrix}\\ &-\frac{1}{2}(h^{ab}_{\tau\tau'},j^{ab}_{\tau\tau'})\cdot\begin{pmatrix}\delta\Sigma^{ab}_{\tau,\tau'}\\ \delta G^{ab}_{\tau\tau'}\end{pmatrix}\end{aligned} \tag{A.23}$$

Correlation functions of the fields δG and $\delta\Sigma$ are obtained by taking derivatives, for instance

$$\langle\delta\Sigma^{ab}_{\tau_1\tau_2}\delta\Sigma^{ab}_{\tau_3\tau_4}(\delta G^{ab}_{\tau_5,\tau_6})^4\rangle=2^6\frac{\delta^6\langle e^{-\delta S^{ab}_{(2)}}\rangle}{\delta h^{ab}_{\tau_1\tau_2}\delta h^{ab}_{\tau_3\tau_4}(\delta j^{ab}_{\tau_5\tau_6})^4} \tag{A.24}$$

Integrating the fields $\delta\Sigma$, δG, we obtain

$$\langle e^{-S^{ab}[j,h]}\rangle = \exp\left[\frac{1}{4N}(h^{ab}_{\tau_1\tau_2}, j^{ab}_{\tau_1\tau_2})\begin{pmatrix} 0 & \delta_{\tau_1,\tau_3}\delta_{\tau_2,\tau_4} \\ \delta_{\tau_1,\tau_3}\delta_{\tau_2,\tau_4} & \mathcal{K}^{\tau_2,\tau_4}_{\tau_1,\tau_3}\end{pmatrix}\begin{pmatrix} h^{ab}_{\tau_3\tau_4} \\ j^{ab}_{\tau_3\tau_4}\end{pmatrix}\right] \quad \text{(A.25)}$$

From Eq. (A.25) we read off the following nonzero contractions of the fields δG and $\delta\Sigma$

$$\langle \delta G^{ab}_{\tau_1,\tau_2}\delta\Sigma^{ab}_{\tau_3,\tau_4}\rangle = \langle \delta\Sigma^{ab}_{\tau_1,\tau_2}\delta G^{ab}_{\tau_3,\tau_4}\rangle = \frac{1}{4N}\delta_{\tau_1,\tau_3}\delta_{\tau_2,\tau_4}, \quad \text{(A.26)}$$

$$\langle \delta G^{ab}_{\tau_1,\tau_2}\delta G^{ab}_{\tau_3,\tau_4}\rangle = \frac{1}{4N}\mathcal{K}^{\tau_2,\tau_4}_{\tau_1,\tau_3} = \frac{1}{4N}G(\tau_3-\tau_1)G(\tau_2-\tau_4). \quad \text{(A.27)}$$

The additive form of the fluctuation action Eq. (A.17) implies the multiplicative form of the correlation function Eq. (3.20) as a product over the pairs of replicas

$$\begin{aligned}\mathcal{D}_{2p}(\tau) &= (2p-1)!!\langle\chi_i^{a_1}(\tau)\chi_i^{a_2}(0)\rangle\langle\chi_j^{a_1}(0)\chi_j^{a_2}(\tau)\rangle...\langle\chi_i^{a_{2p-1}}(\tau)\chi_i^{a_{2p}}(0)\rangle\langle\chi_j^{a_{2p-1}}(0)\chi_j^{a_{2p}}(\tau)\rangle \\ &= (2p-1)!!\left(\mathcal{D}_2(\tau)\right)^p. \end{aligned} \quad \text{(A.28)}$$

Here $(2p-1)!!$ denotes the number of ways to assign pairs of replicas. The fluctuation expansion around the replica-diagonal saddle point results in

$$D_2^{\mathrm{RD}}(\tau) = \frac{3}{2^{10}N^3}G(\tau)G(-\tau) = \frac{3}{4\pi 2^{10}N^3}\frac{1}{|\tau|}. \quad \text{(A.29)}$$

The same conclusion can be made by means of $1/N$ diagrammatic expansion without employing the replica-trick (see Fig. A.1) [15].

A.3 Correlation function in the replica non-diagonal saddle point.

The replica non-diagonal saddle point assigns a non-zero average to the correlation function $\langle\chi_i^a(\tau)\chi_i^b(\tau')\rangle$. Calculation of high-order correlation functions, such as the one defined by Eq. (3.19), requires building of contractions of pairs of fermions corresponding to the nonzero average in the saddle point, which leads to the general form as given by Eq. (A.28), but with the function $\mathcal{D}_2$ calculated in the replica non-diagonal saddle point.

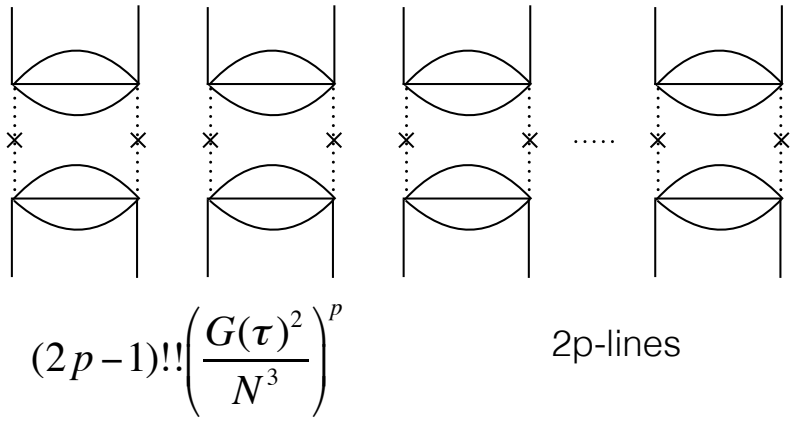

Figure A.1: Diagram for the correlation function $\mathcal{D}_{2p}$. Crossed dashed lines represent averaging over disorder.

Let us now consider the calculation of the function $\mathcal{D}_2$ explicitely. First we note, that the saddle point equations Eqs. (2.56) are invariant with respect to the replica dependent time shift $\tau \to \tau + \tau_a$. This transformation does not change the time dependence in the replica-diagonal elements of saddle point solutions in Eq. (3.1), it influences the replica off-diagonal elements though. As we show below, the time-shift transformation is crucial to obtain the correct time dependence for the correlation functions calculated at the replica non-diagonal saddle point. Consider the correlation function between Majorana fermions on different sites ($i \neq j$)

$$D_2(\tau_1,\tau_2;\tau_3,\tau_4) = \langle\langle \chi_i(\tau_1)\chi_j(\tau_2)\rangle_{\rm QM}\langle\chi_i(\tau_3)\chi_j(\tau_4)\rangle_{\rm QM}\rangle_{\rm dis}\,. \tag{A.30}$$

The correlation function Eq. (A.30) in the replica formalism reads

$$D_2(\tau_1,\tau_2;\tau_3,\tau_4) = \left\langle \chi_i^a(\tau_1)\chi_j^a(\tau_2)\chi_i^b(\tau_3)\chi_j^b(\tau_4)\right\rangle = -\left\langle G^{ab}(\tau_1-\tau_3)G^{ab}(\tau_2-\tau_4)\right\rangle_\Phi, \tag{A.31}$$

where $\langle ...\rangle_\Phi$ denotes the average over the reparametrization fluctuations, and $G^{ab}(\tau-\tau')$ denotes the saddle point replica-off-diagonal Green's function. The time-dependence in

Eq. (A.31) contradicts the quantum mechanical result, which predicts the dependence of correlation function on the differences $\tau_1 - \tau_2$ and $\tau_3 - \tau_4$. However, one can restore the correct quantum mechanical dependence of the correlation function Eq. (A.31) by making appropriate time-shifts in each replica. Namely, for each pair of times belonging to the same replica, the time-shift has to be chosen in such a way, that the shifted times are symmetric with respect to zero. Specifically, in Eq. (A.31), the times τ_1, τ_2, belonging to the replica a, are shifted by $c_a = -(\tau_1 + \tau_2)/2$, so that after the shift $\tau_1' = \tau_1 - c_a = (\tau_1 - \tau_2)/2$, and $\tau_2' = \tau_2 - c_a = -(\tau_1 - \tau_2)/2 = -\tau_1'$. Correspondingly, the times τ_3 and τ_4 are shifted by $c_b = -(\tau_3 + \tau_4)/2$. Let us calculate the correlation function Eq. (A.31) assuming the following ordering of times: $\tau_2 < \tau_3 < \tau_4 < \tau_1$. Using the Liouville quantum mechanical representation for the averaging over the reparametrization fluctuations [16], we obtain

$$\Big\langle G^{ab}(\tau_1 - \tau_3) G^{ab}(\tau_2 - \tau_4) \Big\rangle_\Phi \propto \int_0^\infty \frac{d\alpha d\beta}{\sqrt{\alpha\beta}} \sum_k \langle 0|e^{\frac{1}{4}\phi}|k_\alpha\rangle e^{-\frac{k_\alpha^2}{4M}[(\tau_3-\tau_2)+c_b-c_a)]} \times$$
$$\langle k_\alpha|e^{\frac{1}{4}\phi}|k_{\alpha+\beta}\rangle e^{-\frac{k_{\alpha+\beta}^2}{2M}(\tau_4-\tau_3)} \langle k_{\alpha+\beta}|e^{\frac{1}{4}\phi}|k_\beta\rangle e^{-\frac{k_\beta^2}{4M}[(\tau_1-\tau_3)+c_a-c_b} \langle k_\beta|e^{\frac{1}{4}\phi}|0\rangle =$$
$$\int_0^\infty \frac{d\alpha d\beta}{\sqrt{\alpha\beta}} \sum_k \langle 0|e^{\frac{1}{4}\phi}|k_\alpha\rangle e^{-\frac{k_\alpha^2}{4M}[\frac{1}{2}(\tau_3-\tau_4+\tau_1-\tau_2)]} \times$$
$$\langle k_\alpha|e^{\frac{1}{4}\phi}|k_{\alpha+\beta}\rangle e^{-\frac{k_{\alpha+\beta}^2}{2M}(\tau_4-\tau_3)} \langle k_{\alpha+\beta}|e^{\frac{1}{4}\phi}|k_\beta\rangle e^{-\frac{k_\beta^2}{4M}[\frac{1}{2}(\tau_1-\tau_2+\tau_4-\tau_3)} \langle k_\beta|e^{\frac{1}{4}\phi}|0\rangle$$

One can see, that after the time shifts c_a and c_b, the correlation function depends on the time differences $\tau_1 - \tau_2$ and $\tau_4 - \tau_3$ only. For $\tau_1 = \tau_4 = \tau$, $\tau_2 = \tau_3 = 0$ Eq. (A.32) reduces to the correlation function calculated in Ref. [16], namely

$$\Big\langle G^{ab}(\tau) G^{ab}(\tau) \Big\rangle_\Phi \propto \int_0^\infty \frac{d\alpha d\beta}{\sqrt{\alpha\beta}} \sum_k \langle 0|e^{\frac{1}{2}\phi}|k_{\alpha+\beta}\rangle e^{-\frac{k_{\alpha+\beta}^2}{2M}\tau} \langle k_{\alpha+\beta}|e^{\frac{1}{2}\phi}|0\rangle \sim \frac{1}{\tau^{3/2}}.$$

Let us now consider the higher powers of the site-nonlocal correlation functions, which we define as a product of $2p$ quantum mechanical averages

$$\mathcal{K}(\tau_1, ..., \tau_{4p}) = \langle\langle \chi_i(\tau_1)\chi_j(\tau_2)\rangle_{\rm QM} \langle \chi_i(\tau_3)\chi_j(\tau_4)\rangle_{\rm QM} ... \langle \chi_i(\tau_{4p-1})\chi_j(\tau_{4p})\rangle_{\rm QM}\rangle_{\rm dis} =$$
$$\Big\langle \chi_i^{a_1}(\tau_1)\chi_i^{a_2}(\tau_3)...\chi_i^{a_{2p}}(\tau_{4p-1})\chi_j^{a_1}(\tau_2)\chi_j^{a_2}(\tau_4)...\chi_j^{a_{2p}}(\tau_{4p})\Big\rangle \qquad \text{(A.32)}$$

To facilitate the transition to the limit case, considered in Section 3.2.3

$$\mathcal{D}_{2p}(\tau) = \langle (\langle \chi_i(\tau)\chi_j(0)\rangle_{\rm QM}\langle \chi_j(\tau)\chi_i(0)\rangle_{\rm QM})^p\rangle_{\rm dis} = \\ (-1)^p \langle (\langle \chi_i(\tau)\chi_j(0)\rangle_{\rm QM}\langle \chi_i(0)\chi_j(\tau)\rangle_{\rm QM})^p\rangle_{\rm dis} \tag{A.33}$$

we adopt the following ordering of times in Eq. (A.32)

$$\tau_2 < \tau_3 < \tau_6 < \tau_7 < ... < \tau_{4p-2} < \tau_{4p-1} < \tau_{4p} < \tau_{4p-3} < \tau_{4p-4} < \tau_{4p-7} < \tau_{4p-8} < ... \\ < \tau_5 < \tau_4 < \tau_1 \tag{A.34}$$

The transition to Eq. (A.33) is achieved by taking the limits $\tau_2 = \tau_3 = ... = \tau_{4p} = 0$, $\tau_{4p-3} = \tau_{4p-4} = ... = \tau_1 = \tau$. The correlation function Eq. (A.32) is given by the sum over all possible site-local contractions between the fermions belonging to different replicas. Consider a single contribution, where we denote the pairs of contracted replicas as (a_1, a_2), (a_3, a_4), ... (a_{2p-1}, a_{2p}). Then, employing the Liouville quantum mechanincal treatment of the averaging over reparametrizations and implementing replica-dependent

time shifts $\tau_a \to \tau_a + c_a$, we obtain

$$\mathcal{K}(\tau_1,...,\tau_{4p}) = \langle G^{a_1,a_2}(\tau_1,\tau_3)G^{a_1,a_2}(\tau_2,\tau_4)G^{a_3,a_4}(\tau_5,\tau_7)G^{a_3,a_4}(\tau_6,\tau_8)...$$
$$G^{a_{2p-1},a_{2p}}(\tau_{4p-3},\tau_{4p-1})G^{a_{2p-1},a_{2p}}(\tau_{4p-2},\tau_{4p})\rangle_\Phi \propto$$
$$\int_0^\infty \frac{d\alpha_1...d\alpha_{2p}}{(\alpha_1...\alpha_{2p})^{1/2}} \sum_{k_\alpha,k'_\alpha} \langle 0|e^{\frac{\phi}{4}}|k_{\alpha_1}\rangle \exp\left[-\frac{k^2_{\alpha_1}}{2M}(\tau_3 + c_2 - \tau_2 - c_1)\right]$$
$$\langle k_{\alpha_1}|e^{\frac{\phi}{4}}|k_{\alpha_1+\alpha_2}\rangle \exp\left[-\frac{k^2_{\alpha_1+\alpha_2}}{2M}(\tau_7 + c_4 - \tau_6 - c_3)\right]...$$
$$\langle k_{\alpha_1+\alpha_2+...+\alpha_{2p-1}}|e^{\frac{\phi}{4}}|k_{\alpha_1+\alpha_2+...+\alpha_{2p}}\rangle \exp\left[-\frac{k^2_{\alpha_1+\alpha_2+...+\alpha_{2p}}}{2M}(\tau_{4p} - \tau_{4p-1})\right]$$
$$\langle k_{\alpha_1+\alpha_2+...+\alpha_{2p}}|e^{\frac{\phi}{4}}|k'_{\alpha_1+\alpha_2+...+\alpha_{2p-1}}\rangle \exp\left[-\frac{k'^2_{\alpha_1+\alpha_2+...+\alpha_{2p-1}}}{2M}(\tau_{4p-3} + c_{2p-1} - \tau_{4p} - c_{2p})\right]$$
$$\langle k'_{\alpha_1+\alpha_2+...+\alpha_{2p-1}}|e^{\frac{\phi}{4}}|k'_{\alpha_1+\alpha_2+...+\alpha_{2p-2}}\rangle \exp\left[-\frac{k'^2_{\alpha_1+\alpha_2+...+\alpha_{2p-2}}}{2M}(\tau_{4p-7} + c_{2p-3} - \tau_{4p-4} - c_{2p-2})\right]...$$
$$\langle k'_{\alpha_1+\alpha_2+\alpha_3}|e^{\frac{\phi}{4}}|k'_{\alpha_1+\alpha_2}\rangle \exp\left[-\frac{k'^2_{\alpha_1+\alpha_2}}{2M}(\tau_4 + c_2 - \tau_5 - c_3)\right]$$
$$\langle k'_{\alpha_1+\alpha_2}|e^{\frac{\phi}{4}}|k'_{\alpha_1}\rangle \exp\left[-\frac{k'^2_{\alpha_1}}{2M}(\tau_1 + c_1 - \tau_4 - c_2)\right] \langle k'_{\alpha_1}|e^{\frac{\phi}{4}}|0\rangle. \tag{A.35}$$

To ensure the dependence of Eq. (A.35) on the differences of times belonging to the same replica only, we choose the time shifts c_k as follows

$$c_k = -\frac{1}{2}(\tau_{2k} + \tau_{2k-1}) \tag{A.36}$$

With this choice, the combinations of times entering the exponents in Eq. (A.35) become

$$\tau_{2k-2} + c_{k-1} - \tau_{2k} - c_k = \frac{1}{2}[(\tau_{2k-2} - \tau_{2k-3}) - (\tau_{2k} - \tau_{2k-1}),$$
$$\tau_{2k-1} + c_k - \tau_{2k-3} - c_{k-1} = \frac{1}{2}[(\tau_{2k-1} - \tau_{2k}) - (\tau_{2k-3} - \tau_{2k-2}). \tag{A.37}$$

Therefore, the choice of time shifts in Eq. (A.37) makes the argument of each exponent in Eq. (A.35) to depend only on differences of times in the same replica. Note furthermore, that the time-shifts introduced by Eq. (A.36) are replica-local, hence they ensure the quantum mechanically correct time dependence for any choice of contractions.

In the limit $\tau_2 = \tau_3 = ... = \tau_{4p} = 0$, $\tau_{4p-3} = \tau_{4p-4} = ... = \tau_1 = \tau$, the calculation in Eq. (A.35) reduces literally to the one performed in Ref. [16], hence one obtains for the correlation function Eq. (A.33) the time dependence $\sim 1/|\tau|^{3/2}$ for any power p.

A.4 Reparametrization fluctuations around the replica non-diagonal saddle

In this Appendix we show, that the replica non-diagonal saddle point generates coupling between the reparametrizations in different replicas, leaving only a single soft mode, in which all replicas have the same reparametrization. Consider the replica non-diagonal saddle point given by Eq. (3.1), and consider the replica off-diagonal part of the soft-mode action

$$S_2[f] = \frac{N}{4}\,\mathrm{Tr}(\partial_\tau G \partial_\tau G) = \frac{N}{4}\sum_{ab}\int\limits_{|\tau_1-\tau_2|>1/J} d\tau_1 d\tau_2\,\partial_{\tau_1}\left(G^{ab}[f]_{\tau_1,\tau_2}\right)\partial_{\tau_2}\left(G^{bb}[f]_{\tau_2,\tau_1}\right), \tag{A.38}$$

which is formulated in terms of the reparametrized Green functions

$$G^{ab}[f]_{\tau_1,\tau_2} = f_a'(\tau_1)^{1/4} G^{ab}\Big[f_a(\tau_1) - f_b(\tau_2)\Big] f_b'(\tau_2)^{1/4}, \tag{A.39}$$

with $f_a(\tau)$ being the reparametrization transformation in the replica a. Note, that such form of the Green's function is valid only for times $|\tau - \tau'| > 1/J$. For shorter times, $|\tau - \tau'| \ll 1/J$, the Green's function in the model with finite strength of interaction J should approach a free Majorana correlator, $G^{ab}_{\rm free}(\tau) = -\delta^{ab}\mathrm{sgn}(\tau)/|\tau|$. Therefore we restricted the domain of integration in Eq. (A.38).

If one further changes the time-integration variables to $t_i = f(\tau_i)$, defines the field $\zeta^a_t = [(f_a^{-1})'(t)]^{-1/2}$ and integrates by parts then the action $S_2[f]$ can be cast in the following form (for details see Ref. [16])

$$S_2[f] = \sum_{ab}\int dt_1\, dt_2\, \zeta^a_{t_1}\,\Pi^{ab}(t)\,\zeta^b_{t_2}, \qquad \Pi^{ab}(t_1-t_2) = -\frac{N}{4}\,G^{ab}(t_1-t_2)\overleftrightarrow{\partial}_{t_1}\overleftrightarrow{\partial}_{t_2}G^{ab}(t_2-t_1), \tag{A.40}$$

where we introduced $f_1(t)\overleftrightarrow{\partial_t} f_2(t) \equiv \frac{1}{2}[f_1(t)f_2'(t) - f_1'(t)f_2(t)]$ for any two functions f_1

and f_2. Taking into account the symmetries of the Green's function,

$$G^{ab}(-t) = -G^{ab}(t), \qquad G^{ab}(t) = G^{ba}(t), \tag{A.41}$$

the polarization operator can be represented in the equivalent form,

$$\Pi^{ab}(t) = \frac{N}{8}\Big([\partial_t G^{ab}(t)]^2 - G^{ab}(t)\partial_t^2 G^{ab}(t)\Big). \tag{A.42}$$

This expression needs to be found only for times $|\tau - \tau'| > 1/J$ and therefore one can omit the action of time derivative on the sign-function in Eq. (3.1). Indeed, the resulting δ-function will bring times $t_{1,2}$ infinitely close to each other, but these times are excluded from the integration domain in Eq. (A.38). Bearing this remark one obtains

$$\Pi^{ab}(t) = -\frac{N}{32\sqrt{\pi}J}\frac{g_{ab}^2}{|t|^3}, \tag{A.43}$$

with $g_{aa} = \tilde{g}$ and $g_{ab} = g$ for $a \neq b$ according to Eq. (A.1). Then the soft-mode action assumes the form

$$\begin{aligned} S_2[f] &= -\frac{N}{32\sqrt{\pi}J}\sum_{ab} g_{ab}^2 \iint dt_1 dt_2 \, \frac{\zeta^a_{t_1}\zeta^b_{t_2}}{|t_1 - t_2|^3} \\ &\overset{t_i = f(\tau_i)}{=} -\frac{N}{32\sqrt{\pi}J}\sum_{ab} g_{ab}^2 \iint d\tau_1 d\tau_2 \, \frac{f_a'(\tau_1)^{3/2} f_b'(\tau_2)^{3/2}}{|f_a(\tau_1) - f_b(\tau_2)|^3}. \end{aligned} \tag{A.44}$$

Diagonal matrix elements in this sum produce the Schwarzian action for each function $f_a(\tau)$, see e.g. derivation in Ref. [16], and below we analyze the terms with $a \neq b$. These off-diagonal contributions mainly come from the singularity along the curve $\mathcal{C}$ in the plane (τ_1, τ_2) defined by the equation $f_a(\tau_1) = f_b(\tau_2)$. In the close vicinity of $\mathcal{C}$ one can introduce the new set of coordinates (τ, s), where τ runs along $\mathcal{C}$ and s is the direction which is perpendicular to $\mathcal{C}$, as shown on Fig. A.2. Let $\mathbf{e}_\tau \equiv (\partial_\tau \tau_1(\tau, s), \partial_\tau \tau_2(\tau, s))$ and $\mathbf{e}_n \equiv (\partial_s \tau_1(\tau, s), \partial_s \tau_2(\tau, s))$ be the corresponding tangential and transverse vector fields to the curve $\mathcal{C}$, which in the new coordinates is just a straight line $s = 0$. According to their definitions we have

$$\partial_\tau[f_a(\tau_1(\tau, s)) - f_b(\tau_2(\tau, s))] = (f_a'(\tau_1), -f_b'(\tau_2))^T \cdot \mathbf{e}_\tau = 0, \tag{A.45}$$

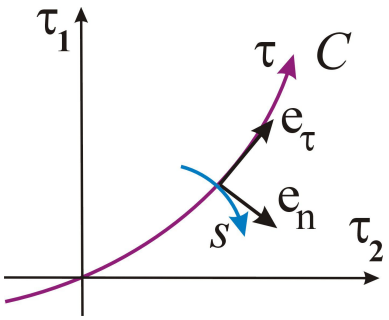

Figure A.2: The curve $\mathcal{C}$ is defined by the relation $f_a(\tau_1) = f_b(\tau_2)$. The new (local) system of coordinates (τ, s) is chosen as described in the main text so that τ runs along $\mathcal{C}$ and s in the orthogonal direction. The main contribution to the action (A.44) stems from the region $|s| \lesssim 1/J$.

which means that $\mathbf{e}_\tau$ should be orthogonal to the vector $\mathbf{f}_{ab} = (f_a'(\tau_1), -f_b'(\tau_2))^T$. On other hand $\mathbf{e}_n$ must be parallel to the same vector $\mathbf{f}_{ab}$. Therefore, the normalized tangential and normal vectors to the line $\mathcal{C}$ can be defined by the following relations

$$\mathbf{e}_\tau = \frac{(f_b', f_a')}{\sqrt{(f_a')^2 + (f_b')^2}}, \qquad \mathbf{e}_n = \frac{(f_a', -f_b')}{\sqrt{(f_a')^2 + (f_b')^2}}. \tag{A.46}$$

From here it follows that the parametrization of the coordinate line s in the perpendicular direction $\mathbf{e}_n$ can be written in the following form

$$\begin{pmatrix} \tau_1 \\ \tau_2 \end{pmatrix} \to \begin{pmatrix} \tau_1 \\ \tau_2 \end{pmatrix} + \frac{s}{\sqrt{(f_a')^2 + (f_b')^2}} \begin{pmatrix} f_a' \\ -f_b' \end{pmatrix} \tag{A.47}$$

The difference $f_a(\tau_1) - f_b(\tau_2)$ transforms under Eq. (A.47) to

$$f_a\left(\tau_1 + s\frac{f_a'}{\sqrt{(f_a')^2 + (f_b')^2}}\right) - f_b\left(\tau_2 - s\frac{f_a'}{\sqrt{(f_a')^2 + (f_b')^2}}\right) \simeq s\sqrt{(f_a')^2 + (f_b')^2}, \tag{A.48}$$

where we took into account that $f_a(\tau_1) = f_b(\tau_2)$. Now using the exponential parametrization

$$f_a' = e^{\phi_a}, \quad f_b' = e^{\phi_b}, \tag{A.49}$$

and substituting Eq. (A.48) into the integration kernel in Eq. (A.44), we obtain

$$S_2[f] = -\frac{N}{32\sqrt{\pi}J}\sum_{a\neq b} g^2 \int\limits_{\sim 1/J}^{+\infty} \frac{ds}{s^3} \int\limits_{\mathcal{C}} \frac{d\tau}{\cosh^{3/2}\left[\phi_a(\tau_1(\tau)) - \phi_b(\tau_2(\tau))\right]}. \tag{A.50}$$

Here we took into consideration that the Jacobian of transformation from (τ_1, τ_2) to (s, τ) variables is unity, because the basis $(\mathbf{e}_\tau, \mathbf{e}_n)$ is orthonormal. The choice of the short-time cutoff $\sim 1/J$ affects the value of the coupling constant in the action Eq. (A.50), it does not change the functional form of the coupling term though.

Considering infinitesimally close transformations in different replicas, we can expand the denominator in small difference $\varphi(\tau) = \phi_a(\tau_1(\tau)) - \phi_b(\tau_2(\tau))$, and after performing the integration over s, we obtain

$$S_2[f] \simeq -\frac{NJ}{2^7\sqrt{2\pi}}\sum_{a\neq b} g^2 \int\limits_{\mathcal{C}} d\tau \left(1 - \frac{3}{4}\varphi^2\right). \tag{A.51}$$

For the 2nd term in the expression, $\propto \varphi_{ab}^2$, the contour $\mathcal{C}$ can be substituted by the straight line ($\tau_1 = \tau_2 = \tau$) if one is interested in the Gaussian order only. As to the 1st part, the line integral

$$L_{ab} = \int_{\mathcal{C}} dl \tag{A.52}$$

by itself has a φ^2–contribution which takes into account the deviation of $\mathcal{C}$ from a straight line. As shown below the length reads

$$L_{\alpha\beta} = \sqrt{2}\int d\tau \left(1 + \frac{1}{8}\varphi_{ab}^2(\tau) + \mathcal{O}(\varphi_{ab}^3)\right), \tag{A.53}$$

and therefore the final result for the action in the Gaussian order in fluctuations assumes the form

$$S_2[f] = \frac{5NJ}{2^{10}\sqrt{2\pi}}\sum_{a\neq b} g_{ab}^2 \int d\tau \varphi_{ab}^2(\tau) + \mathcal{O}(\varphi_{ab}^3), \tag{A.54}$$

which is the last expression in Eq. (3.9).

Let us now derive Eq. (A.53). We assume that both phases are small ($\phi_a \ll 1$ and

$\phi_b \ll 1$) and then parametrize $\mathcal{C}$ by a variable τ as

$$\tau_1(\tau) = \tau + x(\tau), \qquad \tau_2(\tau) = \tau + y(\tau), \tag{A.55}$$

with fluctuations x, y being small in ϕ's . Their role is to take into account a deviation of the curve from the straight diagonal. From the relation $f_a(\tau + x) = f_b(\tau + y)$ we then have (up to 2nd order in ϕ),

$$f_a + e^{\phi_\alpha} x = f_b + e^{\phi_\beta} y, \tag{A.56}$$

where we took into account that next order terms, e.g $f_a'' x^2 \simeq \phi_a' e^{\phi_\alpha} x^2$, are of cubic order in ϕ's. There are many ways to parametrize the same curve and thus equation above does not fix x and y unambiguously. For example one can choose

$$x = -\frac{1}{2} e^{-\phi_a}(f_a - f_b), \qquad y = \frac{1}{2} e^{-\phi_b}(f_a - f_b). \tag{A.57}$$

With this choice one further needs to evaluate

$$L = \int_{\mathcal{C}} dl = \int d\tau \Big[(1 + x_\tau')^2 + (1 + y_\tau')^2 \Big]^{1/2}. \tag{A.58}$$

In the 2nd order in ϕ's one finds

$$1 + x_\tau' = \frac{1}{2}\left[1 + e^{\phi_b - \phi_a} + \phi_a'(f_a - f_b) \right], \tag{A.59}$$

$$1 + y_\tau' = \frac{1}{2}\left[1 + e^{\phi_a - \phi_b} - \phi_b'(f_a - f_b) \right], \tag{A.60}$$

which gives us for the line element

$$dl = \sqrt{2}\left[1 + \frac{3}{8}\varphi_{ab}^2 + \frac{1}{4}\varphi_{ab}'(f_a - f_b) \right] d\tau. \tag{A.61}$$

When performing the integral over $d\tau$ we integrate by parts. Taking into account that $f_a' = e^{\phi_a}$ we finally arrive at

$$L_{ab} \simeq \sqrt{2} \int d\tau \left(1 + \frac{1}{8}\varphi_{ab}^2(\tau) \right), \tag{A.62}$$

as it was claimed above. It is natural that the correction to the geometric length of the curve $\mathcal{C}$ is positive, since it deviates from the straight line.

A.5 Transition to the two-level regime

In this Appendix we give a qualitative explanation as to why the transition from the reparametrization-dominated to the two-level regime occurs at a shorter time-scale for the site off-diagonal correlation functions in comparison to the site-diagonal ones, as observed numerically. Consider first the correlation functions $D_2(\tau)$ and $\langle G_{ii}^2(\tau)\rangle_{\rm dis}$. In the two-level regime, with the levels denoted as $|0\rangle$ and $|1\rangle$, we have

$$D_2(\tau) = \left\langle \langle 0|\chi_i|1\rangle\langle 1|\chi_j|0\rangle\langle 0|\chi_j|1\rangle\langle 1|\chi_i|0\rangle e^{-2E_1\tau}\right\rangle_{\rm dis} = \left\langle |\langle 0|\chi_i|1\rangle|^2|\langle 0|\chi_j|1\rangle|^2 e^{-2E_1\tau}\right\rangle_{\rm dis} \tag{A.63}$$

Here the energy of the ground state is set to zero hence E_1 denotes the energy gap between the ground state and the first excited state. The numerical data in the two-level regime can be fitted with very high accuracy under the assumptions that energies E_1 and the matrix elements $M_i = \langle 0|\chi_i|1\rangle$ are statistically independent Gaussian distributed quantities. Furthermore, to explain the different time scales for the crossover between the reparametrization dominated and two-level regimes, assume the matrix elements for the operators at different sites to be statistically independent of each other, $\langle M_i M_j\rangle_{\rm dis} = 0$. Then, for the correlation function $D_2(\tau)$, we obtain

$$D_2(\tau) = \left(\left\langle |M|^2\right\rangle_{\rm dis}\right)^2 \left\langle e^{-2E_1\tau}\right\rangle_{\rm dis}, \tag{A.64}$$

where $\left\langle |M|^2\right\rangle_{\rm dis} = \left\langle |M_i|^2\right\rangle_{\rm dis}$ independently of i. For $\langle G_{ii}^2(\tau)\rangle_{\rm dis}$ we obtain under the same assumptions

$$\langle G_{ii}^2(\tau)\rangle_{\rm dis} = \left\langle |M|^4\right\rangle_{\rm dis} \left\langle e^{-2E_1\tau}\right\rangle_{\rm dis}. \tag{A.65}$$

Under the assumption of Gaussian distributed matrix elements the results Eqs. (A.64) and (A.65) differ just by an N-independent factor.

The crossover from the reparametization dominated to the two-level regime occurs at the time scale, where the contributions of higher energy levels become suppressed by the corresponding energy exponents $\sim e^{-E_n\tau}$. As a toy model, consider the contribution

of the next exited level, which we denote as $|2\rangle$ with the energy E_2. For the correlation function $D_2(\tau)$ we now obtain

$$D_2(\tau) = \big\langle \big(\langle 0|\chi_i|1\rangle\langle 1|\chi_j|0\rangle e^{-E_1\tau} + \langle 0|\chi_i|2\rangle\langle 2|\chi_j|0\rangle e^{-E_2\tau} \big) \big(\langle 0|\chi_j|1\rangle\langle 1|\chi_i|0\rangle e^{-E_1\tau} + \langle 0|\chi_j|2\rangle\langle 2|\chi_i|0\rangle e^{-E_2\tau} \big) \big\rangle_{\rm dis} = \big\langle |\langle 0|\chi_i|1\rangle|^2 |\langle 0|\chi_j|1\rangle|^2 e^{-2E_1\tau} + |\langle 0|\chi_i|2\rangle|^2 |\langle 0|\chi_j|2\rangle|^2 e^{-2E_2\tau} \big\rangle_{\rm dis} + \Big\langle \big(\langle 0|\chi_i|1\rangle\langle 1|\chi_j|0\rangle\langle 0|\chi_j|2\rangle\langle 2|\chi_i|0\rangle + \langle 0|\chi_j|1\rangle\langle 1|\chi_i|0\rangle\langle 0|\chi_i|2\rangle\langle 2|\chi_j|0\rangle \big) e^{-(E_1+E_2)\tau} \Big\rangle_{\rm dis} \quad \text{(A.66)}$$

Eq. (A.66) is to be contrasted to the 3-level expression for $\langle G_{ii}^2(\tau)\rangle_{\rm dis}$

$$\langle G_{ii}^2(\tau)\rangle_{\rm dis} = \big\langle |\langle 0|\chi_i|1\rangle|^4 e^{-2E_1\tau} + |\langle 0|\chi_i|2\rangle|^4 e^{-2E_2\tau} \big\rangle_{\rm dis} + 2 \Big\langle \langle 0|\chi_i|1\rangle\langle 1|\chi_i|0\rangle\langle 0|\chi_i|2\rangle\langle 2|\chi_i|0\rangle e^{-(E_1+E_2)\tau} \Big\rangle_{\rm dis} . \quad \text{(A.67)}$$

Now let us make the following assumptions: matrix elements between the ground state and the state $|1\rangle$, and between the ground state and the state $|2\rangle$ are statistically independent. Furthermore, the sign of the product $\langle 0|\chi_j|n\rangle\langle n|\chi_i|0\rangle$, $(i \neq j)$ is random, hence the average of such a product over disorder distribution is close to zero. It follows from this assumption, that the terms $\langle 0|\chi_i|1\rangle\langle 1|\chi_j|0\rangle\langle 0|\chi_j|2\rangle\langle 2|\chi_i|0\rangle$ vanish after the average over disorder, in contrast to $\langle 0|\chi_i|1\rangle\langle 1|\chi_i|0\rangle\langle 0|\chi_i|2\rangle\langle 2|\chi_i|0\rangle$, which result in the explicitly positive contribution. Eqs. (A.66), (A.67) become

$$D_2(\tau) \approx \big\langle |M_1|^2 \big\rangle_{\rm dis}^2 \big\langle e^{-2E_1\tau} \big\rangle_{\rm dis} + \big\langle |M_2|^2 \big\rangle_{\rm dis}^2 \big\langle e^{-2E_2\tau} \big\rangle_{\rm dis} . \quad \text{(A.68)}$$

$$\langle G_{ii}^2(\tau)\rangle_{\rm dis} \approx \big\langle |M_1|^4 \big\rangle_{\rm dis} \big\langle e^{-2E_1\tau} \big\rangle_{\rm dis} + \big\langle |M_2|^4 \big\rangle_{\rm dis} \big\langle e^{-2E_2\tau} \big\rangle_{\rm dis} + 2 \big\langle |M_1|^2 \big\rangle_{\rm dis} \big\langle |M_2|^2 \big\rangle_{\rm dis} \Big\langle e^{-(E_1+E_2)\tau} \Big\rangle_{\rm dis} . \quad \text{(A.69)}$$

Here we denoted $M_1 = \langle 0|\chi_i|1\rangle$, $M_2 = \langle 0|\chi_i|2\rangle$. Taking into account $E_1 < E_2$, on can see that the subleading term $\big\langle e^{-(E_1+E_2)\tau} \big\rangle_{\rm dis}$ in Eq. (A.69) leads to a slower time decay of the site diagonal correlation function $\langle G_{ii}^2(\tau)\rangle_{\rm dis}$ at relatively short times than the decay of the site off-diagonal correlation function, where the above mentioned term is absent.

Another, complementary point of view on the spread of the correlation functions in the crossover region between the reparametrization-dominated and two-level regime can

be gained by considering the effective many particle density of states. Namely, assuming the discrete spectrum of energies E_n we conclude that the possible energy factors determining the time decay of the site off-diagonal correlation functions can be only the multiples of the energies E_n (in our previous example $n = 1, 2$), such as $2E_1, 2E_2, ...$ This is due to the vanishing disorder averages of the matrix elements $\langle\langle 0|\chi_i|n\rangle\langle n|\chi_j|0\rangle\rangle_{\rm dis}$ for $i \neq j$. In contrast, for the site diagonal correlation function, the energy factors are built out of all possible sums of pairs of energies, such as $E_n + E_m$, for any two states $|n\rangle$ and $|m\rangle$. Considering each energy factor as an effective multi-particle energy level, we conclude, that the many-particle energy spectrum contributing to the site-diagonal correlation function is more dense, that is it has lower many-particle level spacing. Now, the deviations from the reparametrization dominated regime should happen at the times which are of the order of inverse many-particle level spacing. According to the considerations above, those times are larger for the site-diagonal correlation function that for the site off-diagonal one. This would explain qualitatively why the spreading of the site off-diagonal curves $[D_{2p}/(2p-1)!!]^{1/p}$ in Fig. 3.4 occurs at earlier times than that for the site-diagonal curves $\langle G^p\rangle_{\rm dis}^{1/p}$ in Fig. 3.1.

Appendix B

SYK superconductivity: technical details

B.1 Mean-field treatment of SYK-Hubbard model

In this Appendix we provide details of the mean-field treatment for the model specified by Eqs. (4.9)–(4.12). We employ the standard treatment of SYK model, which includes averaging of the replicated partition function over the distribution of couplings followed by the so-called $G\Sigma$-approach [16]. For the model with *real* couplings, Eq. (4.9), the Gaussian averaging over $J_{ij;kl}$'s produces two kinds of 8-fermion terms, which we call normal and anomalous

$$\left\langle e^{-\sum_{a=1}^{n}\int H_a d\tau}\right\rangle_J = \exp\left\{\frac{J^2}{4(4N)^3}\sum_{a,b=1}^{n}\int d\tau d\tau' \sum_{i,j,k,l=1}^{N}\left(\mathcal{A}_{ijkl}^{a\tau,b\tau'}+\mathcal{N}_{ijkl}^{a\tau,b\tau'}\right)\right\}, \qquad \text{(B.1)}$$

where the anomalous part $\mathcal{A}_{ijkl}^{a\tau,b\tau'}$ is given by a product of fermion operators describing creation and annihilation of on-site Cooper pairs

$$\mathcal{A}_{ijkl}^{a\tau,b\tau'} = \sum_{\sigma\sigma'\rho\rho'}(\bar{c}_{i\sigma}^{a\tau}\bar{c}_{i\rho}^{b\tau'})(\bar{c}_{j\sigma'}^{a\tau}\bar{c}_{j\rho'}^{b\tau'})(c_{k\sigma'}^{a\tau}c_{k\rho'}^{b\tau'})(c_{l\sigma}^{a\tau}c_{l\rho}^{b\tau'}) \qquad \text{(B.2)}$$

and the normal part is given by product of one creation and one annihilation operator at each site

$$\mathcal{N}_{ijkl}^{a\tau,b\tau'} = \sum_{\sigma\sigma'\rho\rho'} (\bar{c}_{i\sigma}^{a\tau} c_{i\rho}^{b\tau'})(\bar{c}_{j\sigma'}^{a\tau} c_{j\rho'}^{b\tau'})(\bar{c}_{k\rho'}^{b\tau'} c_{k\sigma'}^{a\tau})(\bar{c}_{l\rho}^{b\tau'} c_{l\sigma}^{a\tau}). \tag{B.3}$$

Here $\bar{c}$ refers to the Grassmann variable which is the counterpart of $c^\dagger$ in canonical form. Guided by the knowledge that no replica-off-diagonal saddle points exist for the SYK-model [14, 16, 8], we restrict further consideration to the replica-diagonal sector and drop the replica indexes hereafter. In the framework of $G\Sigma$-approach one introduces fields corresponding to the on-site Green's functions. However, the presence of the anomalous term, Eq. (B.2), requires introduction of both normal and anomalous Green's functions. Anticipating spin-singlet superconducting pairing, we assume the anomalous fields $\bar{F}, F$ to have nonzero componens for the opposite spin-indexes only, such as

$$F_{\tau\tau'} = -\frac{1}{N}\sum_{i=1}^{N} c_{i\downarrow}^{\tau} c_{i\uparrow}^{\tau'}, \;\; \bar{F}_{\tau\tau'} = -\frac{1}{N}\sum_{i=1}^{N} \bar{c}_{i\uparrow}^{\tau} \bar{c}_{i\downarrow}^{\tau'}. \tag{B.4}$$

In contrast, since we do not expect magnetic ordering, the normal fields G and Σ are assumed to have nonzero components only for the coinciding spin-indexes,

$$G_{\tau\tau'} = -\frac{1}{N}\sum_{i=1}^{N} \bar{c}_{i\sigma}^{a\tau} c_{i\sigma}^{b\tau'}.$$

Technically, the new fields are embedded into the path integral for partition function by insertion of the functional δ-functions. To this end, we introduce the Nambu-basis $\Psi_i = (c_{i\uparrow}, \bar{c}_{i\downarrow})^T$, $\bar{\Psi}_i = (\bar{c}_{i\uparrow}, c_{i\downarrow})$, and the matrix Green's function

$$\mathbf{G}_{\tau\tau'} = \begin{pmatrix} G_{\tau\tau'} & \bar{F}_{\tau\tau'} \\ F_{\tau\tau'} & -G_{\tau'\tau} \end{pmatrix}. \tag{B.5}$$

Then the functional δ-functions are enforced by the conjugated matrix field

$$\mathbf{\Sigma}_{\tau\tau'} = \begin{pmatrix} \Sigma_{\tau\tau'} & \bar{\Xi}_{\tau\tau'} \\ \Xi_{\tau\tau'} & -\Sigma_{\tau'\tau} \end{pmatrix}. \tag{B.6}$$

as follows

$$\mathbf{1} = \int [D\mathbf{\Sigma}, \mathbf{G}] \exp\left[\sum_{i=1}^{N} \bar{\Psi}_i \mathbf{\Sigma} \Psi_i + N \mathrm{Tr}\left(\mathbf{\Sigma G}\right)\right], \tag{B.7}$$

The dual fields Ξ, $\bar{\Xi}$, and Σ play the role of anomalous and normal self-energies respectively.

Furthermore, we perform Hubbard-Stratonovich transformation to decouple the Hubbard term in the Cooper channel, introducing site-local complex fields Δ_i,

$$\begin{aligned} & \exp\left[U \sum_i \int d\tau \bar{c}^{\tau}_{i\uparrow} \bar{c}^{\tau}_{i\downarrow} c^{\tau}_{i\downarrow} c^{\tau}_{i\uparrow}\right] \\ = & \int [D\bar{\Delta}^{\tau}_i, \Delta^{\tau}_i] \exp\left[-\frac{1}{U} \sum_i \int d\tau \left(\bar{\Delta}^{\tau}_i \Delta^{\tau}_i\right) + \sum_i \int d\tau \left(\bar{\Delta}^{\tau}_i c^{\tau}_{i\downarrow} c^{\tau}_{i\uparrow} + \Delta^{\tau}_i \bar{c}^{\tau}_{i\uparrow} \bar{c}^{\tau}_{i\downarrow}\right)\right]. \end{aligned} \tag{B.8}$$

After the decoupling procedure, the action reads:

$$\begin{aligned} S = & \sum_{i=1}^{N} \int_0^{\beta} d\tau d\tau' \left\{ \sum_{\sigma=\uparrow,\downarrow} \bar{c}^{\tau'}_{i\sigma} \left(\delta_{\tau'\tau} \partial_{\tau} + \Sigma_{\tau'\tau}\right) c_{i\sigma} \right. \\ & \left. + \Xi_{\tau'\tau} \bar{c}^{\tau'}_{i\uparrow} \bar{c}^{\tau}_{i\downarrow} + \bar{\Xi}_{\tau'\tau} c^{\tau'}_{i\downarrow} c^{\tau}_{i\uparrow} + (\bar{\Delta}^{\tau}_i c^{\tau}_{i\downarrow} c^{\tau}_{i\uparrow} + \Delta^{\tau}_i \bar{c}^{\tau}_{i\uparrow} \bar{c}^{\tau}_{i\downarrow}) \delta_{\tau\tau'} \right\} \\ & - N \int_0^{\beta} d\tau d\tau' \left\{ 2\Sigma_{\tau'\tau} G_{\tau\tau'} + \Xi_{\tau'\tau} \bar{F}_{\tau\tau'} + \bar{\Xi}_{\tau'\tau} F_{\tau\tau'} \right. \\ & \left. + \frac{J^2}{64} \left[\bar{F}^2_{\tau\tau'} F^2_{\tau\tau'} + G^4_{\tau\tau'}\right] \right\} + \frac{1}{U} \sum_{i=1}^{N} \int_0^{\beta} d\tau \bar{\Delta}^{\tau}_i \Delta^{\tau}_i. \end{aligned} \tag{B.9}$$

B.1.1 Saddle point ansatz

We assume the fields Δ_i to be time- and site-independent at the saddle point. Then we integrate out fermion fields, and obtain the action in the form

$$\begin{aligned}\frac{S}{N} = &-\sum_{\omega_n} \ln\left[(-i\omega_n + \Sigma(\omega_n))^2\right. \\ &\left.- (\bar{\Xi}(\omega_n) + \bar{\Delta})(\Xi(\omega_n) + \Delta)\right] + \frac{\beta}{U}\bar{\Delta}\Delta \\ &- \int d\tau d\tau' \left(\Xi_{\tau'\tau}\bar{F}_{\tau\tau'} + \bar{\Xi}_{\tau'\tau}F_{\tau\tau'} + 2\Sigma_{\tau'\tau}G_{\tau\tau'}\right) \\ &- \frac{J^2}{64}\int d\tau d\tau' \left[G^4_{\tau\tau'} + \bar{F}^2_{\tau\tau'}F^2_{\tau\tau'}\right]. \end{aligned} \tag{B.10}$$

Variation of the action Eq. (B.10) results in the following set of saddle point equations

$$\frac{\Delta}{U} = T\sum_{\omega_n} \frac{\Delta + \Xi(\omega_n)}{(\omega_n + i\Sigma(\omega_n))^2 + (\bar{\Xi}(\omega_n) + \bar{\Delta})(\Xi(\omega_n) + \Delta)}, \tag{B.11}$$

$$F(\omega_n) = \frac{-(\Delta + \Xi(\omega_n))}{(\omega_n + i\Sigma(\omega_n))^2 + (\bar{\Xi}(\omega_n) + \bar{\Delta})(\Xi(\omega_n) + \Delta)}, \tag{B.12}$$

$$\Xi_{\tau\tau'} = -\frac{J^2}{32}\bar{F}_{\tau\tau'}F^2_{\tau\tau'}, \tag{B.13}$$

$$G(\omega_n) = \frac{-i\omega_n + \Sigma(\omega_n)}{(\omega_n + i\Sigma(\omega_n))^2 + (\bar{\Xi}(\omega_n) + \bar{\Delta})(\Xi(\omega_n) + \Delta)}, \tag{B.14}$$

$$\Sigma_{\tau\tau'} = \frac{J^2}{32}G^3_{\tau\tau'}. \tag{B.15}$$

Note the relation

$$\frac{\Delta}{U} = -T\sum_{\omega_n} F(\omega_n) = -F_{\tau\tau}. \tag{B.16}$$

Hereafter we restrict ourselves to the case of the half-filling, where, due to the particle-hole symmetry, the normal components are odd, while anomalous are even functions of time, eg., $\Xi_{\tau'\tau} = \Xi_{\tau\tau'}$, $\Sigma_{\tau'\tau} = -\Sigma_{\tau\tau'}$.

B.1.2 Approximate solution of the mean-field equations

The anomalous fields Ξ and F, entering the saddle point equations, admit non-zero solutions only in the presence of Δ. Similarly to the BCS case, we'll find that $F \propto \Delta$. According to Eq. (B.13), $\Xi \propto F^3 \propto \Delta^3$. Therefore in the limit of (exponentially) small Δ one may consider dropping Ξ from the set of the mean-field equations and restricting them down to:

$$G(\omega_n) = \frac{-i\omega_n + \Sigma(\omega_n)}{(\omega_n + i\Sigma(\omega_n))^2 + \Delta^2}, \tag{B.17}$$

$$\Sigma_{\tau\tau'} = \frac{J^2}{32} G^3_{\tau\tau'}, \tag{B.18}$$

$$F(\omega_n) = -\frac{\Delta}{(\omega_n + i\Sigma(\omega_n))^2 + \Delta^2}, \tag{B.19}$$

where we fixed the phase of Δ to make the latter real. We'll see below that neglecting Ξ is not, strictly speaking, justified, even for the small Δ. Nevertheless Eqs. (B.17)–(B.19) will be shown to be a qualitatively (if not quantitatively) accurate representation of the full set. Eqs. (B.17), (B.18) are the known saddle point equations of the SYK model, modified by the presence of a finite Δ. In the normal phase ($\Delta = 0$) Eqs. (B.17), (B.18) exhibit an approximate conformal invariance at long times. Their solutions behave like $G(\tau) \sim \mathrm{sign}(\tau)/\sqrt{J|\tau|}$ and $\Sigma(\tau) \sim \mathrm{sign}(\tau)\sqrt{J}/|\tau|^{3/2}$. Assuming for a moment that $\Sigma \gg \Delta, \omega_n$, one finds $F(\omega_n) \propto \Delta/(J|\omega_n|)$. In the time representation this amounts to $F(\tau) \propto (\Delta/J)\ln(\tau_\Delta/\tau)$, where τ_Δ is a long time cutoff to be discussed momentarily.

A finite Δ creates a gap in the many-body spectrum, forcing the exponential decay of the correlation functions at a long imaginary time. We denote the corresponding time scale, given by the inverse of the energy gap, as τ_Δ. Following Ref. [82, 83], based on these considerations we adopt the following variational ansatz for the normal and anomalous Green functions:

$$G(\tau) = -\frac{e^{-|\tau|/\tau_\Delta}}{\sqrt{2\pi\tilde{J}|\tau|}}\,\mathrm{sgn}(\tau); \tag{B.20}$$

$$F(\tau) = -\frac{\Delta}{\pi\tilde{J}}\, e^{-|\tau|/\tau_\Delta} \ln\left(1 + c\,\frac{\tau_\Delta}{|\tau|}\right), \tag{B.21}$$

where $\tilde{J} = J/(4\sqrt{2\pi})$ and parameters τ_Δ and c are to be determined to satisfy Eqs. (B.17),

(B.19) in the limit of small frequencies.

To execute this program we first perform the Fourier transforms of $G(\tau)$ and $\Sigma(\tau) = J^2 G^3(\tau)/32$, finding:

$$G(\omega_n) = \frac{\mathrm{sgn}(\omega_n)}{i\sqrt{\tilde{J}|\omega_n|}}; \qquad \Sigma(\omega_n) = -i\sqrt{\tilde{J}|\omega_n|}\,\mathrm{sgn}(\omega_n), \tag{B.22}$$

for $\omega\tau_\Delta \gg 1$ and

$$G(\omega_n) = \frac{\tau_\Delta^{3/2}\,\omega_n}{i\sqrt{2\tilde{J}}}; \qquad \Sigma(\omega_n) = -i\frac{\sqrt{\tilde{J}\tau_\Delta}\,\omega_n}{\sqrt{6}}, \tag{B.23}$$

for $\omega\tau_\Delta \ll 1$. One notices that in both limits $\Sigma(\omega_n) \gg \omega_n$ and therefore the latter may be neglected in Eqs. (B.17), (B.19). In the limit $\omega\tau_\Delta \gg 1$ one also notices that $\Sigma(\omega_n) \gg \Delta$ and thus $G(\omega_n) = -1/\Sigma(\omega_n)$, which is consistent with Eq. (B.22). This consistency is a consequence of our choice of $\tilde{J}$. In the opposite limit, $\omega\tau_\Delta \ll 1$, $\Sigma(\omega_n) \ll \Delta$ and thus $G(\omega_n) = \Sigma(\omega_n)/\Delta^2$. Combining this with Eq. (B.23), one finds for the inverse energy gap

$$\tau_\Delta = \frac{\tilde{J}}{\sqrt{3}\,\Delta^2}. \tag{B.24}$$

Notice that the gap scales as $\Delta^2/J \ll \Delta$. This is a consequence of the superconductivity being formed from the non Fermi liquid normal state.

We turn now to the anomalous function. According to Eqs. (B.19) and (B.22) its high energy limit is given by:

$$F(\omega_n) = \frac{\Delta}{\Sigma^2(\omega_n)} = -\frac{\Delta}{\tilde{J}|\omega_n|}. \tag{B.25}$$

It's Fourier transform is $F(\tau) = -(\Delta/\pi\tilde{J})\ln(\tau_\Delta/\tau)$, where τ_Δ is adopted as a long time cutoff. This is exactly the variational form, Eq. (B.21) at $\tau \ll \tau_\Delta$. Finally to fix the constant c in Eq. (B.21) we demand the correct asymptotic at $\omega_n \to 0$, which is, according to Eqs. (B.19) and (B.23), $F(\omega_n = 0) = \int d\tau F(\tau) = -1/\Delta$. Integrating Eq. (B.21) with τ_Δ given by Eq. (B.24), one finds $c = 7.58$.

Finally, we can self-consistently determine Δ using Eq. (B.16). To this end one needs the anomalous function at the coinciding times: $F_{\tau\tau} = F(\tau = 0)$. Putting UV

cutoff instead, $\tau \sim 1/\tilde{J}$, one finds

$$\frac{\Delta}{U} = \frac{\Delta}{\pi\tilde{J}} \ln\Big(\tilde{J}\tau_\Delta\Big) = \frac{2\Delta}{\pi\tilde{J}} \ln\left(\frac{\tilde{J}}{\Delta}\right), \tag{B.26}$$

where the coefficient inside the logarithm is somewhat arbitrary. As a result, one finds

$$\Delta \sim \tilde{J}\, e^{-\frac{\pi\tilde{J}}{2U}}. \tag{B.27}$$

We conclude that, within the mean-field treatment, the superconducting order parameter Δ is present at an infinitesimally small Hubbard attraction U.

Let us now discuss the omission of the anomalous component of the self-energy, $\Xi(\omega_n)$, in Eqs. (B.11)–(B.15). One expects that, since $\Xi \propto F^3$ and $F \propto \Delta \propto e^{-\frac{\pi\tilde{J}}{2U}}$, the anomalous self-energy is exponentially suppressed. In reality this is not entirely the case. Indeed, let's evaluate $\Xi(\omega_n = 0) \sim J^2 \int d\tau F^3(\tau) \sim J^2(\Delta/J)^3\tau_\Delta \sim \Delta$, where we have employed Eqs. (B.21) and (B.24). Therefore at small energies, $\omega_n\tau_\Delta \ll 1$, $\Xi(\omega_n) \sim \Delta$, while for $\omega_n\tau_\Delta \gg 1$, $\Xi(\omega_n) \sim \Delta/(|\omega_n|\tau_\Delta) \propto \Delta^3$, as expected. Nevertheless, we observe that in the entire energy range $\Xi(\omega_n) \lesssim \Delta$ and therefore omitting Ξ in Eqs. (B.11)–(B.15) is not affecting the qualitative behavior of the Green functions, Eqs. (B.20), (B.21), and the scaling of the inverse gap, Eq. (B.24). It may affect, though, some of the numerical coefficients.

In the opposite limit of large Hubbard coupling, $U > J$, the spectral gap is of the order of U. Being the largest energy scale, the gap suppresses the SYK non Fermi liquid regime. This leads to $|\omega_n| \gg \Sigma(\omega_n), \Xi(\omega_n)$ and thus Eq. (B.16) yields:

$$\Delta = U \int \frac{d\omega}{2\pi} \frac{\Delta}{\omega^2 + \Delta^2} = \frac{U}{2}. \tag{B.28}$$

B.2 Interaction constant in the quantum Kuramoto action

Here we derive the interaction term for the phase fluctuations of the local order parameters on different sites, Eq. (4.26). As explained below Eq. (4.26), the corresponding coupling constant is proportional to the off-diagonal susceptibility to variations of the local order parameter, $\kappa_{ij} = \partial^2 E_{\rm GS}/\partial\Delta_i\partial\bar{\Delta}_j$. We thus consider the order parameters,

Δ_i, to be externally applied (proximitized) through an extra term in the Hamiltonian, $\sum_i \bar{\Delta}_i c_{i\downarrow} c_{i\uparrow} + h.c.$, and evaluate an induced energy change. Diagrammatically the latter is given by the order $1/N$ diagrams, Fig. B.1, which involve normal and anomalous Green's functions, as well as the paired interaction vertices $\langle J^2_{ik;lj} \rangle = J^2/(4N)^3$.

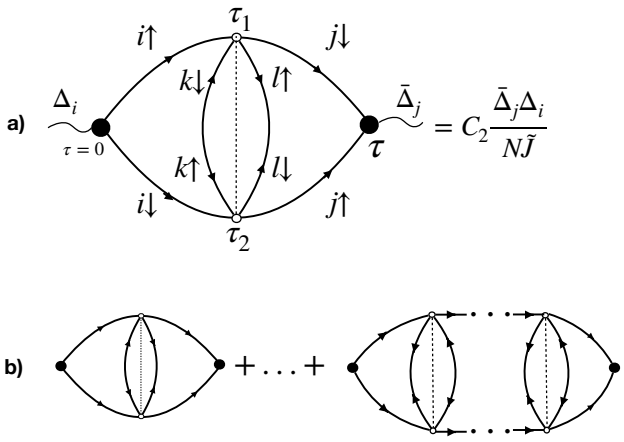

Figure B.1: Diagrammatic representation of the off-diagonal Cooper susceptibility: a) the lowest order diagram; b) the ladder series.

Since all propagators are site-diagonal, correlations between distinct sites appear in the order $1/N$ in expansion of the action. The physical mechanism of correlations between the superconducting fluctuations at different sites consists of correlated hopping of Cooper pairs facilitated by SYK-interactions $J_{ik;lj} c^\dagger_{i\sigma} c^\dagger_{k\sigma'} c_{l,\sigma'} c_{j,\sigma}$. Because all four sites here are distinct, no direct hopping of a Cooper pair is possible. Rather, a transfer of a single Cooper pair from a site i to another site j involves at least two correlated acts of interaction that cause transfer of two Cooper pairs from the sites i, k to the sites ℓ, j. Thereby the second Cooper pair plays the role of an assisting agent for the hopping of the first one. The amplitude of an elementary jump of a Cooper pair from a site i to a different site j, assisted by a hopping of another Cooper pair from a site k to a site ℓ is represented by the diagram in Fig. B.1a). The hopping of the assisting Cooper pair is depicted by the insertion of an anomalous loop between the normal Green's functions. Thus, insertion of anomalous loops is a necessary ingredient of diagrammatic representation of interaction between superconducting fluctuations at different sites.

Taking into account summation over the spin indexes and over the intermediate sites k, ℓ, one obtains contribution to the average susceptibility, $\kappa_{ij}^{(1)}$, from the lowest order diagram in Fig. B.1a):

$$\kappa_{ij}^{(1)} = \frac{J^2}{16N} \int d\tau d\tau_1 d\tau_2 \, G(\tau_1) G(\tau_2) \\ \times \bar{F}(\tau_1 - \tau_2) F(\tau_1 - \tau_2) G(\tau - \tau_1) G(\tau - \tau_2). \tag{B.29}$$

Substituting the variational solutions, Eqs. (B.20), (B.21), for normal and anomalous propagators and introducing dimensionless time-variables $t = \tau/\tau_\Delta$, $t_{1,2} = \tau_{1,2}/\tau_\Delta$, one finds

$$\kappa_{ij}^{(1)} = \frac{C_2^{(1)}}{N\tilde{J}}, \tag{B.30}$$

where $C_2^{(1)}$ is given by a convergent integral, which does not depend on any parameters,

$$C_2^{(1)} = \frac{1}{2\sqrt{3}\pi^3} \int dt dt_1 dt_2 \, \mathrm{sign}(t_1) \mathrm{sign}(t_2) \\ \mathrm{sign}(t - t_1) \mathrm{sign}(t - t_2) \ln^2 \left(1 + \frac{7.58}{|t_1 - t_2|} \right) \times \\ \frac{\exp\left[-|t_1| - |t_2| - |t - t_1| - |t - t_2| - 2|t_1 - t_2| \right]}{\sqrt{|t_1||t_2||t - t_1||t - t_2|}} = 1.58.$$

This numerical constant should not be taken too seriously. Indeed, our variational ansatz for the propagators, Eqs. (B.20), (B.21), is not exact but only interpolates between correct short and long time asymptotics. The reason of presenting this calculation is to point out the absence of logarithmic factors. The latter may be naively expected, due to the presence of two runs of the Cooper ladder in the diagram of Fig. B.1a). If the anomalous loop in the middle would be confined in time to some scale $\tau_0 \ll \tau_\Delta$, the diagram would be $\propto \ln^2(\tau_\Delta/\tau_0) \gg 1$. This is because the two integrals over τ and $\tau_1 \approx \tau_2$ would be logarithmic. In this case summation of the entire Cooper ladder, Fig. B.1b), would be of a crucial importance. However, our case happens to be different. The reason is that the anomalous loop has the same characteristic time scale, τ_Δ, as the normal Green functions, which form runs of the Cooper ladder. As a result, logarithms are not present and all the terms of the ladder have the same order of magnitude as the

first diagram, Fig. B.1a). Therefore the ladder summation only changes the numerical coefficient, C_2, rather than the large logarithmic factor. Let us note in passing that Hubbard U, being time-local, induces the conventional logarithmic Cooper ladder and thus Eq. (B.27). This ladder, however, is strictly diagonal in the site index (and is already incorporated in diagonal G and F, Eqs. (B.20), (B.21)). The off-diagonal ladder and thus the off-diagonal susceptibility, κ_{ij}, needed in the quantum Kuramoto action, requires long-range anomalous loops inserted in each run of the ladder as in Fig. B.1b).

Another consequence of the long-range nature of the anomalous loop is that the susceptibility, κ_{ij}, Eq. (B.30), is not proportional to Δ, despite each of the two anomalous propagators, F, being proportional to Δ, Eq. (B.21). The reason is that the integrations range, given by τ_Δ, is inversely proportional to Δ^2, Eq. (B.24). In the absence of other long time cutoffs, e.g. a finite size gap, this leads to Δ-independent susceptibility, Eq. (B.30).

Finally, the interaction term in the quantum Kuramoto action, Eq. (4.26), is given by $\kappa_{ij}\Delta_i\bar{\Delta}_j + h.c. \sim \kappa_{ij}|\Delta|^2\cos(\phi_i - \phi_j)$. As a result, the interaction constant, g, in the quantum Kuramoto action, Eq. (4.26), is given by

$$g = C_2\,\frac{\Delta^2}{\tilde{J}} \propto \tilde{J}e^{-\frac{\pi\tilde{J}}{U}}, \tag{B.31}$$

where constant $C_2 \sim O(1)$ remains undetermined by these considerations. The fact that g is linearly proportional to the *energy gap*, Eq. (B.24), (both being $\sim \Delta^2$) is analogous to the conventional $T = 0$ Josephson energy.

B.3 Richardson model and its generalizations

In this Appendix we review some general aspects of the Richardson model and its generalizations for completeness.

B.3.1 Richardson model

The truncated BCS-like Richardson model of superconductivity [89] involves some number of doubly degenerated fermionic levels with the set of energies $\epsilon_j/2$, where $j =$

$1, \ldots, N$. It describes the system with a fixed number, $M \leq N$, of the Cooper pairs. It is assumed that several energy levels are populated by Cooper pairs while levels with the single fermions are blocked. The Hamiltonian reads as

$$H_R = \frac{1}{2} \sum_{j,\sigma=\uparrow\downarrow}^{N} \epsilon_j c_{j\sigma}^{\dagger} c_{j\sigma} - G \sum_{jk} c_{j\uparrow}^{\dagger} c_{j\downarrow}^{\dagger} c_{k\downarrow} c_{k\uparrow}, \tag{B.32}$$

where $c_{j\sigma}^{\dagger}$ are the fermion operators and G is a coupling constant providing the attraction between fermions. In terms of the hard-core boson operators it reads as

$$H_R = \sum_{j} \epsilon_j b_j^{\dagger} b_j - G \sum_{jk} b_j^{\dagger} b_k, \tag{B.33}$$

where

$$[b_j^{\dagger}, b_k] = \delta_{jk}(2N_j - 1), \qquad b_j = c_{j\downarrow} c_{j\uparrow}, \qquad N_j = b_j^{\dagger} b_j. \tag{B.34}$$

The eigenfunctions of the Hamiltonian can be written as

$$|M\rangle = \prod_{i}^{M} B_i^{\dagger} |\mathrm{vac}\rangle, \qquad B_i^{\dagger} \equiv \sum_{j}^{N} \frac{b_j^{\dagger}}{\epsilon_j - E_i}, \tag{B.35}$$

provided the set of energies E_i, where $i = 1, \ldots, M$ satisfies the Bethe Anzatz (BA) equations

$$G^{-1} = -\sum_{j}^{N} \frac{2}{\epsilon_j - E_i} + \sum_{j}^{M} \frac{1}{E_j - E_i}. \tag{B.36}$$

The many-body energies of the corresponding states read as

$$E(M) = \sum_{i}^{M} E_i. \tag{B.37}$$

For nontrivial degeneracies of the energy levels, d_j, the BA equations read as

$$G^{-1} = -\sum_{j}^{N} \frac{d_j}{\epsilon_j - E_i} + \sum_{j}^{M} \frac{1}{E_j - E_i}. \tag{B.38}$$

It is convenient to introduce the pseudospin $Sl(2,R)$ algebra in terms of the creation-annihilation operators for the Cooper pairs

$$t_j^- = b_j \qquad t_j^+ = b_j^\dagger \qquad t_j^0 = N_j - 1/2. \tag{B.39}$$

The Richardson Hamiltonian commutes with the set of operators R_j [133]

$$R_i = -t_i^0 - 2G \sum_{i \neq j}^{N} \frac{\sum_{a=\pm,0} t_i^a t_j^a}{\epsilon_i - \epsilon_j}, \tag{B.40}$$

which are identified as the Gaudin Hamiltonians

$$[H_R, R_j] = [R_i, R_j] = 0. \tag{B.41}$$

Moreover the Richardson Hamiltonian itself can be expressed in terms of the operators R_i as

$$H_R = \sum_j \epsilon_i R_i + G \left(\sum_i R_i \right)^2 + \text{const.} \tag{B.42}$$

The number of orbitals, N, coincides with a number of sites in the Gaudin model and a coupling constant in the Richardson Hamiltonian corresponds to the "boundary twist" in the Gaudin model. The commuting operators, R_i, are the residues of the transfer matrix of the inhomogeneous twisted XXX spin chain in the semi-classical limit taken at inhomogeneities, ϵ_i. The BA equations for the Richardson model, Eq. (B.36) and for the Gaudin model exactly coincide. The Richardson model can be described in terms of the conformal field theory, where the Cooper pairs correspond to screening operators [134].

B.3.2 Russian Doll model and twisted inhomogeneous XXX spin chains

A generalization of the Richardson model - the so-called Russian Doll (RD) model [135], involves TRI breaking parameter, α. It's Hamiltonian is given by

$$H_{\text{RD}} = 2 \sum_i^N (\epsilon_i - G) N_i - \bar{G} \sum_{j<k} (e^{i\alpha} b_k^\dagger b_j + e^{-i\alpha} b_j^\dagger b_k). \tag{B.43}$$

The two parameters $G, \bar{G}$ can be related to α as

$$\alpha = \operatorname{arctanh}\left(\frac{\eta}{G}\right), \tag{B.44}$$

where $\eta = \sqrt{\bar{G}^2 - G^2}$. It is also useful to consider dimensionless parameters g, θ defined as $G = gd$ and $\eta = \theta d$, where d is a mean value of $(\epsilon_{i+1} - \epsilon_i)$ sequence. The RD model reduces to the Richardson model in the limit $\eta \to 0$.

The RD model turns out to be integrable as well. Now instead of the Gaudin model a proper spin chain counterpart is the generic quantum twisted inhomogeneous XXX spin chain [136]. The equation defining a spectrum of the RD model reads as

$$\exp(-2i\alpha) \prod^{N} \frac{E_j - \epsilon_k - i\eta/2}{E_j - \epsilon_k + i\eta/2} = \prod^{M} \frac{\epsilon_j - \epsilon_k - i\eta}{\epsilon_j - \epsilon_k + i\eta} \tag{B.45}$$

and coincides with the BA equations for the spin chain. It reduces to the BA equation of the Richardson model (B.36) in the limit $\eta \to 0$.

The RD model enjoys the gap equation, which reads as follows:

$$\tilde{\Delta}_j = \sum_{i \neq j} V_{ij} \frac{\tilde{\Delta}_i}{\sqrt{(\epsilon_i - V_{ii})^2 + |\Delta_i|^2}}, \qquad \tilde{\Delta}_j = \Delta_j e^{i\phi_i}, \tag{B.46}$$

where V_{ij} is a scattering potential, which depend on the parameters G, α. In the thermodynamical limit it becomes an integral equation with multiple solutions for the gaps. Different solutions to the gap equation yield different superconducting states.

Solutions of the gap equation in the large N limit are parametrized as follows:

$$\Delta_n = \frac{\omega}{\sinh t_n}, \quad t_n = t_0 + \frac{\pi n}{\theta} \quad n = 0, 1 \ldots, \tag{B.47}$$

where t_0 is a solution to the following equation:

$$\tan(\theta t_0) = \frac{\theta}{g} \qquad 0 < t_0 < \frac{\pi}{\theta} \tag{B.48}$$

and $\omega = dN$ for equal spacing $(\epsilon_{i+1} - \epsilon_i) = \text{const}$. This behavior can be derived in the

mean-field approximation [135]. In the limit $\theta \to 0$ the gaps $\Delta_{n>0} \to 0$ and

$$t_0 = \frac{1}{g}, \qquad \Delta_0 = 2\omega e^{-\frac{1}{g}}. \tag{B.49}$$

This way the standard BCS expression for the gap is recovered. At a weak coupling the gaps behave as

$$\Delta_n \propto \Delta_0 e^{-\frac{n\pi}{\theta}}. \tag{B.50}$$

For Cooper pair degeneracies on orbitals, d_i, the RD model is modified a bit and is related to the higher spin XXX spin chain. The local spins s_i are determined by the corresponding pair degeneracy, d_i, of the i-th orbital

$$s_i = d_i/2 \tag{B.51}$$

and the corresponding BA equations read as

$$\exp(-2i\alpha)\prod^{N}\frac{E_j-\epsilon_k-i\eta/2+i\eta s_i}{E_j-\epsilon_k+i\eta/2-i\eta s_i}=\prod^{M}\frac{\epsilon_j-\epsilon_k-i\eta}{\epsilon_j-\epsilon_k+i\eta}. \tag{B.52}$$

The RD model involves an interesting RG behavior of couplings with respect to RG time $s = \log N$, [135]. The coupling constant exhibit the cyclic RG flow (a recent review on the cyclic RG can be found in [137]), while the TRS parameter does not renormalize

$$g_{N-1} = g_N + \frac{1}{N}(g_N^2 + \theta^2), \qquad \theta_{N-1} = \theta_N \tag{B.53}$$

$$g(s+\lambda) = g(s), \qquad g(e^{-\lambda}N) = g(N). \tag{B.54}$$

The RG period reads as

$$\lambda = \frac{\pi}{\theta} \tag{B.55}$$

and the total number of the independent gaps in the model is

$$N_{\text{gaps}} \propto \frac{\theta}{\pi}\log N. \tag{B.56}$$

The cyclic RG behavior reflects the breaking of the scale invariance down to the discrete

subgroup and the spectrum of gaps manifests in the Efimov scaling

$$\Delta_{n+1} = e^s \Delta_n \tag{B.57}$$

The sizes of the Cooper pairs in the n-th condensates also have the Efimov-like scaling.

B.3.3 Possible generalizations

Here we consider generalizations of the Richardson model, involving four-boson interactions. The Hamiltonian (4.20), appropriate for large U, is

$$H_{\rm gR} \propto -\sum_{ijkl}^{N} b_i^\dagger b_j^\dagger b_k b_l. \tag{B.58}$$

Hence one may question if Hamiltonians with four-boson interactions can be derived from the commuting set, R_i. Such representation would prove the integrability of the model. It is known that the Hamiltonians, R_i, obey a nontrivial algebraic relation [138]

$$R_i^2 = G^2 + \sum_j \frac{R_j}{\epsilon_i - \epsilon_j} + \frac{3}{4} \sum_{i \neq j} \frac{1}{(\epsilon_i - \epsilon_j)^2} \tag{B.59}$$

which follows from the hidden algebraic structure of the Gaudin model. Therefore R_i^2 yield two-boson interaction term only.

To obtain the four-boson interaction term we can consider the quadratic form

$$H_4 = \sum_{ij} A_{ij}(\epsilon_i) R_i R_j \tag{B.60}$$

with arbitrary matrix, A_{ij}. The integrable Hamiltonians, H_4, involve the desired four-boson interactions. In general, if $\epsilon_i \neq 0$, the resulting interaction coupling constants are site- and ϵ_i-dependent. In our case all $\epsilon_i = 0$ and hence the Hamiltonian (B.58) can be considered as the peculiar limit of the generic quadratic form, Eq. (B.60). Moreover, all Bethe states creation operators, B_i, at $\epsilon_i = 0$ reduce to the single operator $B_0 = \sum_i b_i^\dagger$.

B.4 Towards a holographic interpretation

We briefly comment on a possible holographic interpretation of our findings. Recall that at $T = 0$ we have seen formation of local Cooper pairs at arbitrary small attraction between fermions. Their phases are incoherent at intermediate U, separated by the continuous QPT from the superfluid phase with ODLRO at large U. The complex SYK dot we work with is now used as a toy model for "near AdS/almost CFT" correspondence in quantum mechanics. From a higher-dimensional perspective the Reissner-Nordstrom (RN) black hole (BH) is considered as the bulk whose geometry involves a long AdS_2 throat near the horizon. The large N SYK quantum mechanics lives at the boundary of the throat and in low energy sector is described by the Schwartzian action which on the other hand is the boundary action in JT gravity.

To translate our findings into the holographic framework we have to answer a few questions

- How the Hubbard scaleful parameter U enters the holographic picture?
- What is the holographic interpretation of the Goldstone $U(1)$ phase field?
- Can we identify holographically the individual Cooper pair?
- Can we identify holographically the synchronization of phases via all-to-all SYK interactions?

The answers on two first questions are relatively clear. Fortunately, the Hubbard model has been treated in the holographic approach for Bose [139] and Fermi systems [140], where it was realized that the Hubbard coupling U is to be identified with the radial position of the hard wall $r_U = U$. Therefore the control parameter, U/J, tells how close to the horizon the hard wall is placed. Small U corresponds to IR near horizon region, while large U corresponds to the hard-wall at UV near the boundary of AdS_2.

To identify the Goldstone phase field consider for a moment the $U(1)$ bulk $2d$ field (A_τ, A_r) with the boundary behavior involving chemical potential and density

$$A_\tau(r \to 0) = \mu + \rho r, \qquad F_{\tau,r} = \rho. \tag{B.61}$$

In the boundary theory the density, ρ, and the phase, ϕ, are conjugated variables

$$[\rho, \phi] = i. \tag{B.62}$$

Hence the phase has to be canonically conjugated to $F_{\tau r}$ in the bulk. To get the correct conjugated variable recall the canonical pair in $2d$ gauge theory

$$[E_r(\tau, r), A_r(\tau, r')] = i\delta(r - r'), \tag{B.63}$$

which allows to identify the phase field, $\phi(\tau)$, as the gauge holonomy along the radial direction, r.

$$\phi(\tau) = \int dr\, A_r(\tau, r). \tag{B.64}$$

Note that if we choose $A_r = 0$ gauge, the holonomy factor appears in the boundary conditions.

A somewhat similar identification of the Goldstone phase modes has been developed in holographic QCD [141] and in the holographic hydrodynamics [142]. In QCD the bulk flavor gauge group $SU(N_f)_L \times SU(N_f)_R$ is broken by the Higgs mechanism down to the diagonal $SU(N_f)$ and the pions π^a, which are non-abelian Goldstone phases, of the chiral (excitonic) condensate are identified as $\exp(i\pi^a t^a) = P \exp \int dr A_r(r, x)$. In the holographic hydrodynamics a similar identification of the Goldstone phase is emerging upon breaking of $U(1) \times U(1)$ symmetry to the diagonal subgroup.

The answers to the rest of the questions are conjectural. As follows from our analysis, a perturbation induced by the IR wall at small U amounts to the instability of the extremal RN geometry and formation of the Cooper pairs. At large U the gap of an individual Cooper pair, $\Delta \sim U$, fits the length of two strings extended up to the U scale, representing two fermions at the boundary.That is we assume that individual Cooper pair is represented by two such strings.

The last question concerns the synchronization of the phases of the Cooper pairs that is large number of strings. We conjecture that the following analogy works. Remind that the holographic Skyrmion can be equally represented as the instanton in the bulk [143] or the baryonic vertex [144]. In the case of one compact coordinate the instanton or baryon vertex gets splitted into constituents- fractional Skyrmions [145]. The mechanism of

splitting is dictated by the dynamically induced potential for interaction between phases of constituents. Let's assume that our large N SYK+Hubbard dot is a kind of Skyrmion-instanton state that is a baryon vertex placed at r_U in the throat region like it happens in holographic QCD. It can be splitted in some parameter regime when all-to-all SYK Hamiltonian apparently induces an all-to-all interaction between phases of individual components. The fractional Skyrmion hosts now *two* strings instead of N strings and therefore amounts to the pair of fermions at the boundary. Hence the fractionalized Skyrmion is a candidate for a bulk counterpart of an ensemble of individual Cooper pair.

Note some analogy with QCD at non-vanishing density. It is well-known that at large baryonic density QCD is in the color-flavor locking phase with the Cooper condensate of quarks. However it was argued in [146] that at smaller chemical potential there is a transition from Skyrmions into half-Skyrmions. It is assumed that at the transition the common gap and exciton(chiral) condensate disappears. Still there are "islands" of gapped phase with disordered chiral phases. This resembles the behavior of our model near the QPT.

Two additional remarks are in order. The insulator-superfluid QPT in $2+1$ has been discussed in the holographic framework in [147] and has clear parallels with our $0+1$ case. The insulator phase was related with the AdS soliton background while the superfluid phase with the AdS BH background. The AdS soliton solution has the effective IR cut-off at a tip of the cigar, which is an analogue of our small U regime, since U provides the IR cut-off as well. When U is large it no longer serves as an IR parameter, yielding the UV scale instead. The BH physics starts to dominate in the superfluid phase in IR similar to our case.

Let us emphasize that the relation between the SYK model and 2D JT gravity is valid only for parts of spectra described by the Schwarzian action emergent at both sides. Away from this limit the JT gravity can be considered as a dimensional reduction of 4D black hole [148], where the higher modes do not fit with SYK spectrum well (see, extended discussion in [28]). On the other hand, 4D Einstein-Maxwell action can be considered as a possible UV completion of the JT gravity.

The discussion in this Appendix is clearly only qualitative and tentative. We postpone a more detailed analysis of the holographic picture for a separate study.